Connectable solar air collectors

Connectable solar air collectors

Søren Østergaard Jensen
Miroslav Bosanac
Solar Energy Centre Denmark
Danish Technological Institute

February 2002

Preface

The present report concludes the work within the project "Connectable solar air collector/PVT collector" (Sammenkoblelig luftsolfanger/PVT-fanger), journal no. 51181/99-0059 and part of the work within the project "Cheap solar air heating system for combined DHW and space heating – phase 2" (Prisbilling kombineret rum- og brugsvandssolvarmeanlæg – fase 2. Luft-solvarme- og PVT-anlæg), journal no. 51181/99-0057 both financed by the development programme for renewable energy of the Danish Energy Agency.

The project group behind the project was:

<u>Solar Energy Centre Denmark, Danish Technological Institute</u>

Søren Østergaard Jensen. M.Sc.
Miroslav Bosanac, M.Sc., Ph.d.
Hossein Gohari, B.Sc.
Lars Molnit, student (B.Sc.)
Trine Dalsgaard Jacobsen, M.Sc.
William Otto, laboratory technician

<u>Aidt Miljø A/S</u>

Hans Jørgen Christensen
Torkil Forman

List of content

1. Introduction

There has during the later years been an increasing interest in pre-heating of fresh air to buildings by means of solar air collectors. The reason for this is that pre-heating of fresh air with solar air collectors is a simple and cheap technology – specially if the building has or otherwise need a ventilation system as the price of the ventilation system and the cost of running the fans doesn't influence the economy of the solar air heating system.

Today solar air collectors are either small separate panels up to about 3 m² or site built if larger areas are required. Figure 1.1 shows an example of a small panel, which is very popular in Denmark – the solar air collector of the Summer House Package from Aidt Miljø A/S. The Summer House Packages which consists of a 1.28 m² solar air collector and a PV driven fan (PV panel of 0.3 m²) is mainly utilized for keeping summer cottages dry during the winter – a data sheet for the system may be found in Appendix A.

Figure 1.1.   Example of a small solar air collector – the collector of the Summer House Package.

If larger areas are desired the collector array either has to be built up of smaller panels, which are connected by often bulky and expensive ductworks as shown in figure 1.2 or special purpose site built – an example of such a collector is shown in figure 1.3.

However, in order to increase the utilization of solar air heating systems there is a need for development of solar air collectors, which are easy and cheap to connect into larger areas without loosing efficiency.

Figure 1.2.   Example of two hybrid solar air/liquid collectors (solar air collectors where liquid is circulated in the absorber) connected by means of ducts.

Figure 1.3.   150 m² roof space collector on an apartment block in the centre of Copenhagen.

1.1. The idea behind the project

In the IEA Task 19 project "Solar Air Systems" the efficiency of several commercial solar air collectors were measured (Fechner, 1999). Figure 1.4 shows the results of the performed tests.

One of the investigated solar air collectors was the solar air collector of the Summer House Package shown in figure 1.1. Although very simple this collector proved to be the second most efficient only surpassed by a very expensive German solar air collector.
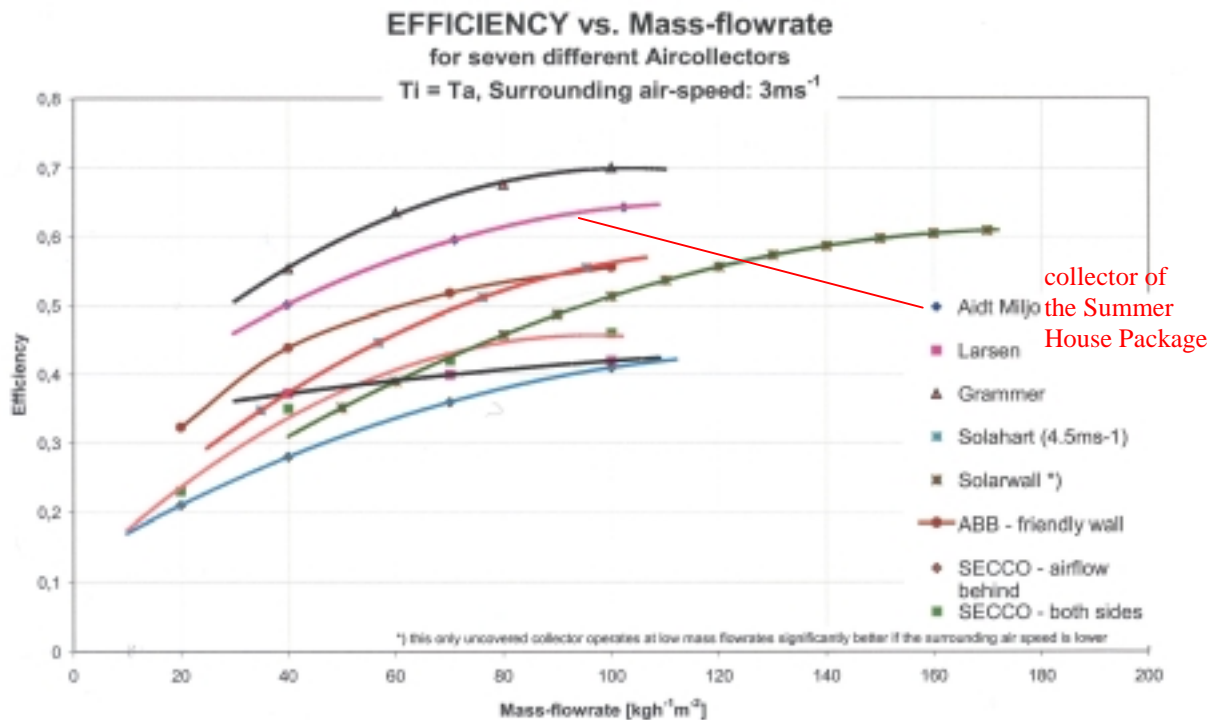

Figure 1.4.   The efficiency of 8 commercial solar air collectors (Fechner, 1999).

The reason for the high efficiency of the solar air collector of the Summer House Package is the applied matrix absorber in the form of a black 2 mm felt mat. In traditional solar air collectors the air is heated when passing along the absorber as shown in figure 1.5, while the air in a solar air collector with a matrix absorber is heated when passing through the absorber – also shown in figure 1.5. The main problem in solar air collectors is the often rather low heat transfer coefficient between the absorber and the air. The heat transfer coefficient in a matrix absorber is, however, much higher than when the air flows along the absorber. This leads to higher efficiencies for the matrix absorbers. The pressure loss across the matrix absorber may further ensure a more even air flow through the collector.

Due to the benefit of the matrix absorber and because Aidt Miljø already has experience regarding this type of absorber it was decided to apply this technology. Figures 1.6 and 1.7 show the principle behind the concept of connectable solar air collectors. From the figures it is seen that each collector has an air intake in the middle at the back (could also be at the front at one of the smaller sides in the cover for building integration where air cannot be taken from the backside of the collectors). The air is sucked into the air gap between the cover and the absorber making this the coldest spot of the collector, which again leads to a lower heat loss through the cover and thereby to a higher efficiency. The air passes through the absorber and enters an air gap below the absorber. The air cap behind the absorber acts as a manifold and as ductworks for the heated air from both the collector in question and for the collectors located before this collector. The main pressure drop should occur across the absorber in order to create an even air flow not only over the absorber in the collector in question but over all the

collectors in the array. The lowest pressure drop should occur in the air gap behind the absorber.
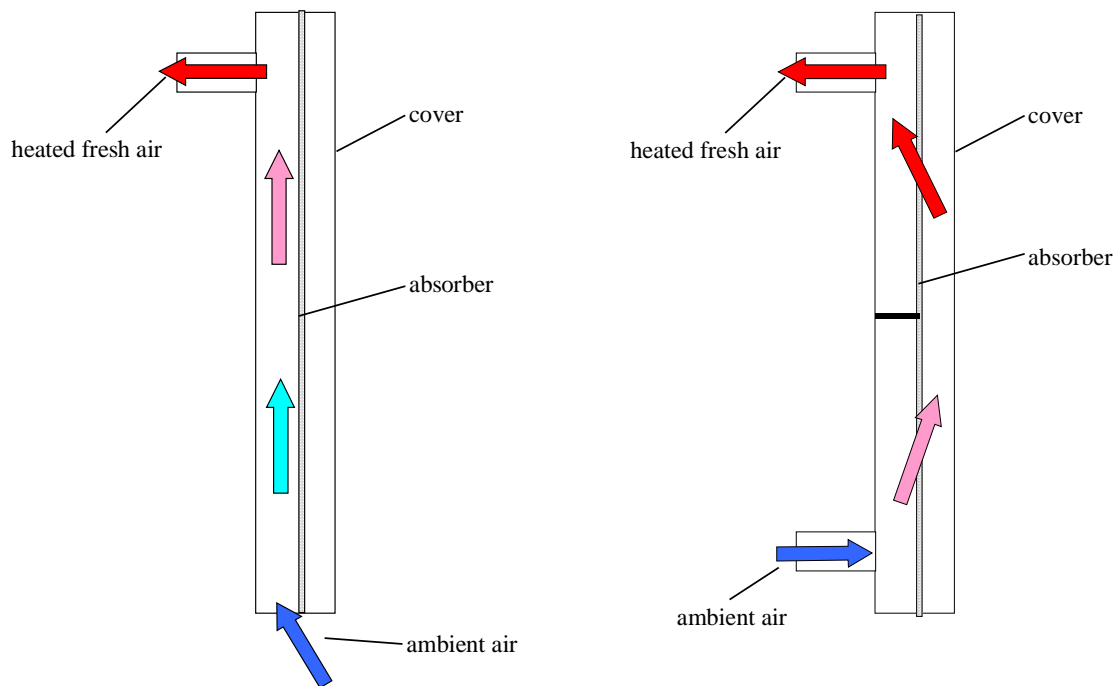

Figure 1.5. The principle in a traditional solar air collector (to the left) and in the solar air collector of the Summer House Package (to the right).
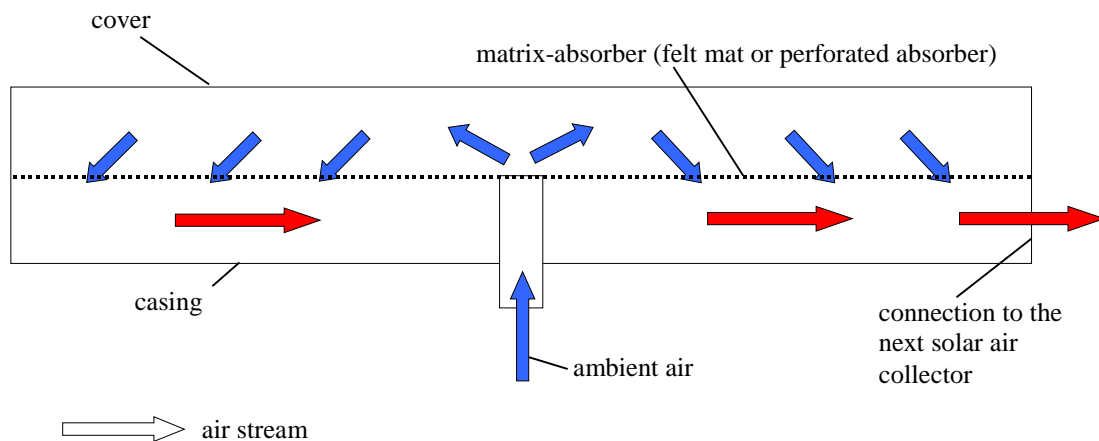

Figure 1.6. The principle of the connectable solar air collectors.
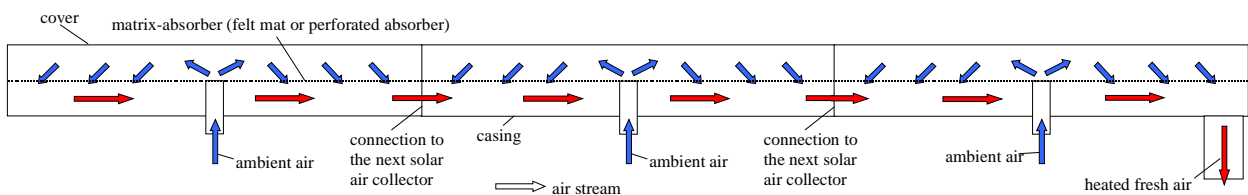
Figure 1.7. The principle of the connections between the connectable solar air collectors.

2. The investigated solar air collectors

Three solar air collectors have been investigated in the projects: one large solar air collector made of three connectable solar air collectors with a total transparent area of 9.22 m² and two single solar air collectors both with a transparent area of 2.98 m². The reason for the two small solar air collectors was to allow comparison of the efficiency of the large solar air collector with traditional sized solar air collectors. The two small solar air collectors further had two different absorbers as described below.

2.1. Absorbers

Originally it was the intention to manufacture the connectable solar air collectors with the same absorber as the solar air collector in the Summer House Package – i.e. a black felt mat/fibre cloth. However, it was decided instead to use a newly developed 0.8 mm perforated dark grey aluminium plate with a perforation of little under 1 %. Figure 2.1 shows a close up of such an absorber. The diameter of the holes is approximately 1.35 mm and the distance is 11 and 15 mm. The rigid metal absorber eases the construction of the connectable collectors.
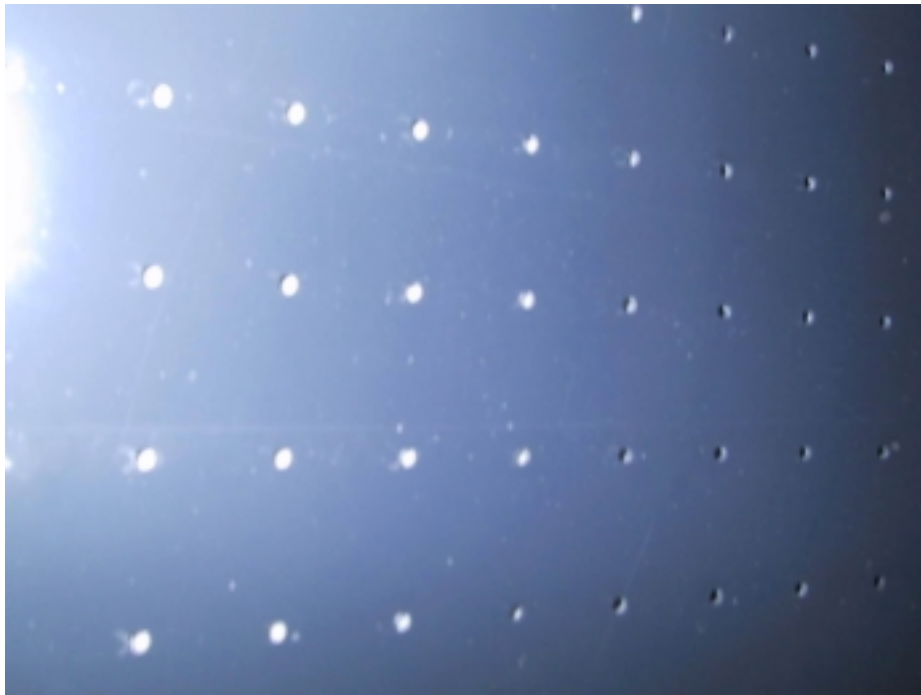
Figure 2.1.   The used absorber – a perforated metal plate.

A small investigation was conducted in order to determine the pressure drop of the perforated metal plate compared to the pressure drop across the fibre cloth.

The measuring of the pressure drop across the two absorbers was performed by the arrangement shown in figure 2.2. The arrangement consisted of a "funnel" with a well defined (although small) cross section of ø280 mm = 0.06158 m². The funnel was located at the end of a ø100 mm duct with a speed-controlled fan at the other end. The pressure drop across the absorber was measured by means of a calibrated micro manometer while the air speed and

thereby the air flow rate was measured by an calibrated air speed meter. Both instruments are shown in figure 2.2 and further described in section 3.2.7.
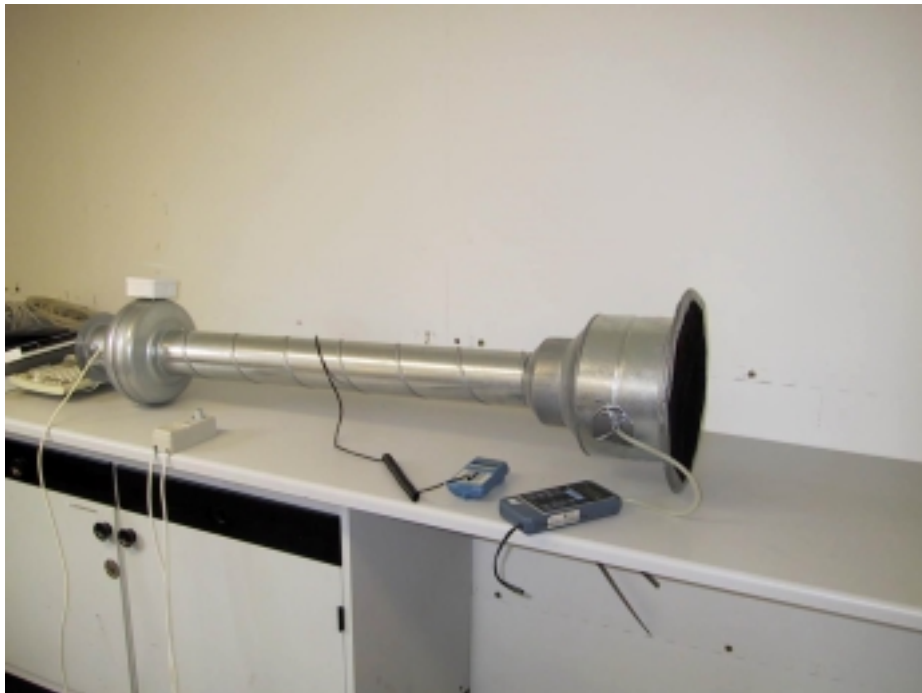
Figure 2.2.   The arrangement for measuring of the pressure drop across the absorbers.

Based on the measurements the dependency of the air flow rate on the pressure drop across the absorbers was found – see figure 2.3. The figure shows that the pressure drops increases more rapidly by increasing air flow rate for the perforated metal plate than for the fibre cloth. However, due to the rather small samples of the absorbers it was only possible to measure the pressure drop at high air flow rates – higher air flow rates than normally used in solar air collectors. The pressure drops are, therefore, shown at lower air flow rates in figure 2.4. The values in figure 2.4 are found by interpolation between 0 and the actual measured values.

Figure 2.4 shows that although higher pressure drops across the perforated metal plates at high air flow rates the pressure drop at flow rates normally used in solar air collectors is very similar for the two absorber types. It is, therefore, expected that the two absorber types will have almost the same ability to create an even air flow rate over the absorbers.

However, in order to determine if the performance of the two absorbers is identical as expected, the performance of the connectable collectors have been compared with the performance of two small collectors – a collector with each of the two absorbers.

The actual construction of the solar air collectors is described in the following section. The solar air collectors were all developed and manufactured by the solar collector manufacture Aidt Miljø A/S, which also manufacture the Summer House Package described earlier.

Pressure drop across matrix absorbers

Figure 2.3. The pressure drop across the absorbers dependent on the air flow rated per m² absorber.
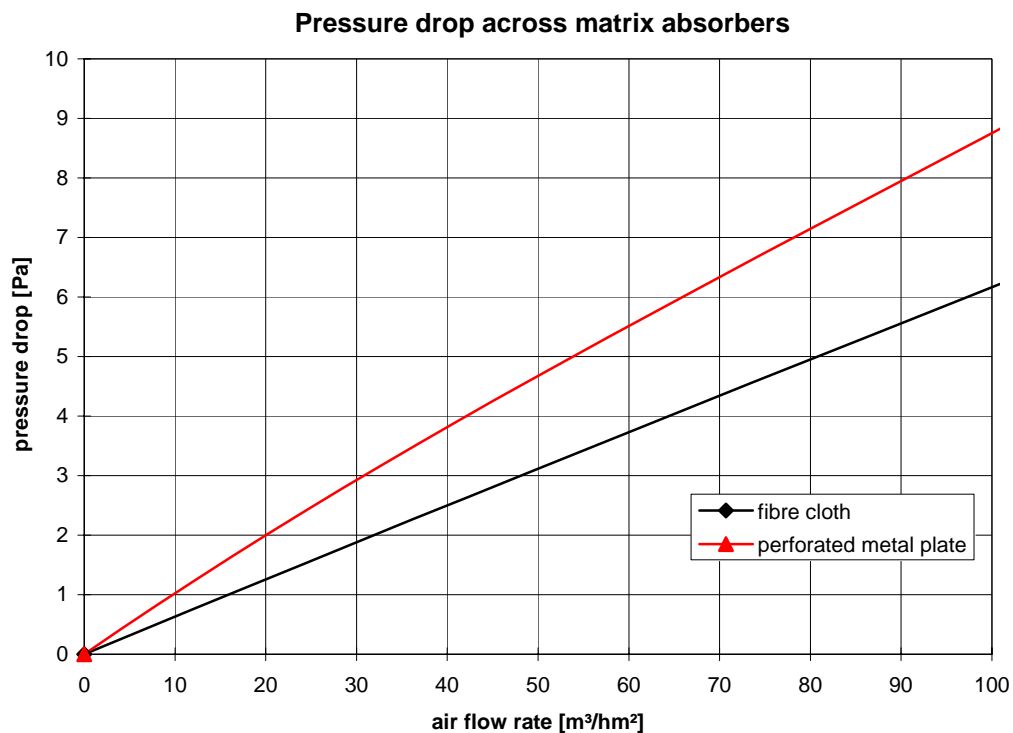
Pressure drop across matrix absorbers

Figure 2.4. The pressure drop across the absorbers dependent on the air flow rated per m² absorber found by interpolation between 0 and the measured values.

2.2. Description of the solar air collectors

The main features of the three tested solar air collectors are described in the following.

2.2.1. Description of the connectable solar air collectors

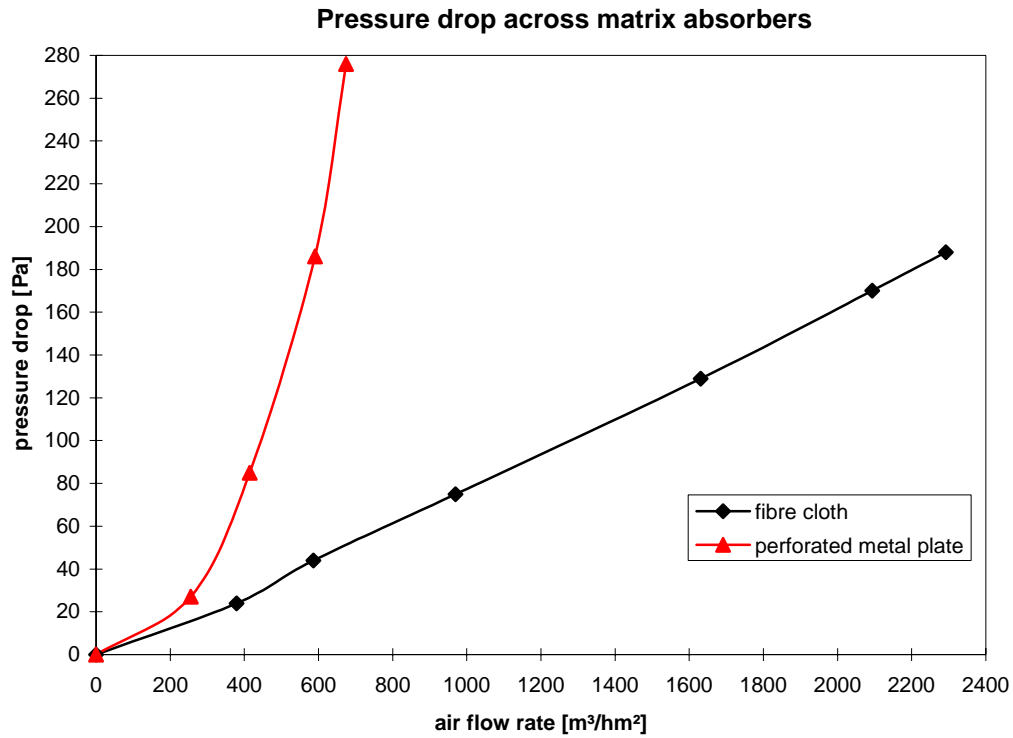The large collector with a transparent area of 9.22 m² is in principle built as shown figure 1.7 except that the air is not taken out directly from the last collector but via a small 0.28 m² manifold collector as seen later.

Figure 2.5 shows in more details the construction of the connectable collectors: The cover consists of double walled UV-stabilized ribbed polycarbonate with a thickness of 10 mm. The air gap between the cover and the absorber was 15 mm while the air gap below the absorber was 43 mm. The backside of the collectors was insulated with 20 mm mineral wool with a 3.5 mm wooden fibreboard facing the air gap and a 0.7 mm aluminium plate against exterior. The long sides of the collectors and one short side of the first collector were insulated with 7-8 mm foam insulation with a 3.5 mm wooden fibreboard on top. Figure 2.6 shows a view inside the air gap behind the absorber of one of the connectable solar air collectors. Please also refer to appendix B, which contains working drawings of the connectable solar air collectors, however, with some smaller differences between the drawings and the final collectors.

cover 10 mm

air gap 15 mm

absorber

air gap 43 mm

fibreboard 3.5 mm

insulation 20 mm

aluminium sheet
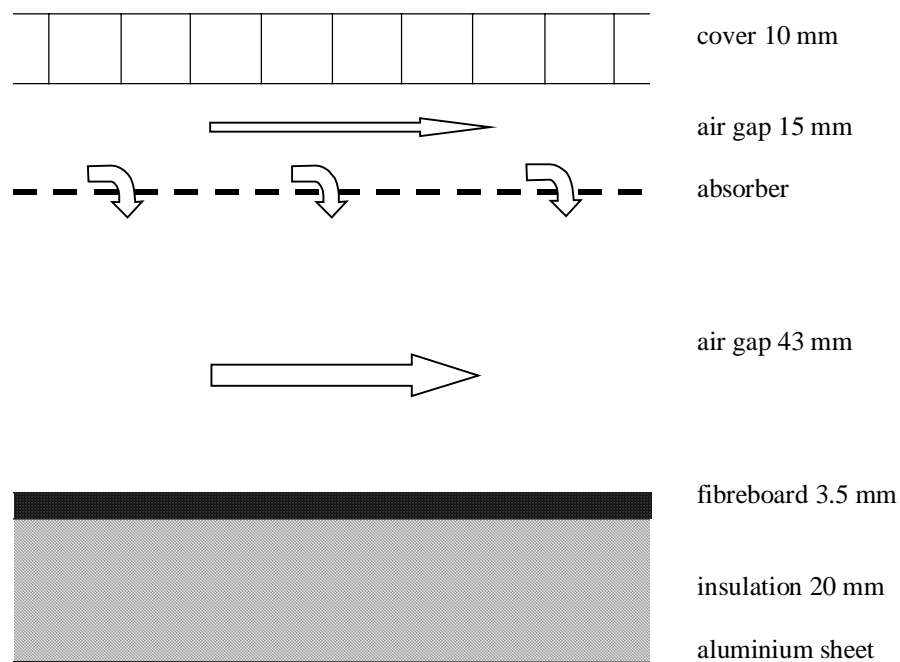
Figure 2.5.   The construction of the connectable solar air collectors.

The transparent area of each of the solar air collectors is 2.473 x 1.205 = 2.98 m². Figure 2.7 shows the first solar air collector mounted on the test rig. The test rig is orientated due south and has a tilt of 45°.

Figure 2.8 shows a close up of the connections between the solar air collectors. The collectors were developed with an easy connection system with aluminium profiles, which fits directly

into the folds of the casing profiles. Weather strips ensure the tightness of the connections. Figure 2.9 shows two of the connectable collectors mounted on the test rig.

perforated absorber

air intake

temperature sensor
(see later)
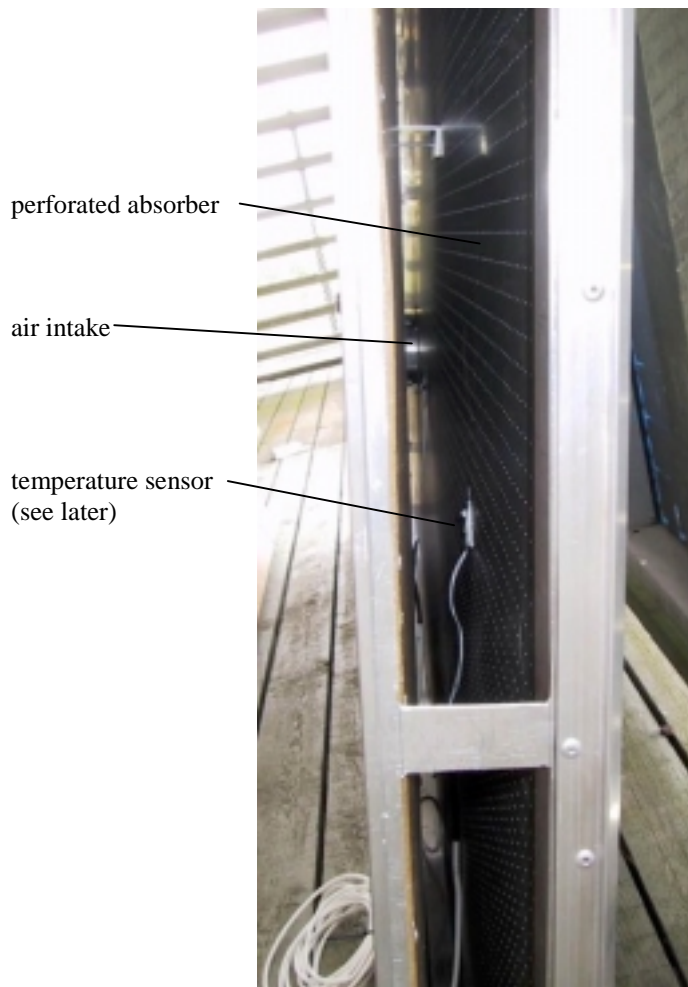
Figure 2.6.   View inside one of the connectable solar air collectors

The air intake to the solar air collectors was as shown in figures 1.6 and 2.6 via a duct through the backside. The ø125 mm duct was situated in the middle of the backside. Figure 2.10 shows a close up of one of the air intakes. Figure 2.10 shows the diffuser located between the inlet duct and the cover. The purpose of the diffuser was to turn the direction of the incoming air from being perpendicular to the cover to be along the cover. The aim was that the diffuser should create a lower pressure drop than if the direction of the air was turned by the air hitting the cover. Figure 2.11 shows the principle of the diffuser. The diffuser was fastened to the absorber by blind rivets. The diffusers were manufactured of the same material as the absorbers. In real life filters will be located in the air intakes in order to prevent insects and dust in getting into the solar air collectors. However, in order to facilitate the measurements on the solar air collectors these were not mounted in the investigated solar air collectors.

Figure 2.12 shows the small manifold collector to be connected to the end of the connectable solar air collectors. No perforated absorber was located in the manifold collector as shown in figure 2.12. The wooden fibreboard above the insulation acted here as absorber. The outlet was made of a ø200 mm duct. The aluminium profiles for the connection to the solar air collector is clearly shown to the right of the manifold collector.

Figure 2.7.   The first of the three connectable solar air collectors mounted on the test rig.
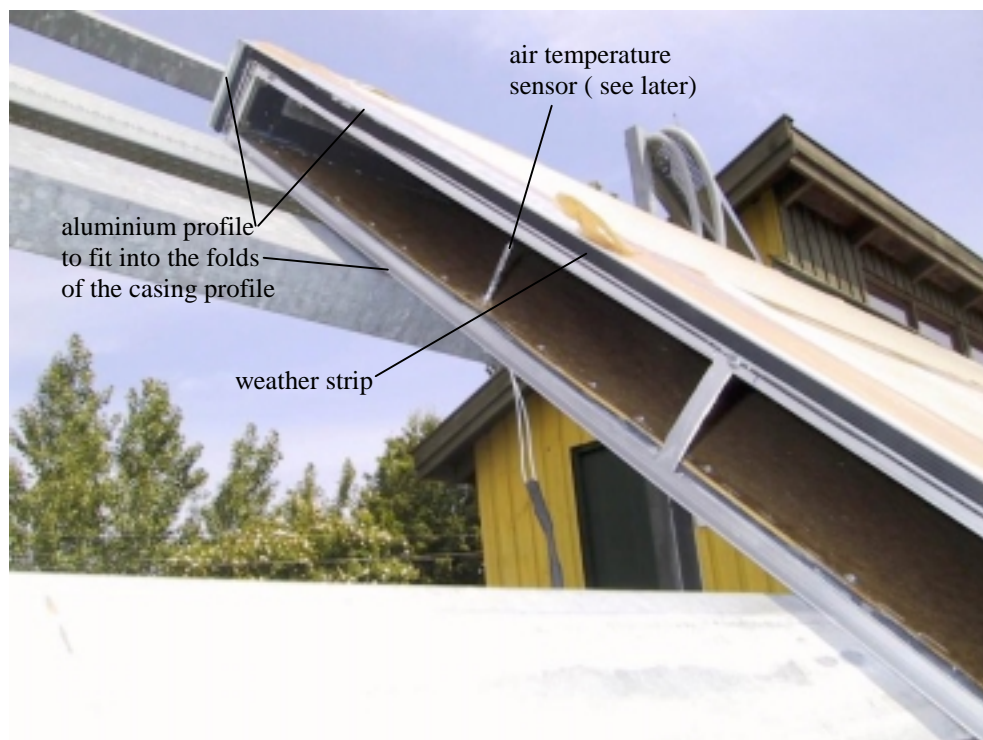
Figure 2.8.   Close up of the connection shown in figure 2.7.

Figure 2.9.   Two of the three connectable collectors mounted on the test rig.
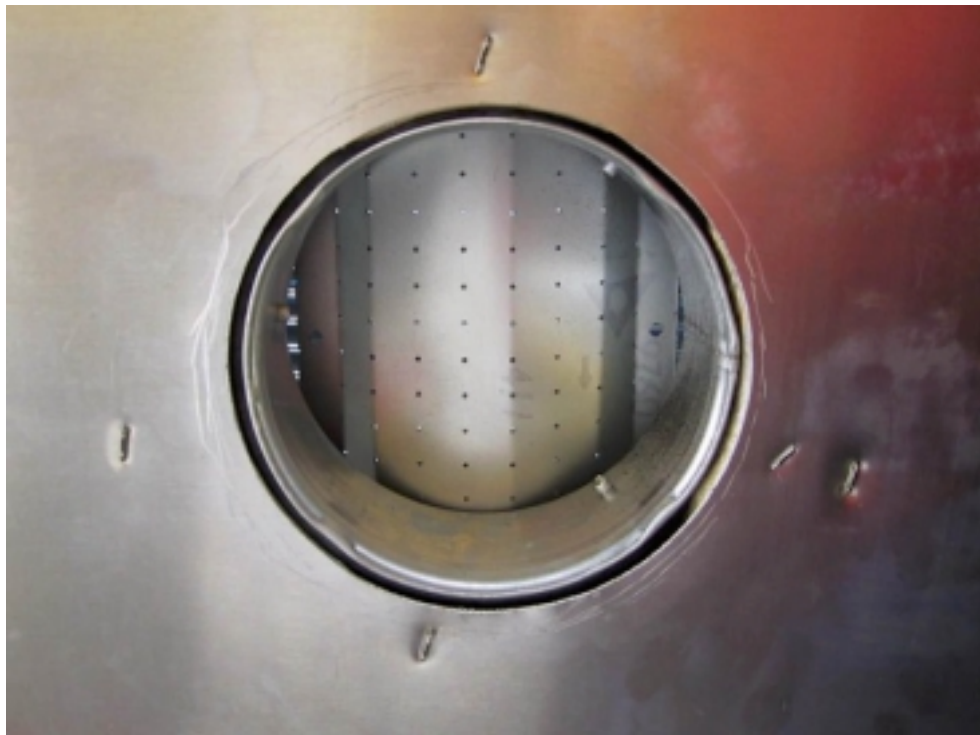
Figure 2.10. One of the air intakes of the connectable solar air collectors.
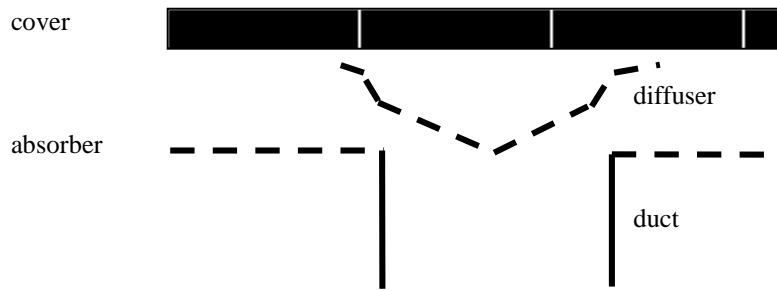
Figure 2.11. The principle of the diffuser at the air intakes.

aluminium profile to fit into the folds of the casing of the last connectable solar air collector

Figure 2.12. The manifold collector with the outlet duct.

Figure 2.13 shows the three collectors and the manifold collector mounted on the test rig together with the single collector also with a perforated metal absorber.

Figure 2.13. The 9.22 m² solar air collector consisting of three connectable collectors of each 2.98 m² and a manifold collector of 0.28 m². At the far back of the collector array is seen the single collector also with a perforated metal absorber.

2.2.2. Description of the single solar air collector with perforated metal absorber

The intention of the single solar air collector with perforated metal absorber was to compare the dependency of size and inlet arrangement on the efficiency of the solar air collectors. The single solar air collector is as already mentioned shown in figure 2.13. The size of the single solar air collector is identical to one of the connectable solar air collectors – i.e. 2.473 x 1.205 = 2.98 m². The main difference between the single and the connectable solar air collectors is the flow pattern within the solar air collectors. The flow pattern of the connectable solar air collectors is shown in figures 1.6-7, while the flow pattern of the single solar air collector is shown in figures 2.14. The distance between cover and absorber is 20-30 mm and the air gap behind the absorber is likewise 20-30 mm. The backside insulation has a thickness of 30 mm and the sides 7-8 mm.
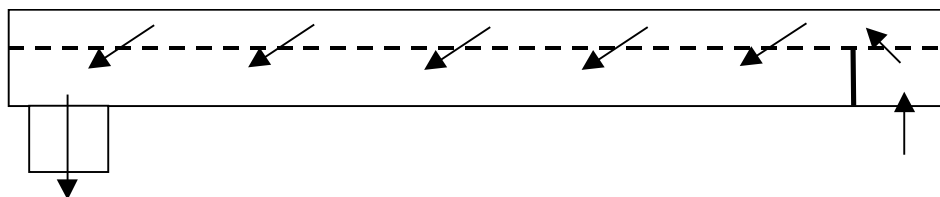
Figure 2.14. The flow pattern of the single solar air collector with perforated metal absorber.

In the single solar air collector the air passes the absorber twice as seen in figure 2.14. This very much help to even out the air flow over the entire solar air collector.

Instead of a central air intake in the connectable solar air collectors the air is in the single solar air collector with perforated metal absorber taken in at one of the short ends through 7 ø5.5 mm holes with insect net at the backside as shown in figure 2.15.

15

Figure 2.15. The middle and three top air intakes of the single solar air collector with perforated metal absorber.

2.2.3. Description of the single solar air collector with fibre cloth absorber

The single solar air collector with fibre cloth absorber is in principle identical to the single solar air collector with perforated metal absorber. The main difference being the absorber, which was a black fibre cloth as described in section 2.1. The distance between absorber and cover is here 15-25 mm and behind the absorber 20-30 mm. 30 mm insulation at the back and 7-8 mm on the sides. Another small difference is the location of the air intake at the back as shown in figure 2.16, which, however, is believed to have small if any influence on the performance of the collector as the air also here has to pass the absorber twice.

The intention of the single solar air collector with fibre cloth absorber is to compare the dependency of size, inlet arrangement and absorber material on the efficiency of the solar air collectors

Figure 2.17 shows the single solar air collector with fibre cloth absorber mounted on the roof of the laboratory of Solar Energy Centre Denmark, Danish Technological Institute. The orientation of the roof is due south with a tilt of 45°. The collector was actually part of another project as mentioned in the preface. The collector was connector to a DHW tank where the heat from the collector was transferred to the water via the surface of the tank – please refer to

(Jensen and Bosanac, 2002) for further details if interested. But as the projects were run in parallel the benefit of the present project was easy to enhanced by including measured data from the project with the fibre cloth absorber.
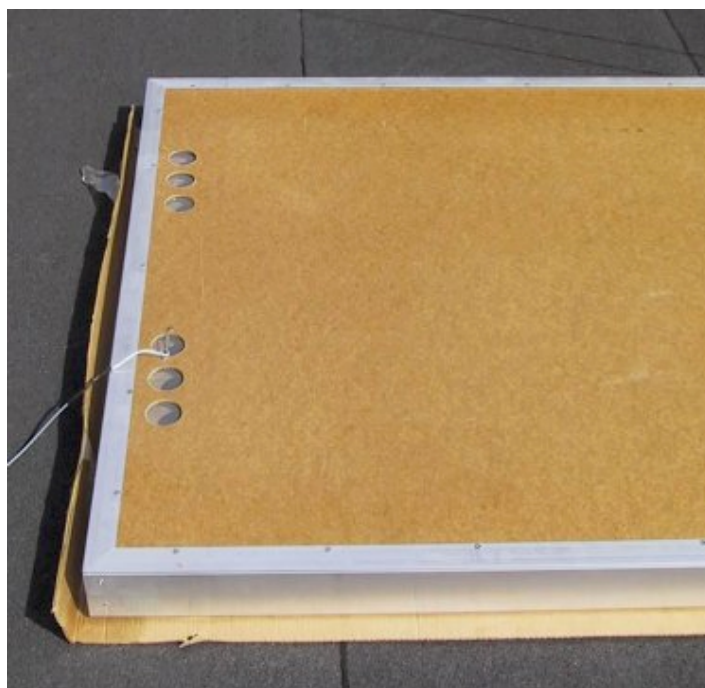
Figure 2.16. The air intake of the single solar air collector with fibre cloth absorber.

Figure 2.17. The single solar air collector with fibre cloth absorber mounted at the roof of the laboratory of Solar Energy Centre Denmark, Danish Technological Institute.

2.3. Air flows

In order to be able to determine the efficiency of the solar air collectors, the solar air collectors were connected to fans, which established the desired flow rate though the collectors. Figure 2.18 shows the fans connected to the connectable solar air collectors and the single solar air collector with perforated metal absorber. The fan connected to the connectable solar air collectors was a ø250 mm axial variable speed controlled fan while a similar, however, ø125 mm fan was connected to the single solar air collector with perforated metal absorber.

Figure 2.18. The fans for dragging air trough the connectable solar air collectors and the single solar air collector with perforated metal absorber. The different measuring features shown on the picture will be discussed in the following chapter.

The single solar air collector with fibre cloth collector was as explained earlier part of another project where the hot air was utilized for preheating domestic hot water. The aim of the system is to produce usable hot water temperatures – i.e. high temperatures from the solar air collector are desired. PV panels therefore, drove the fan. In this was the air flow rate was directly dependent on the solar irradiation – high air flow rates at high irradiation levels and low air flow rates at low irradiation levels. This leads to higher air temperatures from the collector at low irradiation levels, which is desired – the price is, however, a decrease in efficiency as shown in figure 1.4. The fan was a small DC 12 V/12 W axial fan. The fan is seen in figure 2.19. Figure 2.20 shows the PV panels for driving the fan. In order to investigate the influence of the max. air flow rate the fan was either connected to one PV panel (14 W_p) or two PV panels (24 W_p). The small DC fan could as seen later only create a small air flow rate – enough for the actual system though, but for this project a higher air flow rate was also desired. So at the end the DC fan was replaced with a fan similar to the fan applied on the single solar air collector with perforated metal absorber.
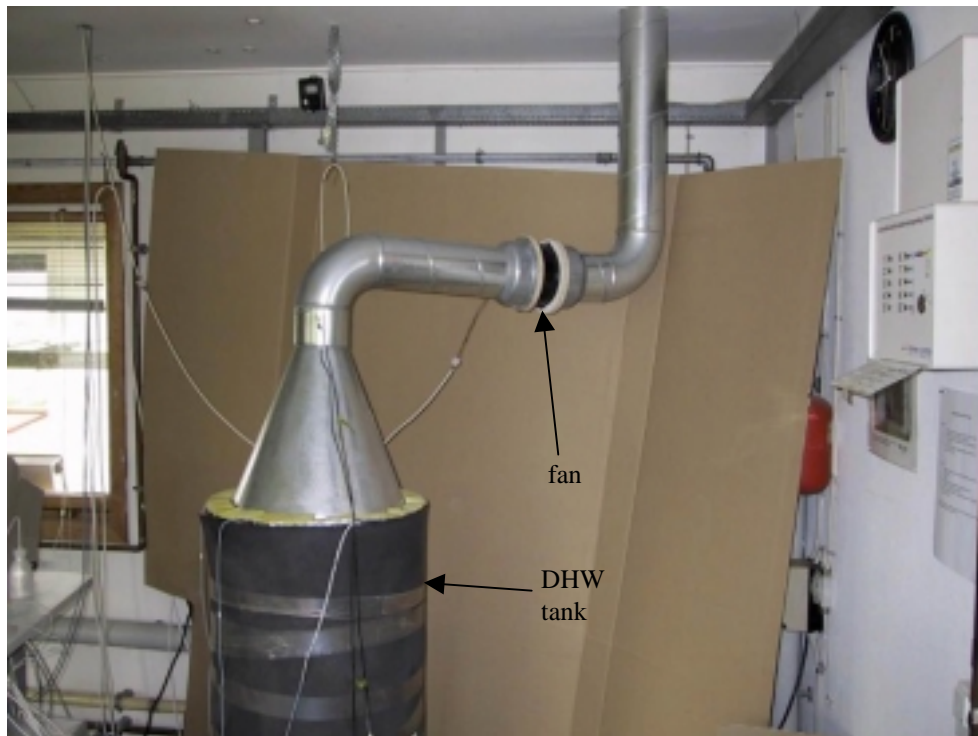
Figure 2.19. The fan connected to the single solar air collector with fibre cloth absorber.
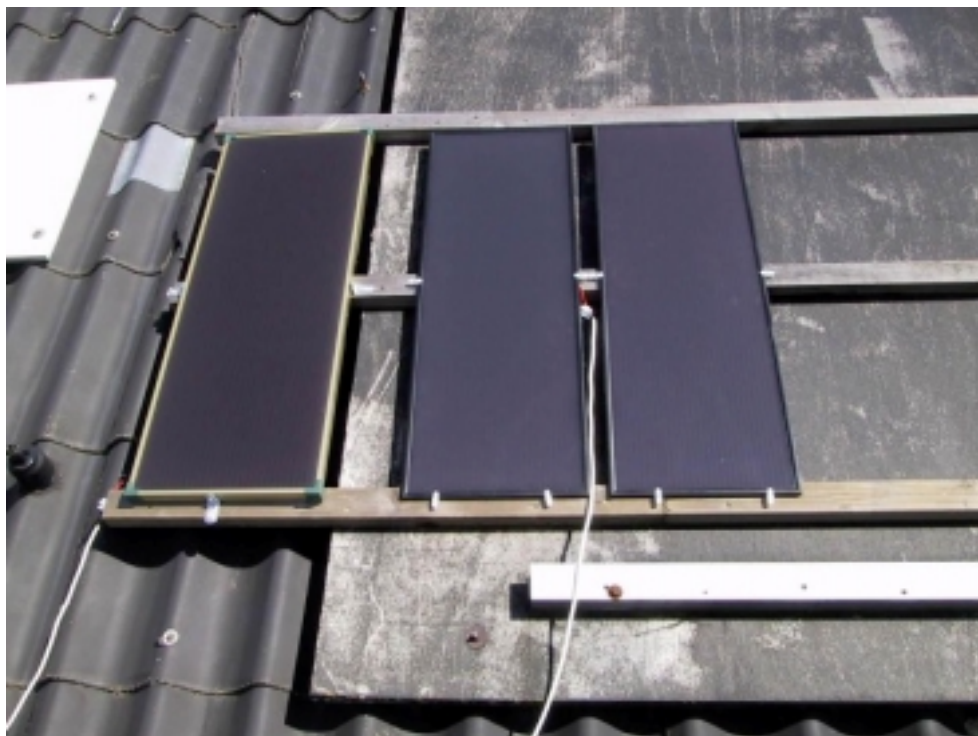
Figure 2.20. The PV panels for running the fan connected to the single solar air collector with fibre cloth absorber.

3. Measuring system

The aim of the project was to thermally characterise the above-described solar air collectors – especially to determine the efficiency of the collectors. In order to allow this it was necessary to design and run a comprehensive measuring system where all relevant parameters were measured with a sufficient accuracy. The measuring system will be described in the following.

As the two projects were run in parallel on the test area of Solar Energy Centre Denmark, Danish Technological Institute the two measuring systems were combined into one measuring system. However, only the sensors on the system with the single solar air collector with the fibre cloth absorber relevant to the present project will be discussed here.

3.1. Outline of the measuring system

Figures 3.1-3 shows the locations of the sensors connected to the solar air collectors. In addition the solar radiation on a plane parallel to the cover of the solar air collectors was measured.

● absorber temperature
● air temperature
◇ air speed

Figure 3.1.   The sensors connected to the connectable solar air collectors.

● air temperature
◇ air speed
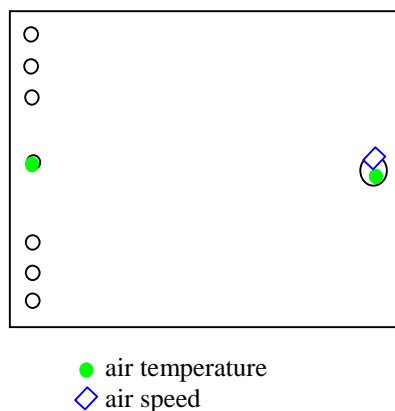
Figure 3.2.   The sensors connected to the single solar air collector with perforated metal absorber.

● air temperature
◇ air speed
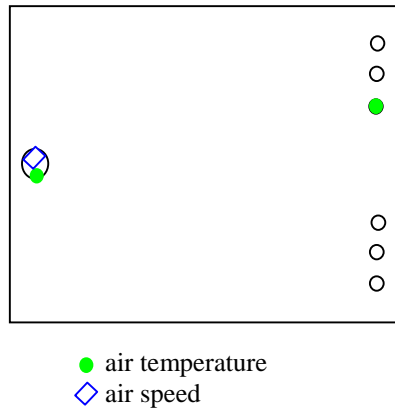
Figure 3.3. The sensors connected to the single solar air collector with fibre cloth absorber.

3.2. Sensors

The following sensors were applied in the measuring system.

3.2.1. Absorber temperature sensors

The six absorber temperatures in figure 3.1 were measured using PT100 class A sensors fastened to the back side of the absorbers with good thermal connection between the sensors and absorbers. The location of the sensors was as indicated in figure 3.1 either 300 mm from the inlet duct or 300 mm from the edge of the absorber. The intention with these sensors was to investigate the distribution of the air flow over the absorber. Poor distribution will give a large temperature difference between the two sensors on one absorber. The sensors were further used to illustrate any increase in absorber temperature between the first and last absorber. Figure 2.6 shows one of the absorber temperature sensors.

3.2.2. Air temperature sensors

The four air temperatures in figure 3.1 and two air temperatures in figures 3.2-3 were also measured using PT100 class A sensors. The intention of the temperature sensors in the inlet and outlet of the collectors was together with the air speed sensors to facilitate the calculation of the energy output from the collectors. Only one temperature sensor was located in one of the inlets (the middle inlet) to the connectable air collectors. The reason for this was that the distance between the inlets is only about 2.5 m. The temperature of the inlet air was, thus, identical for all three inlets. Figures 3.4-6 show the location of the inlet temperature sensors while figures 3.7-8 show the location of the outlet temperature sensors. The in and outlet temperature sensors where all expect the outlet temperature sensor for the connectable solar air collectors shielded from the sun due to the location behind an absorber or an inlet diffuser. However, as no absorber was present in the manifold collector it was necessary to shield the outlet temperature sensor from the sun by external shading as seen in figure 3.9. The area of this shading is 0.06 m² and has in the following evaluation of the measurements been subtracted the total area of the connectable solar air collectors so that the area for determination of the efficiency is 9.16 m² instead of 9.22 m².
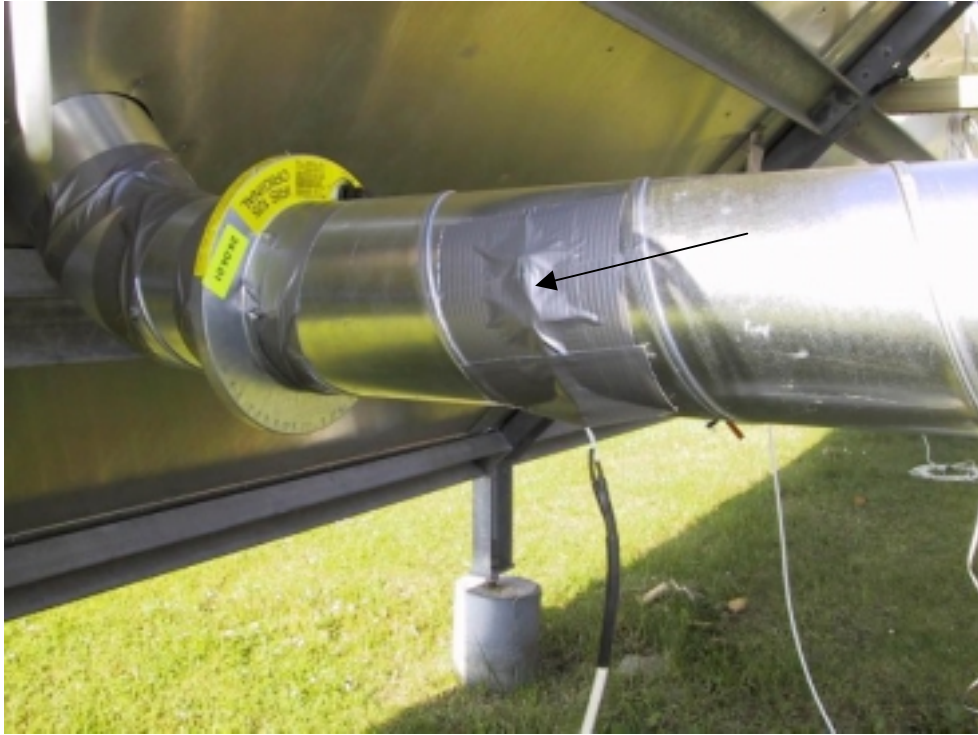
Figure 3.4.   Location of the inlet temperature sensor for the connectable solar air collectors.

Figure 3.5.   The inlet temperature sensor for the single solar air collector with perforated metal absorber.

Figure 3.6.   The inlet temperature sensor for the single solar air collector with fibre cloth absorber.
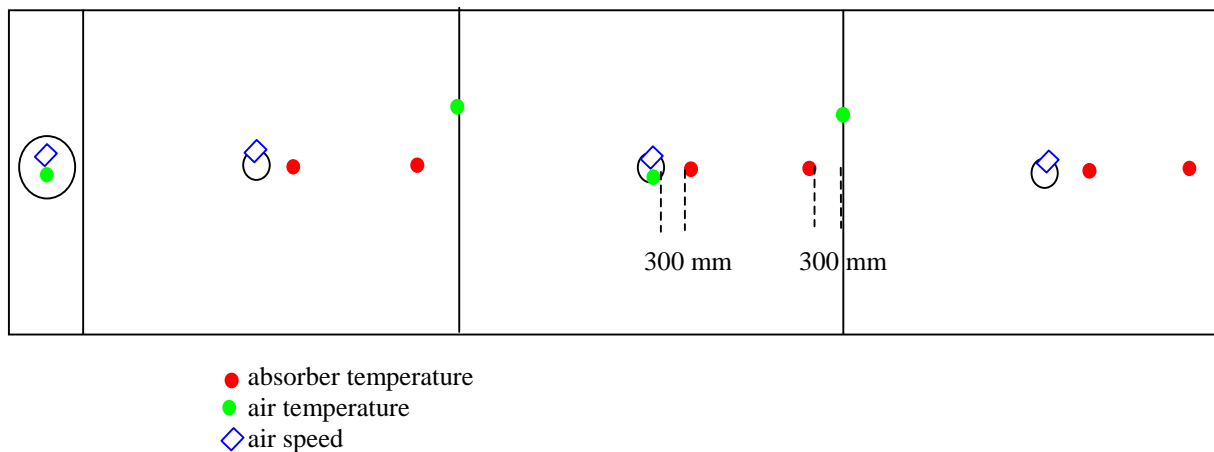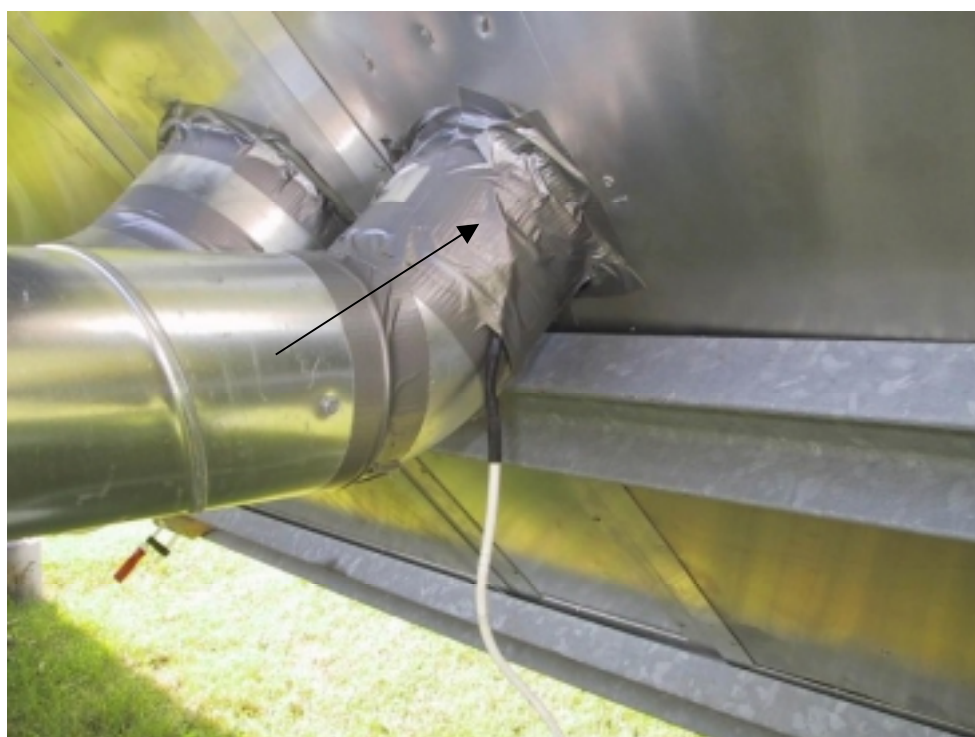

Figure 3.7.   Location of the outlet temperature sensor for the single solar air collector with perforated metal absorber – the location for the connectable solar air collectors was similar.

Figure 3.8.   Location of the outlet temperature sensor for the single solar air collector with fibre cloth absorber.
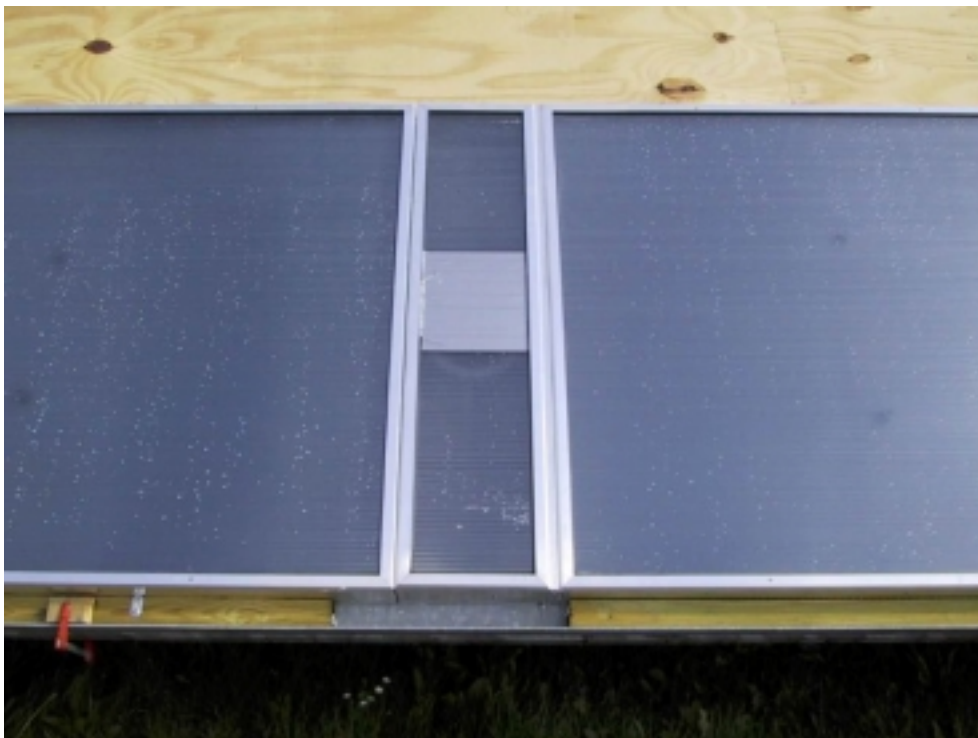
Figure 3.9.   External shading of the outlet temperature sensor for the connectable solar air collectors.

Two further air temperature sensors were located in the connections between the three connectable solar air collectors. These two sensors were also measured using PT100 class A sensors. The intention with these sensors together with the outlet sensor of the connectable solar air collectors was to determine the temperature increase of the air flowing behind the absorbers of the collectors. Figure 3.10 shows one of these sensors. One sensor is also shown in figure 2.8.

Figure 3.10. One of the two air temperature sensors in the connection between the connectable solar air collectors in the air stream behind the absorbers.

3.2.3. Air speed sensors

The air speed from all of the collectors were measured using calibrated Envic air speed sensors type AFT-10. Figure 3.11 shows an example of an Envic AFT-10 sensor mounted in the outlet of the connectable solar air collectors. The air speed sensors were all calibrated on location as also seen in figure 3.11. The air speed sensors were calibrated by comparing the reading at different air speeds with the readings from a calibrated air speed sensor by which the air speed in the ducts was measured in a well-defined net as seen in figure 3.12.

The air speed at the inlets to the connectable solar air collectors were measured by means of calibrated VentCaptor air speed sensors. An example of a VentCaptor mounted in the inlet is shown in figure 3.13. These three air speed sensors were calibrated on location in the same way as the Envic AFT-10 air speed sensors. The VentCaptors were mounted in a 1100 mm long ducts with smooth inlets in order to create a fully developed and stable air flow before the air speed sensors as seen both in figure 2.18 and figure 3.13.

The aim of the connectable solar air collectors is to create an even air flow over each of the three absorbers – i.e. an identical air flow through each of the three air intakes. In order to be able to correct for any unbalance in the air flows in the three air intakes an iris diaphragm was installed in each air intake as shown in figures 3.13-14.

Figure 3.11. Envic AFT-10 air speed sensor and set-up for calibration of the air speed sensor.

ø125 mm

ø250 mm
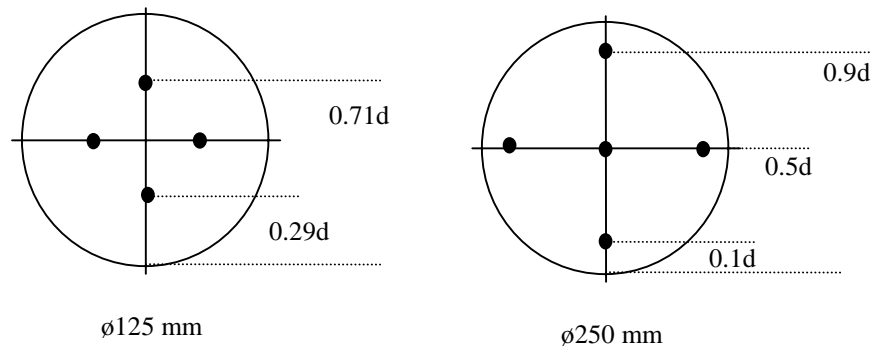
Figure 3.12. Measuring net for determination of the mean air speed in a duct for calibration purposes.

3.2.4. Pyranometers

The solar radiation on the solar air collectors was measured in two different ways: a simple way by measuring the total radiation using a PV pyranometer and in a detailed way by measuring both total and diffuse radiation using more precise instruments. The PV pyranometer was a type 80SP from SolData (see figure 3.15) while the pyranometers for the detailed measuring of solar radiation were for total radiation an Epply pyranometer type PSP and for diffuse radiation a Kipp&Zonen CM11 with shading ring. The latter two instruments are part of the certified test rig for determination of the efficiency of solar liquid collectors. This test rig with the pyranometers is shown in figure 3.16. All applied pyranometers were calibrated instruments. The orientation and tilt of the pyranometers were identical to the orientation and tilt of the solar air collectors.

26

Figure 3.13. Example of an VentCaptor air speed sensor in the air intake of one of the connectable solar air collectors.

Figure 3.14. An iris diaphragm was installed in each air intake of the connectable solar air collectors for balancing the air flows to the three solar air collectors.

Figure 3.15. The applied PV pyranometer mounted above of the connectable solar air collectors.
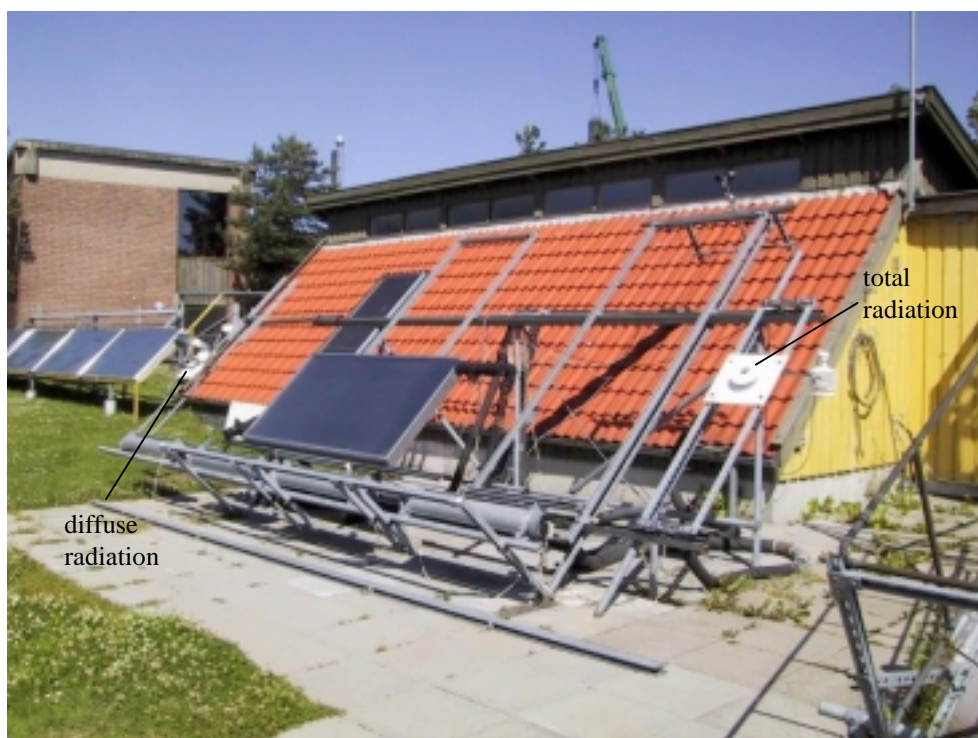
Figure 3.16. The test rig for determination of the efficiency of solar liquid collectors with the applied pyranometers.

The reason for applying two different ways of measuring the solar radiation on the solar air collectors was to test two different ways of determination of the efficiency of the solar air collectors: a simple easy way and a detailed way using statistical identification as seen later.

3.2.5. Data collection

All sensors were connected to a data logger system with modules from Analog Devices. Each sensor were scanned each 5th second and averaged into one or five minutes mean values and stored on the hard disk of a PC.

The PC controlled via the software Labview 5.0 the data logger system. Spot values of the sensor readings together with curves showing several hours of measurements for some values were continuously shown on the screen of the PC.

3.2.6. Treatment of measured data

Using the data logger system/PC the measured values were either directly translated into physical understandable values like temperatures and solar radiation while the air flow rates through the collectors were found using the equations found as a result of the calibration of the air speed sensors. Both raw data and calculated values were stored on the hard disk of the PC. The thermal performance of the solar air collectors was later evaluated in the form of energy output and efficiency of the solar air collectors.

3.2.7. Other sensors

The above sections describe the sensors applied in the data logger system. However, a couple of hand held sensors were used for spot measuring. One of the sensors was the already mentioned calibrated air speed sensor for calibration of the air speed sensors of the data logger system. The instrument was a Velocicheck Model 8330 from TSI. This instrument was also applied together with a calibrated measuring funnel for spot measuring of the air flows to the connectable solar air collectors.

The other applied sensor was a calibrated micro manometer for determination of the pressure drop across the solar air collectors. The sensor was an Airflow-PVM100 micro manometer.

3.2.8. Other matters

When comparing figures 3.9 and 3.15 with 2.18 it is seen that fibreboard were located above the connectable solar air collectors and the single solar air collector with perforated metal absorber after the installation of the solar air collectors. The fibreboard ensured that no solar radiation hits the inlet ducts to the connectable solar air collectors. If solar radiation was allowed to hit the inlet ducts part of the air to the collectors would be heated by the sun leading to an undesirable uncertainty in the measuring of the inlet temperature of the air to the collectors.

4. Measurements

The aim of the measurements was to allow for a thermal characterization of the solar air collectors – especially to determine the efficiency of the collectors. The measuring campaign was started with pressure loss measurements by end June-beginning July 2001. The data logger system was started in the beginning of July 2001 with an initialization phase. Real measurements started by mid July 2001 and lasted to the end of October 2001.

The first section of the chapter deals with the performed measurements of pressure losses, balancing of the air flow in the inlets to the connectable solar air collectors and leakage of the connectable solar air collectors. The second section shows graphs of the obtained measurements and some calculated values including the efficiency of the solar air collectors over the day. A more thorough evaluation of the efficiency of the solar air collectors will be given in the following chapter.

4.1. Pressure losses and leakage

The intention was as mentioned earlier to obtain almost identical air flow through the absorber of each of the three connectable solar air collectors. For obtaining this an iris diaphragm was installed in each inlet for balancing the air flows.

4.1.1. Balancing of the air flows

Firstly the pressure loss over the inlets and the total collector was measured with fully open iris diaphragms. Figure 4.1 shows where the pressure losses were measured: over the inlet arrangements for measuring the inlet air flows (for the connectable collectors) and over the entire collector incl. inlet arrangements for both the connectable and single collector with metal absorber. Figure 4.2 shows the numbering of the inlets used in figure 4.3.
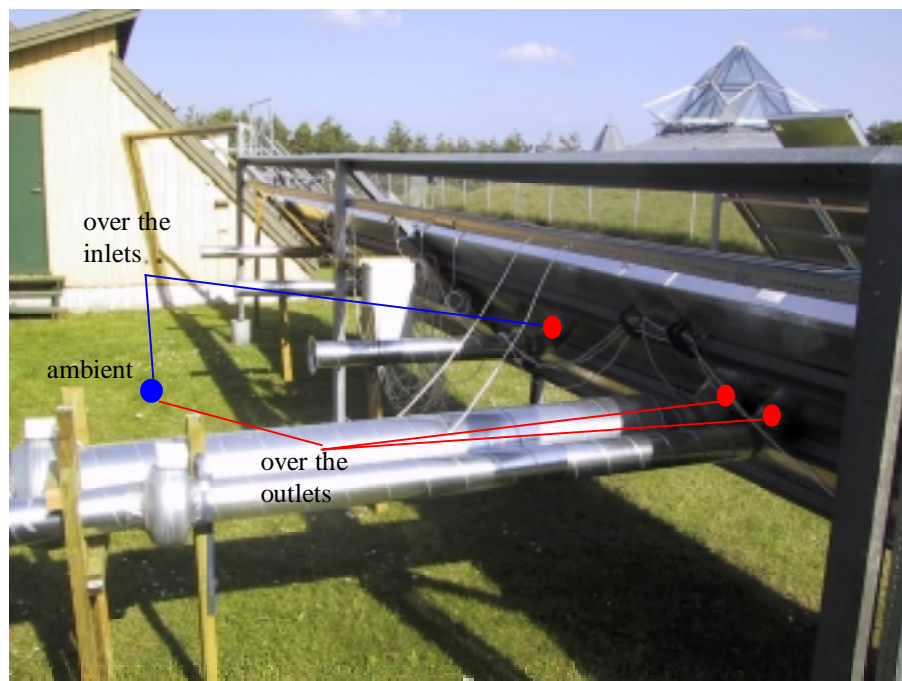
Figure 4.1.   The location of the measured pressure losses.
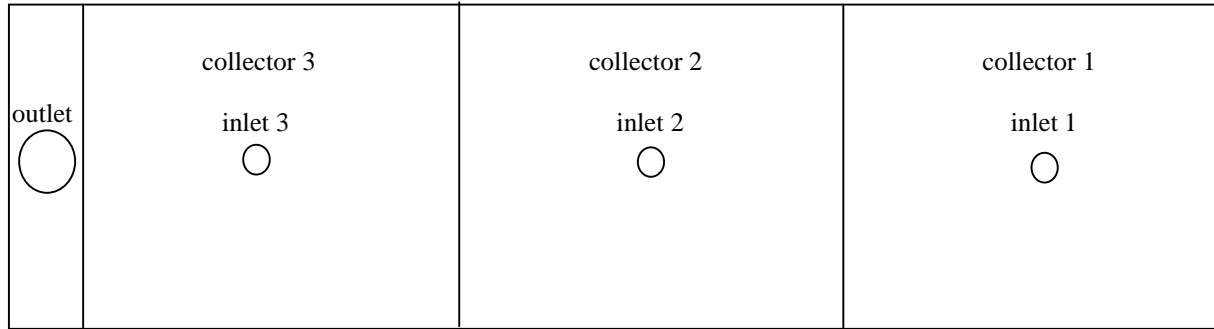
Figure 4.2.   Numbering of the inlets of the connectable solar air collectors.

Figure 4.3. shows the measured pressure drop across the inlet arrangements and the total collector incl. inlet arrangements of the connectable solar air collectors. The pressure drops are shown as a function of the normalized air flow rate through the collector.
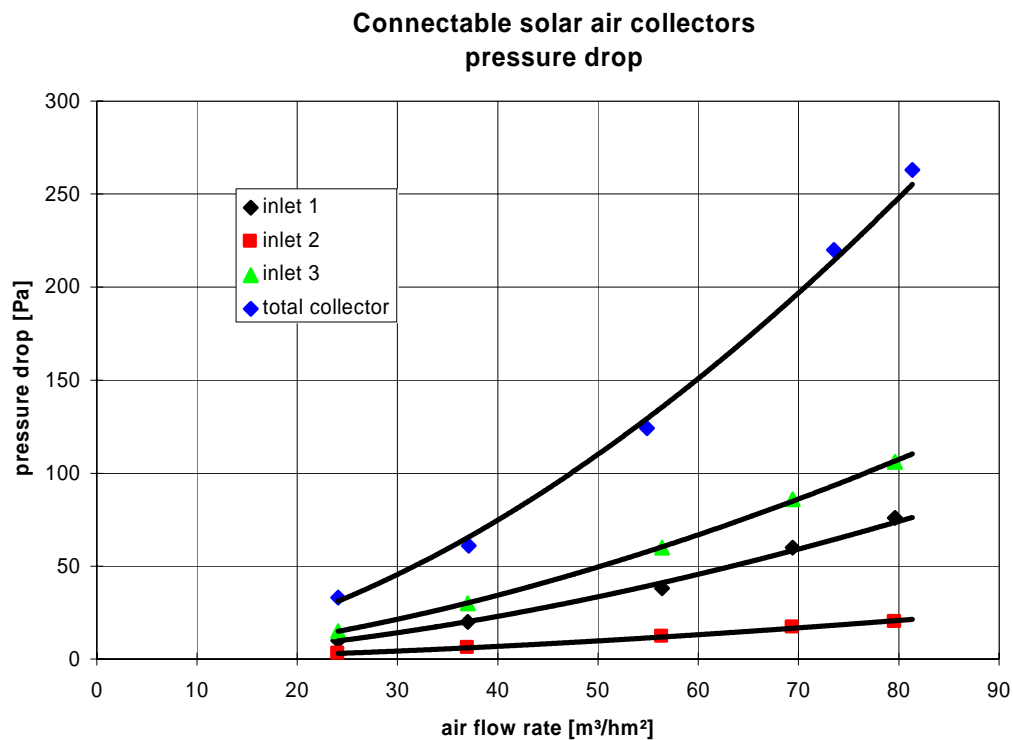
Figure 4.3.   The pressure drop across the inlet arrangements and the total collector incl. inlet arrangements of the connectable solar air collectors.

The inlet arrangements are identical for the three connectable solar air collectors. The difference in pressure drop is due to the fact, that the air flow rate was not identical for the three inlets as seen in figure 4.4, where the mass flow rate through each inlet is shown dependent on the total mass flow rate through the total solar air collector. When comparing figures 4.3 and 4.4 it is seen that the lowest pressure drop over the inlets occurs for the inlet with the lowest mass flow rate. Figure 4.4 shows that the mass flow rate through inlet 1 and 3 is almost identical, while the mass flow rate through inlet 2 is somewhat lower.

**Connectable solar air collectors
unbalance in the inlet air mass flows**
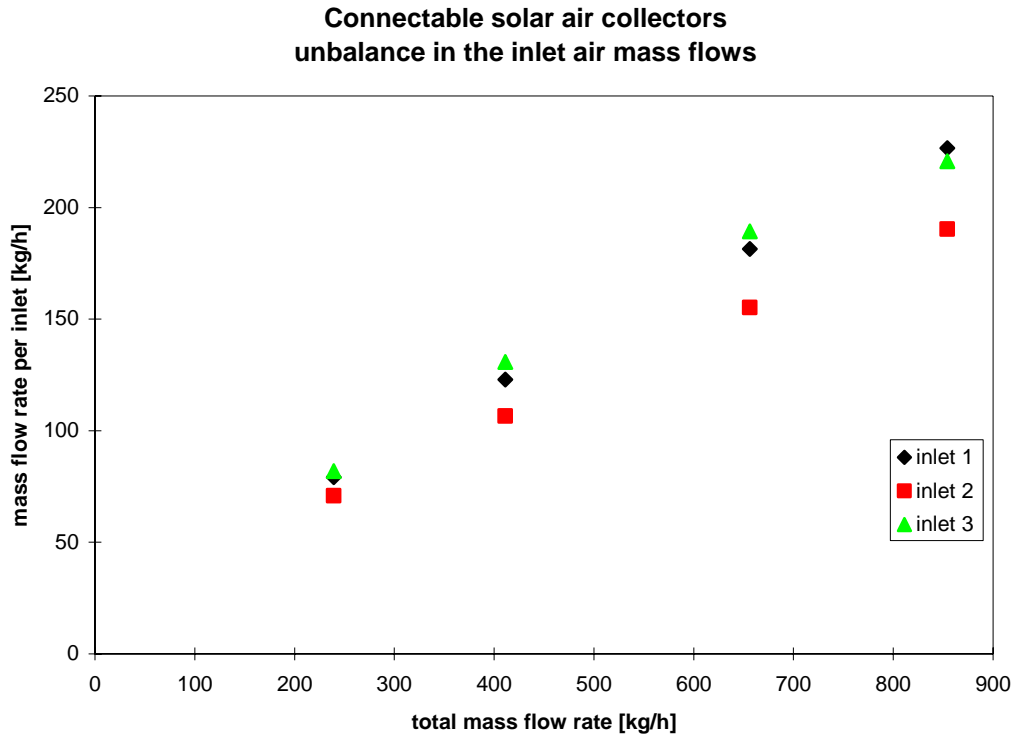
Figure 4.4. The mass flow rates of each inlet dependent on the total mass flow rate through the connectable solar air collectors.

If the main pressure loss appeared in the "manifold" air gap behind the absorbers, the mass flow rate at the inlets to the connectable solar air collectors should increase when going from inlet 1 towards inlet 3. However, the mass flow rate through inlet 1 and 3 is almost identical. This indicates that the main pressure drop occurs at the inlet diffuser (see figure 2.11) as the pressure drop across the absorbers have to be more or less identical and far lees than the pressure drop over the total solar air collector (compare figure 4.3 with figure 2.4). The pressure drop behind the absorber is small due to the rather large air gap – figure 2.5. The pressure drop at the outlet does due to the location not influence the balancing of the air flows through the inlets. The unbalance of the air flows through the inlets must, therefore, be due to the difference in the pressure drop at the diffusers – which seems very likely, as the diffusers were handmade in this test version of the connectable solar air collectors and, therefore, very likely rather different.

The iris diaphragms were operated in order to obtain an equal air flow rate through the three inlets to the connectable solar air collectors. Figures 4.5-6 show measured pressure drops over the connectable solar air collectors incl. inlet arrangements as a function of both the air and mass flow rates including regression lines and equations. The figures show that the balancing of the air flows as expected increases the pressure drop across the total collector incl. inlet arrangement.

Connectable solar air collectors pressure drop

$y = 0.0745x^{1.9217}$
$R^2 = 0.9977$

$y = 0.1273x^{1.7285}$
$R^2 = 0.996$

♦ before balancing
■ after balancing

pressure drop [Pa]

air flow rate [m³/hm²]

Figure 4.5. The pressure drop across the connectable solar air collectors incl. inlet arrangements dependent on the normalized air flow rate.

Connectable solar air collectors pressure drop

$y = 0.0727x^{1.8672}$
$R^2 = 0.9969$

$y = 0.094x^{1.7259}$
$R^2 = 0.996$

♦ before balancing
■ after balancing

pressure drop [Pa]

mass flow rate [kg/hm²]
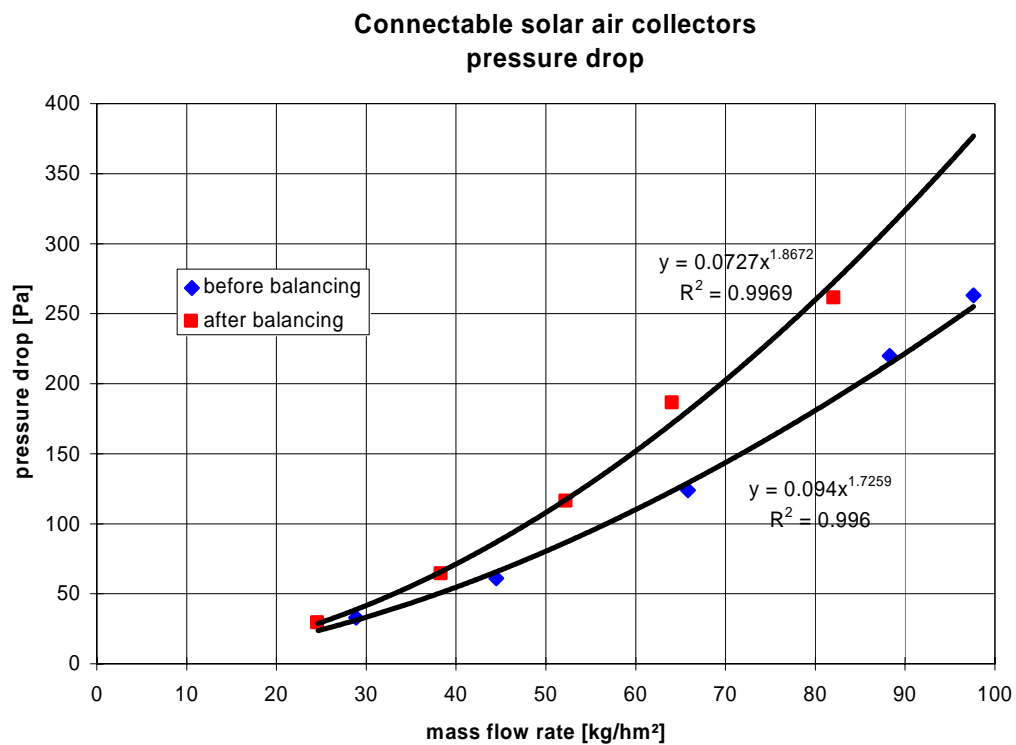
Figure 4.6. The pressure drop across the connectable solar air collectors incl. inlet arrangements dependent on the normalized mass flow rate.

4.1.2. Pressure drop across the solar air collectors

Figure 4.7 shows the measured total pressure drop across the three solar air collectors: connectable solar air collectors, single solar air collector with metal absorber and single solar air collector with fibre cloth absorber. Regression lines and equations are also included in the figure.

Solar air collectors pressure drop
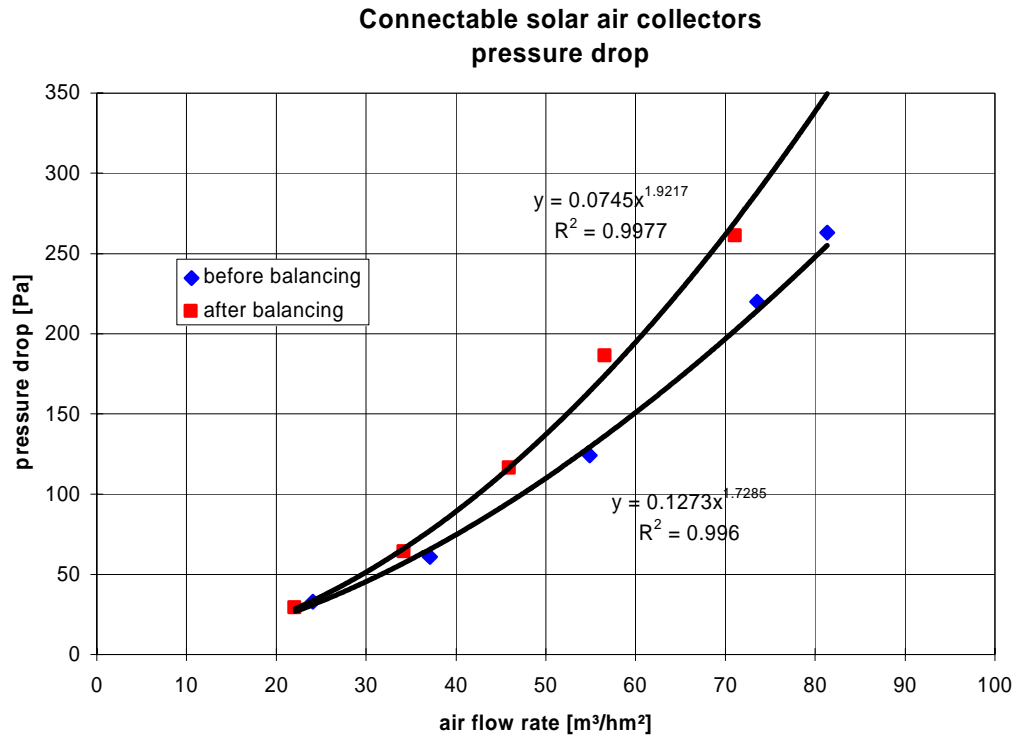

$$y = 0.0745x^{1.9217}$$
$$R^2 = 0.9977$$

$$y = 0.0073x^2 + 1.0712x$$
$$R^2 = 0.9748$$

$$y = 0.0453x^{1.7401}$$
$$R^2 = 0.9992$$

- connectable collectors
- single collector
- fibre collector
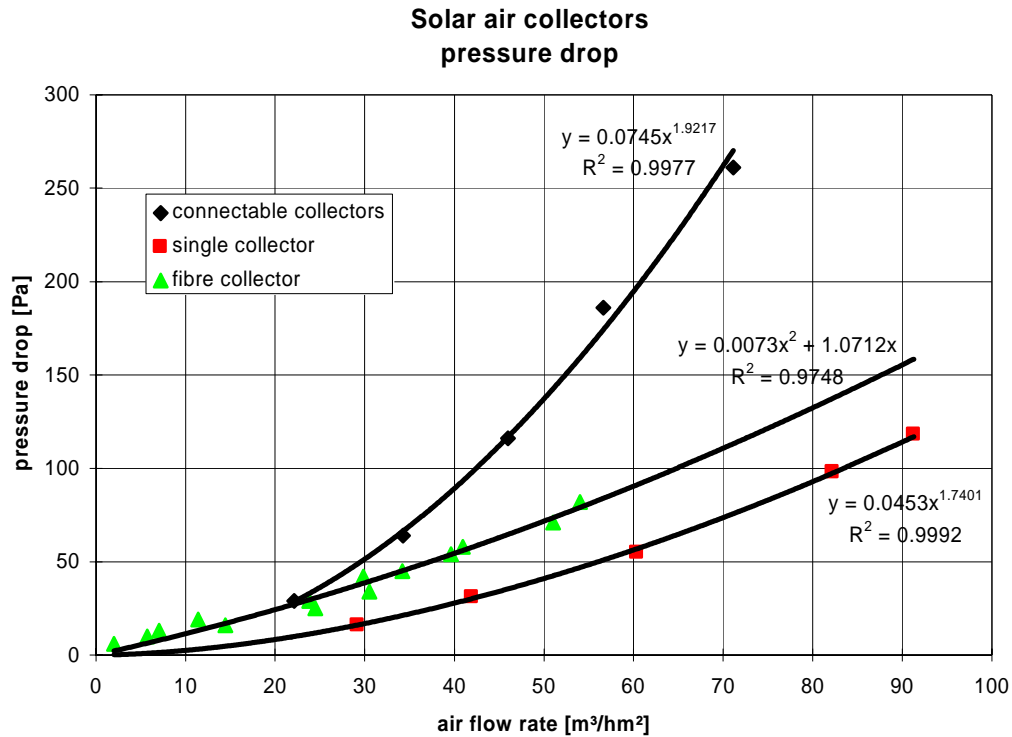
Figure 4.7.   The measured total pressure drop across the three different types of solar air collectors.

Figure 4.7 shows that although very similar with regard to construction the pressure drops for the two single solar air collectors are rather different. As the pressure drop across the fibre cloth is lower than across the perforated metal plate (see figure 2.4) it was expected that the pressure drop across the solar air collector with fibre cloth absorber would be lower than across the single solar air collector with metal absorber. The reason for the opposite may be the location of the two solar air collectors. The solar air collector with fibre cloth absorber is mounted directly on top of roof plates as seen in figure 2.17. This creates an extra pressure drop, while the inlet to the single solar air collector with metal absorber is freely exposes as seen in figure 2.15.

The pressure drop across the collectable solar air collectors is at flow rates above 50 m³/hm² far higher than across the two single absorbers. However, the pressure drop of the inlet arrangements is included in the curve in figure 4.7 for the collectable solar air collectors. Figure 4.3 suggests that the pressure drop across the inlet arrangements accounts for about one third of the total pressure drop shown in figure 4.7 for the connectable solar air collectors. However, no filter was included in the inlet to the connectable solar air collectors when obtaining the values in 4.7. Dependent on the type of filter, these will introduce a pressure drop. As the air in the connectable solar air collectors is blow directly into the space between the cover and

absorber, the filter should be more fine-meshed than in the single solar air collectors – actually a dust filter rather than only an insect net. The reason for this is that the first part of the absorber acts as a filter in the single solar air collectors and the first part of the air gab behind the absorber further acts as a dust catcher due to the very low air speed here – see figure 2.14. In the connectable solar air collectors the dust is blow directly into the space between the cover and absorber. The absorber will, therefore, rather quickly get dirty. The thermal performance is, however, not expected to change very much (unless a rather thick layer of dust is being build up) but the appearance will.

Figure 4.8 shows the pressure drop dependent on the mass flow rate for several of the solar air collectors investigated in IEA Task 19 (Fechner, 1999) – for four of the collectors shown in figure 1.4. Figure 4.7 and 4.8 are not directly comparable due to different units on the x-axis: air flow rate in figure 4.7 and mass flow rate in figure 4.8. However, figure 4.6 gives the pressure drop for the connectable solar air collectors based on mass flow rate. For the two single collectors the values on the x-axis in figure 4.7 should be multiplied with 1.2 to allow comparison between figures 4.7 and 4.8 as the air flow rate here were measured at an air temperature of approx. 20°C – i.e. 50 m³/hm² for the single collectors relate to approx. 60 kg/hm². So when comparing 4.6-8 it is seen that the pressure loss across the here investigated solar air collectors is higher than for the solar air collectors in IEA Task 19 expect the pressure drop across the single solar air collector with metal absorber which is rather similar to the pressure drop for the collector of the Summer House Package (Aidt Miljø) in figure 4.8.

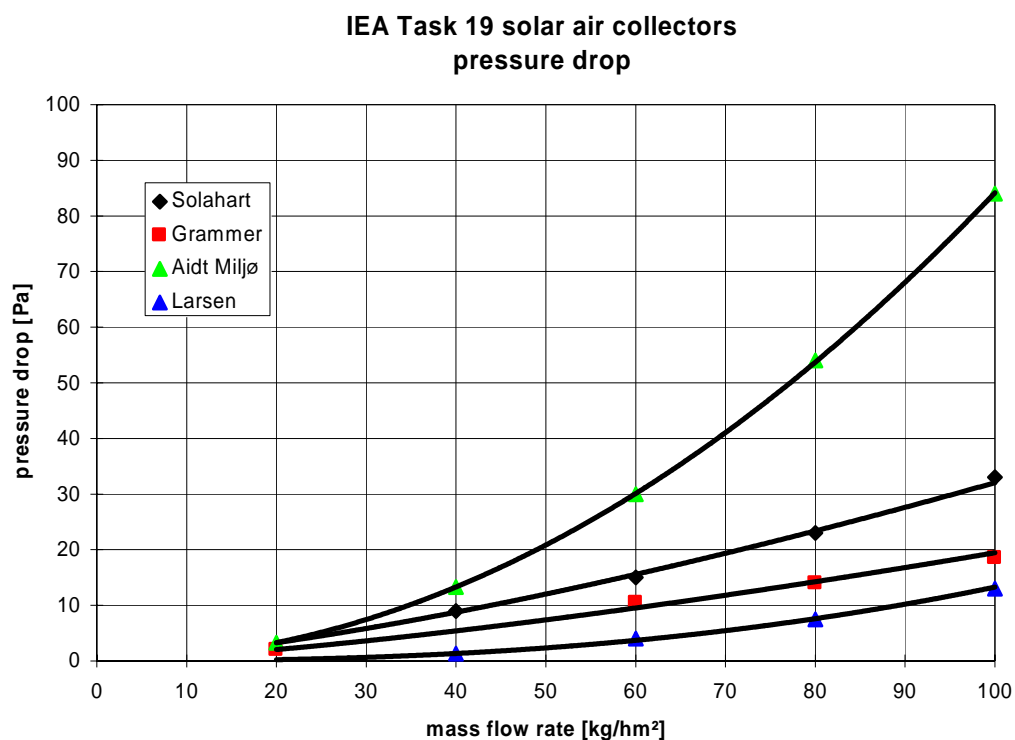Figure 4.8.   The pressure drop across some of the solar air collectors shown in figure 1.4 – based on (Fechner, 1999).

The higher pressure drop of the here investigated single solar air collectors compared to traditional solar air collectors is across the matrix absorber. Figure 2.4 only indicates a small increase in pressure drop due to the matrix absorber. It should, however, be remembered, that in

the two single solar air collectors the matrix absorber is passed twice (se figure 2.14) and further that the area of the first passage is rather small (figure 2.14) leading to a high air speed through the first part of the absorber and thereby to a high pressure drop. The first (inlet) part of the absorber is about 6 % of the total area of the single solar air collectors. An overall air flow rate of 50 m³/hm² leads thus to an specific air flow rate of 830 m³/hm² over the first part of the absorber and 53 m³/m² over the second part. Referring to figures 2.3-4 this leads to a pressure drop for the single solar air collector with fibre cloth absorber across the first part of the absorber of 64 Pa and 3.3 Pa across the second part = 67.3 Pa in total. This is in the same order of magnitude as the value for the single solar air collector with fibre cloth absorber at an air flow rate of 50 m³/hm² in figure 4.7. There must further be a considerable pressure drop across the inlet and outlet as these have sharp edges at both sides. However, the measurements in both figures 2.3-4 and 4.7 have a high degree of uncertainty. According to figures 2.3-4 the single solar air collector with metal absorber should at an air flow rate of 50 m³/hm² and the same considerations as above have a pressure drop above 500 Pa, which is not the case as seen in figure 4.7.

In any case it should be considered to lower the pressure drop across the absorber in the single solar air collectors by increasing the area of the first part (in figure 2.14) of the absorber. The pressure drop ensures an even distribution over the absorber, but it is judged that this could be obtained with a lower pressure drop. Making more smooth inlet and outlet may further lower the pressure drop. In another project also including a solar air collector with matrix absorber (a fibre cloth identical to the here applied) the pressure drop was decreased from 35 to 17 Pa by introducing more aerodynamic correct inlet and outlet without decreasing the efficiency of the solar air collector (Jensen, Kristensen and Forman, 2001).

Pressure drops at proper locations in solar air collectors are important in order to obtain an even air distribution over the absorber and thereby ensuring a high efficiency. But increasing pressure drops lead to increasing power demand of the fan. The pressure drop across a solar air collector should, thus, be designed very carefully.

The main pressure drop across the connectable solar air collectors is as earlier mentioned believed to be at the inlet diffuser. Due to the mounting of the diffuser – by blind rivets to the absorber – the air is not blown in all the way round the diffuser as illustrated in figure 4.9. Figure 4.9 is taken a morning with some dew in the connectable solar air collectors and an air flow rate of approx. 50 m³/hm². Figure 4.9 clearly shows the main flow path of the air – the air starts by flowing to the sides at high speed. Depending on the pressure drop across the absorber (again dependent on the air flow rate) the air will more or less even out over the absorber before passing the absorber. It is, thus, expected that the air flow over the absorber will be more even at high air flow rates than at low air flow rates – i.e. a faster decrease in efficiency is expected for the connectable solar air collectors when going towards lower air speeds than for the single solar air collectors – please refer to the next chapter where the efficiency of the three solar air collectors is investigated.

The pressure drop across the diffusers of the connectable solar air collectors should be minimised. The inlet and outlet should further be made more aerodynamic by smoothening the edges as also indicated in appendix B.

Figure 4.9.   The air flow path in one of the connectable solar air collectors.

4.1.3. Leakage

A careful investigation of figure 4.4 reveals that the sum of the mass flow rates to the connectable solar air collectors is lower than the mass flow rate out of the collector. The reason for this is the location of the fan behind the solar air collector. The fan creates an under pressure in the collector which sucks air through the collector. But if leakage are present part of the mass flow rate at the outlet will come in through these leakage instead of through the inlets. This will not influence the performance of the collector if the leakage are at the edges of the cover as the ambient air any way is let in to the space between the cover and absorber. But if the leakage are to the air gap behind the absorber, heated air will be mixed with ambient air leading to a lower air flow rate through the absorbers resulting in a lower efficiency as seen in figure 1.4 and further lead to lower outlet temperature of the air.

Figure 4.10 shows how large a fraction of the total mass flow rates is sucked in through leakage (false air) instead of through the inlets. The fraction is found in the following way: (1 - (sum of mass flow rates through the inlet)/(mass flow rate out of the collector)). Figure 4.10 shows the fraction before and after balancing the air flow rates through the inlets. Figure 4.10 shows nearly no difference before and after the balancing of the inlets (extra-added pressure loss due to the balancing) with maybe a small increase due to the balancing.

The leakage give rise to 15 % false air at a mass flow rate of 50 kg/hm². In order to evaluate this figure 4.11 has been developed based on values from the investigation in IEA Task 19 (Fechner, 1999). Only data for two solar air collectors are in the form where they can be compared with figure 4.10 – one of the solar air collectors in figure 4.11 is the collector of the Summer House Package utilizing the same basic principle as the here investigated solar air

collectors. The false air introduced at 50 kg/hm² lays is in figure 4.11 between 7-14 % and is not much dependent on the mass flow rate.

Connectable solar air collectors
false air sucked in through leakage
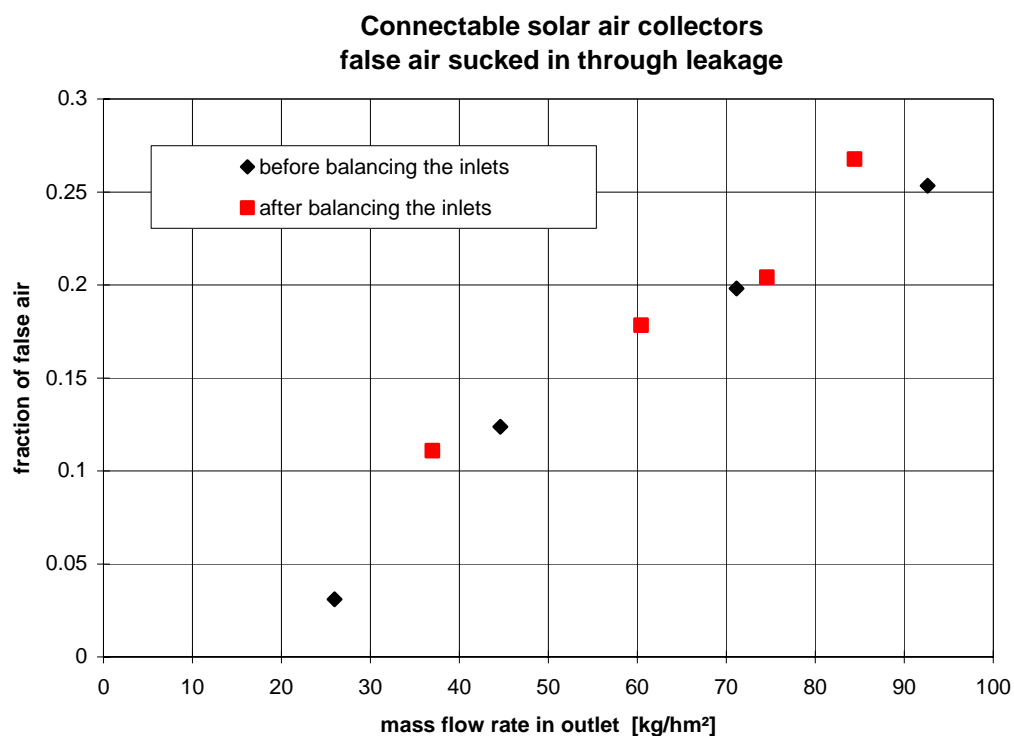
Figure 4.10. Amount of false air sucked into the connectable solar air collectors due to leakage.

IEA Task 19 solar air collectors
false air sucked in throuth leakage

Figure 4.11. Amount of false air sucked into some of the solar air collectors shown in figure 1.4 – based on (Fechner, 1999).

One of the week spots with regards to leakage is the connections between the connectable solar air collectors. The collectors were assembled at the manufacture while the collectors were connected at site. The risk of leakage is, thus, highest at the connections. The connections were therefore sealed carefully with silicone at the site before a new measurements of the leakage were conducted. The result of this investigation together with the values from figure 4.10 is shown in figure 4.12. Figure 4.12 shows that the fraction of false air decreased considerably at mass flow rates below 75 m³/hm² when sealing the connections between the connectable solar air collectors. The sealing had only marginal effects at higher mass flow rates. However, mass flow rates below 75 m³/hm² is of main interest. Compared with figure 4.11 the amount of false air is now in the same order of magnitude as for the solar air collector of the Summer House Package at 50 kg/hm². 7 % at 50 kg/hm² is satisfactory.
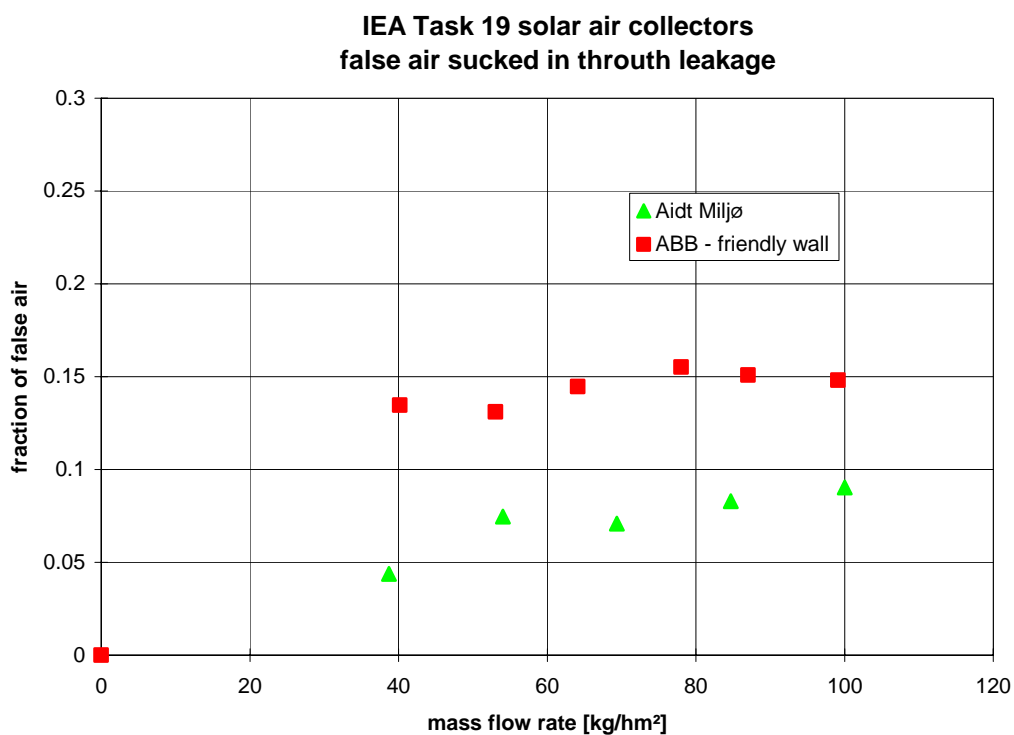
Connectable solar air collectors
false air sucked in through leakage
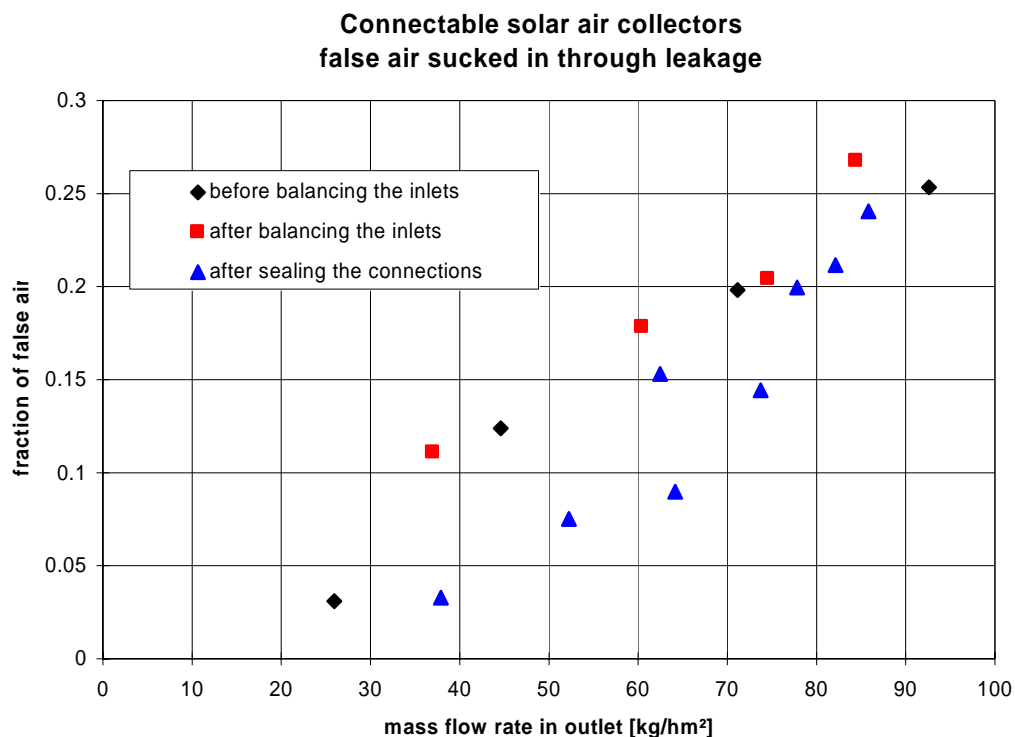
Figure 4.12. Amount of false air sucked into the connectable solar air collectors due to leakage before and after the sealing of the connections.

Figure 4.12 reveals that an extra effort should be put in making the connections more air tight as leakage here as seen in figure 2.6 will let false air into the air gap behind the absorber where it will reduce the efficiency of the connectable solar air collectors.

The leakage level of the single solar air collector with metal absorber was tried determined, however, the used method lead to an unrealistic leakage level – false air intake of above 40% of the mass flow rate out of the collector. Due to the configuration of the inlets (see figure 2.15), the air intake could not be measured. Instead combined pressure levels and air flow rates at the outlet were measured with the inlets either open or sealed. The reason for the high level of false air is believed to be, that the sealing of the inlets totally change the pressure conditions within the collector. However, as the single solar air collectors are made by the same manufacture as the collector of the Summer House Package using more or less the same technique it is believe that the leakage level for the single solar air collectors is about the same

as for the collector of the Summer House Package – Aidt Miljø in figure 4.11 – and thereby in the same order of magnitude as the connectable solar air collectors with sealed connections.

4.2. Measurements from specific days

The present sub-chapter contains graphs showing some of the obtained measured values and calculated values based on the measured values. The aim of the sub-chapter is to illustrate the performance of the solar air collectors.

The measuring campaign lasted as earlier mentioned from mid July until end October. The relatively long measuring period was due to the fact that measurements at different air flow rates through the collectors were required in order to obtain efficiency curves like the ones shown in figure 1.4. For each air flow rate specific weather conditions were further required in order to allow for the determination of the efficiency at that specific air flow rate – the requirements were basically related to the solar radiation. The requirement regarding the solar radiation was different for the two earlier mentioned methods for determination of the efficiency. The simple method requires at least one day with almost clear sky conditions while the detailed method requires a specific amount of solar radiation over a period and not necessarily clear sky conditions.

Figures 4.13-14 show the weather conditions (total radiation and ambient air temperature) for the weeks 30-31, 2001 (July 23-August 5). The total radiation was measured by the PV pyranometer (figure 3.15) while the ambient temperature was the inlet temperature to the connectable solar air collectors (fig 3.1). The two weeks in figures 4.13-14 were characterized by four days with clear sky conditions or almost clear sky conditions while the solar radiation the other days was rather scattered. The ambient temperature was between 13 and 28°C.

Figures 4.15-16 show the mass flow rates through the solar air collectors for the same two weeks as figures 4.13-14. Figures 4.15-16 show three levels of mass flow rates for the collectable solar air collectors and the single solar air collector with metal absorber. The mass flow rate of the single solar air collector with fibre cloth absorber follows the solar radiation. However, on day number 207 the power supply of the fan was switched from being two PV panels to be one PV panel. This halve as seen the mass flow rate through the single solar air collector with fibre cloth absorber.

Figures 4.15-16 reveals a problem with the fans used for the connectable solar air collectors and the single solar air collector with metal absorber: the fans were very temperature dependent – i.e. decreasing mass flow rate by increasing temperature of the air passing the fans. However, the mass flow rates were sufficiently stable during noon in order to allow for determination of the efficiency of the solar air collectors. The main problem with the temperature dependency of the fans was that the highest possible mass flow rate was lower than originally wished, however, sufficiently high in order to determine the efficiency in the main operation area of the solar air collectors. Figure 4.16 further reveals that the mass flow rate especially through the connectable solar air collectors at low flow rates and fluctuating solar radiation is very unstable.
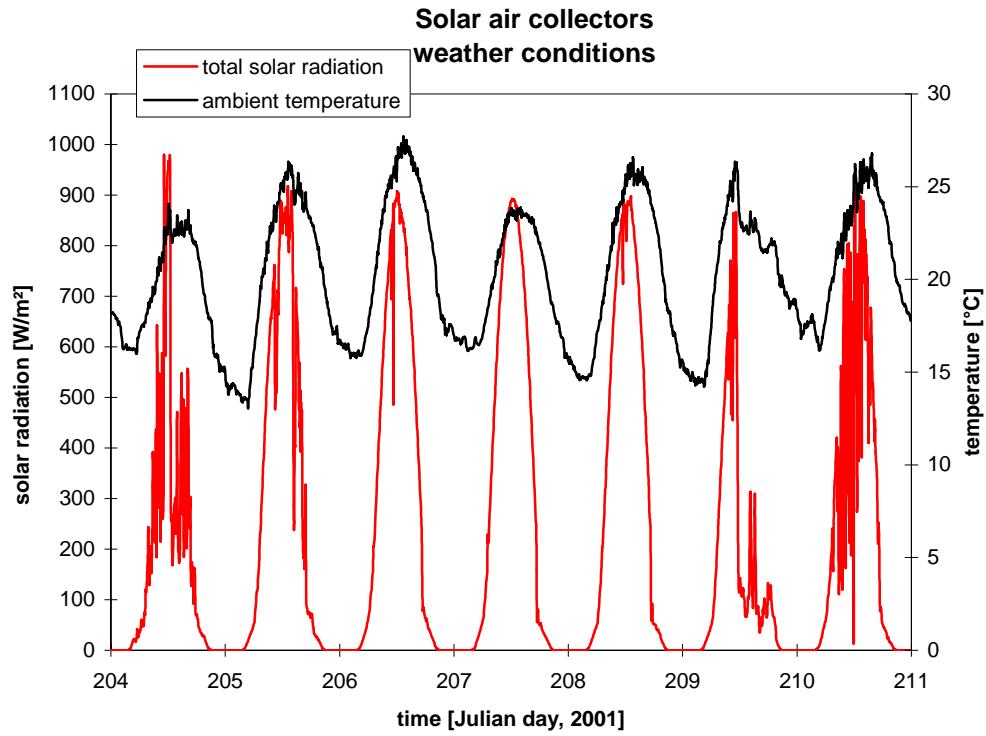
Figure 4.13. Weather conditions during week 30, 2001 – July 23-29.
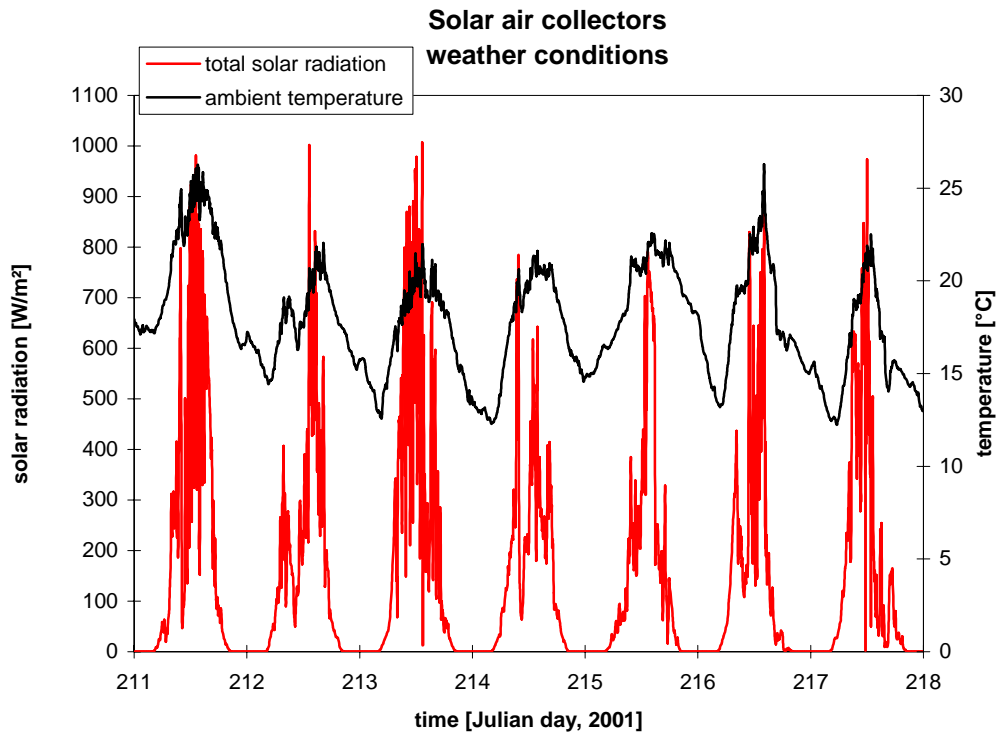

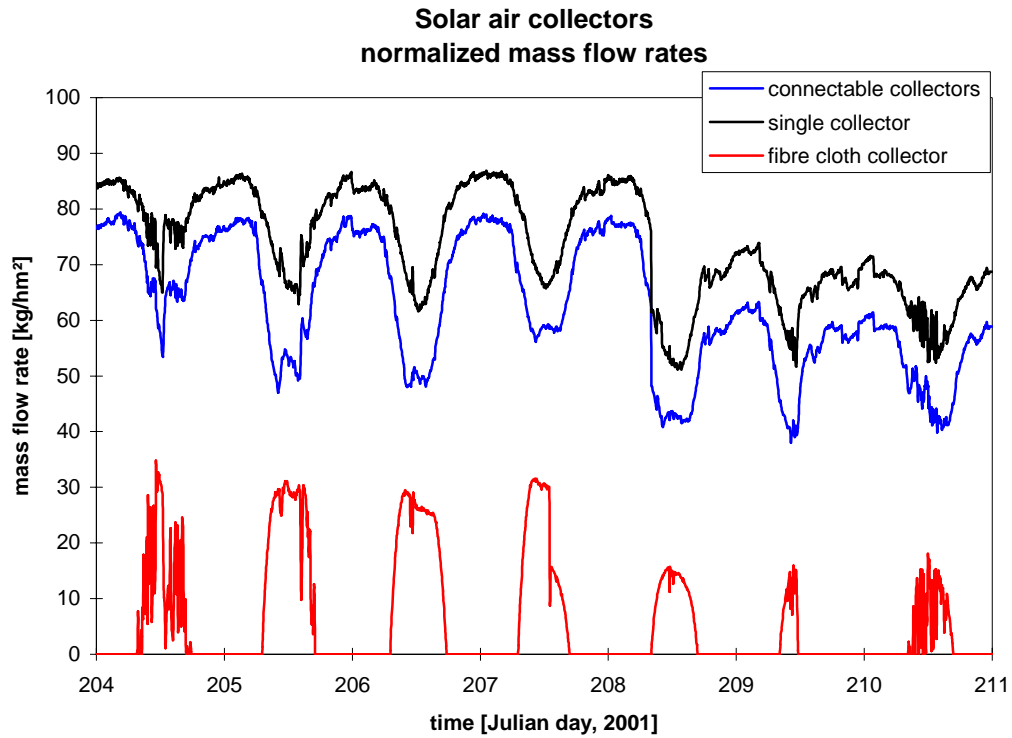Figure 4.14.   Weather conditions during week 31, 2001 – July 30-August 5.

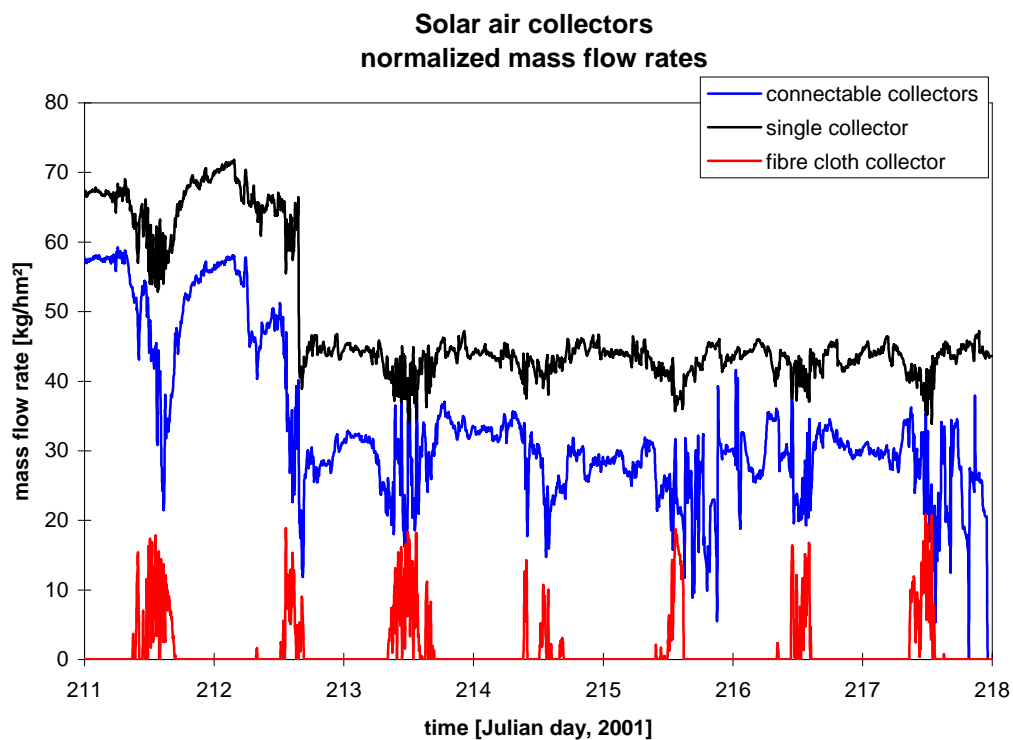Figure 4.15. Mass flow rate through the solar air collectors during week 30, 2001 – July 23-29.

Figure 4.16. Mass flow rate through the solar air collectors during week 31, 2001 – July 30-August 5.

In order to illustrate the thermal performance of the solar air collectors, one day – July 25 (day number 206) - has primarily been chosen for showing measured and calculated values over the day. Figures 4.17-19 show the weather conditions, the air flow rates and normalized mass flow rates through the solar air collectors. There was nearly clear sky conditions on July 25 except for a few clouds before noon and an ambient temperature of up to 28°C.

Figures 4.17-18 shows that the fan connected to the single solar air collector with fibre cloth absorber started at a total radiation level of 200 W/m² and stopped at a total radiation level of 100 W/m². For more information on the function of the combination of fan and PV panels please refer to (Jensen and Bosanac, 2002).

Figure 4.19 shows together with figures 4.20-21 the temperature dependency of the fans connected to the collectors with metal absorbers.

4.2.1. Inlet and outlet temperatures of the solar air collectors

Figures 4.20-22 show the inlet and outlet temperatures of the solar air collectors on July 25.

Figures 4.20-22 show the same pattern in the outlet temperature for the three collectors. The difference in temperature level is partly due to the difference in mass flow rate through the collectors – see figure 4.19 – partly due to different inlet temperatures to the collectors as seen in figure 4.23. The inlet temperature to the two solar air collectors with metal absorbers were very similar while the inlet temperature to the single solar air collector with fibre cloth absorber was much higher – up to 7 K higher. The reason for this is the location of the collectors. The inlets of the two solar air collectors with metal absorbers were freely exposed to the ambient – see figure 4.1 while the single solar air collector was mounted on top of dark roof sheets see figure 2.17. The dark roof sheets absorb heat from the solar radiation and heat the inlet air to the single solar air collector with fibre cloth absorber. Due to the differences in mass flow rates and inlet temperatures the outlet temperatures i figures 4.20-22 cannot be compared directly. In order to compare the performance of the collectors one have to look at the efficiencies – this will be done in the next chapter.

4.1.2. Temperature increase across the connectable solar air collectors

Figure 4.24 shows the inlet and outlet temperature of the connectable solar air collectors together with the air temperatures in the air cab behind the absorbers at the connections of the three collectors. The location of the temperature sensors is shown in figure 4.26. Figure 4.25 shows the temperature increase across the connectable solar air collectors at each hour from 6:00 to 14:00. Figures 4.24-25 show that the main temperature increase occurs when passing the absorber: at 13:00 the inlet temperature was 27°C while the temperature of the air between the two first collectors was 48°C – i.e. an temperature increase over the absorber of 21 K. When passing behind the absorbers the temperature of the air increased from 48°C to 51°C between the second and third collector and ended up with an temperature at the outlet of 55°C. The temperature increase of the air when passing behind the absorber was thus 55-48 = 7 K. This means that ¾ of the temperature increase occurred through the absorbers, while the last ¼ occurred when passing behind the absorbers. Figure 4.24 shows that the intention of having the main heating of the air to occur when passing the absorber has been fulfilled.

Solar air collectors
weather conditions
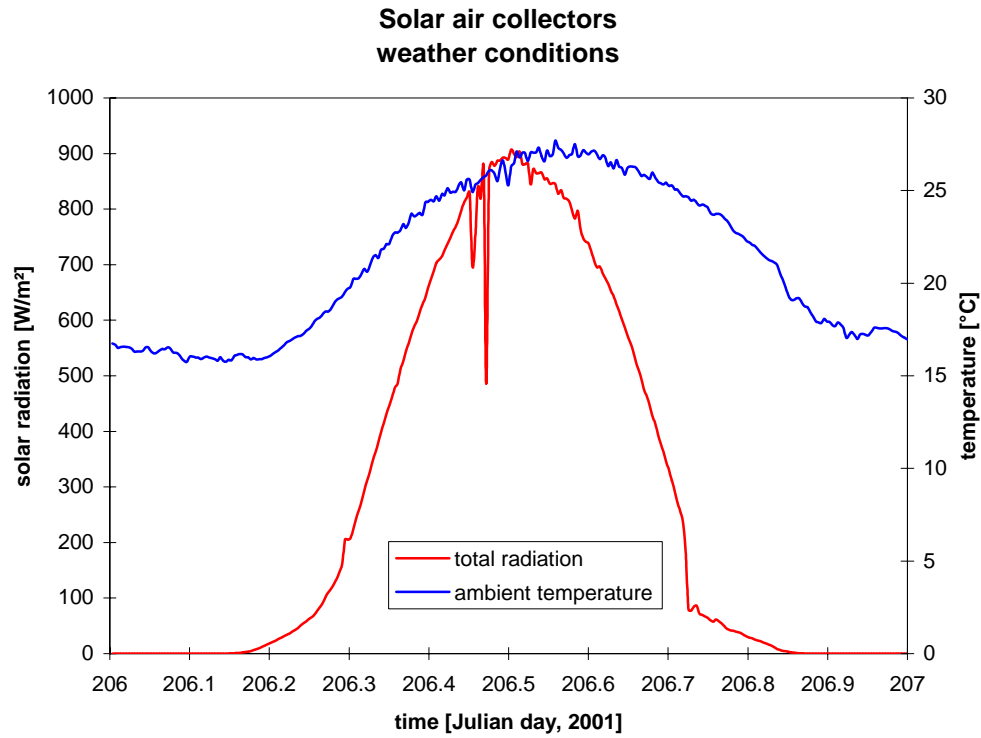
Figure 4.17. The weather conditions on July 25.

Solar air collectors
air flow rates
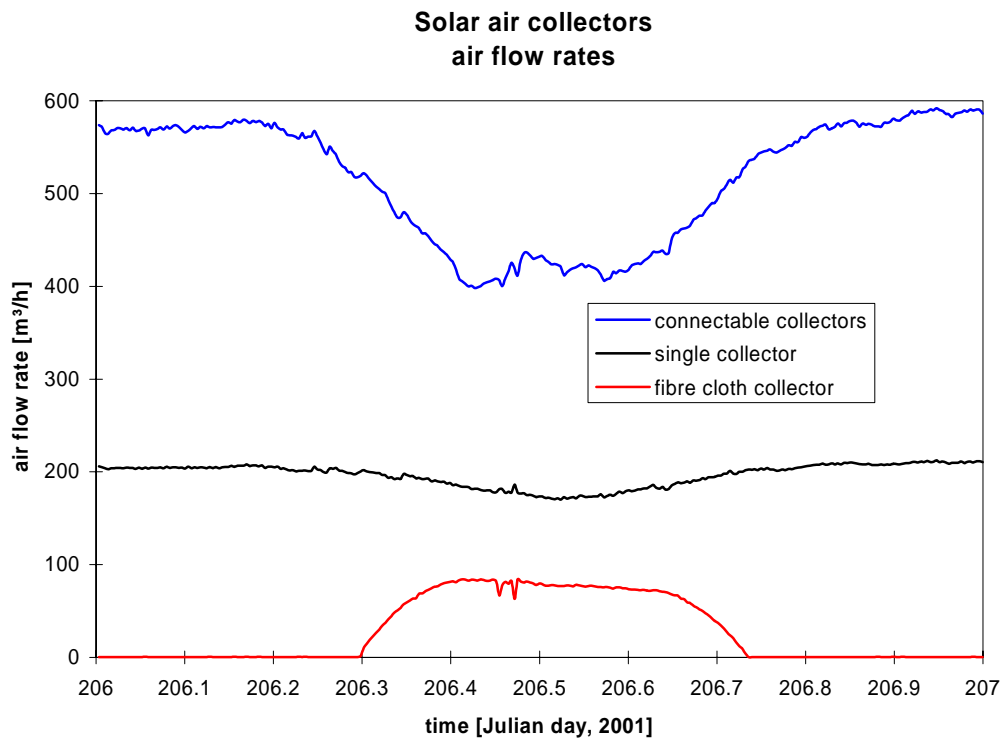
Figure 4.18. The total air flow rate through the solar air collectors on July 25.
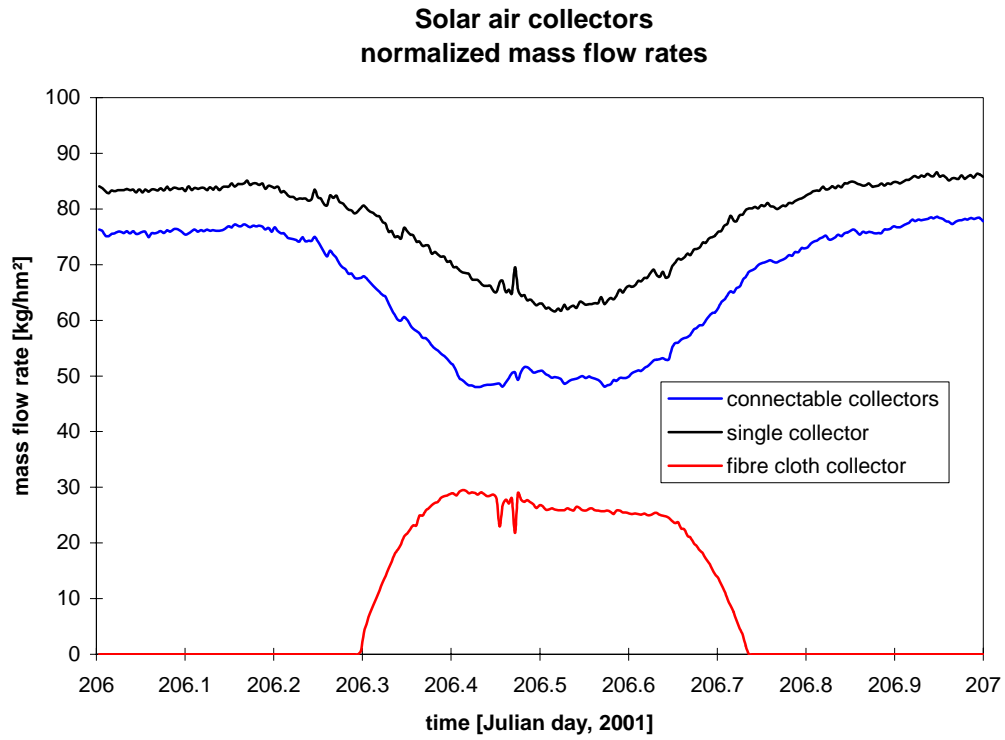
Figure 4.19.   The normalized mass flow rate through the solar air collectors on July 25.
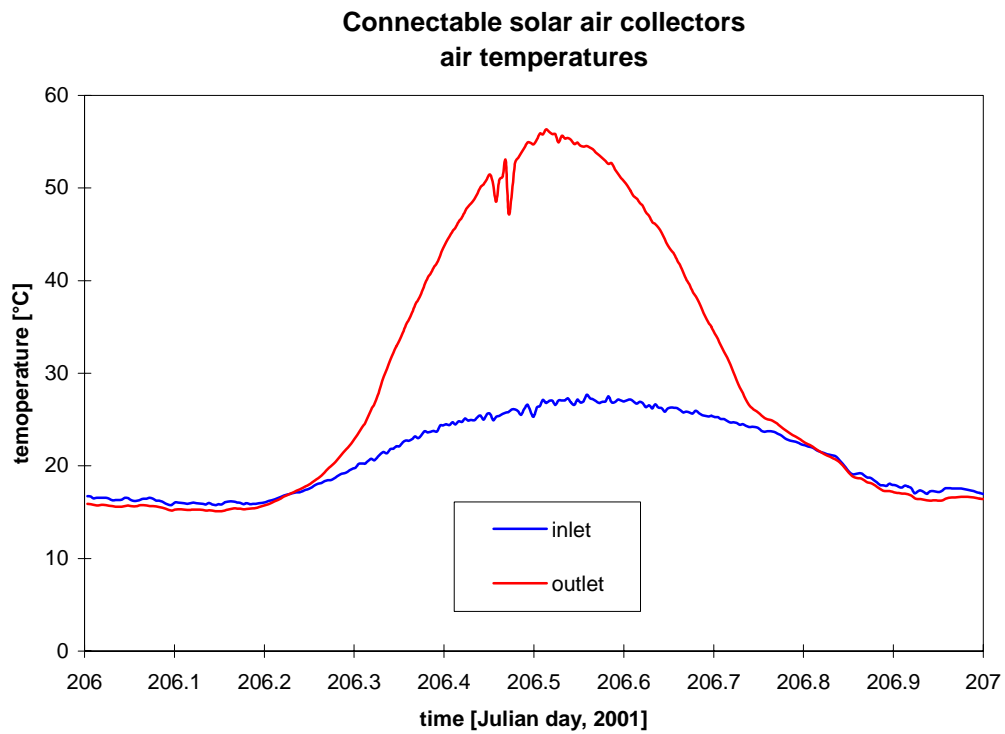
Figure 4.20. The inlet and outlet temperature of the connectable solar air collectors on July
                25.
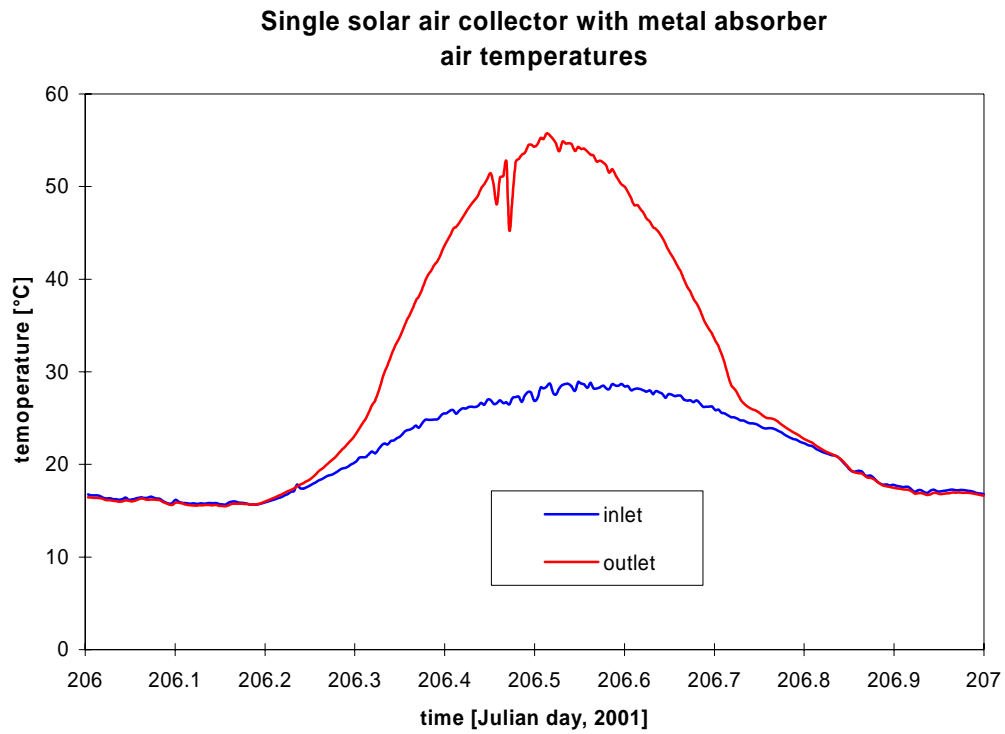
Figure 4.21. The inlet and outlet temperature of the single solar air collector with metal absorber on July 25.
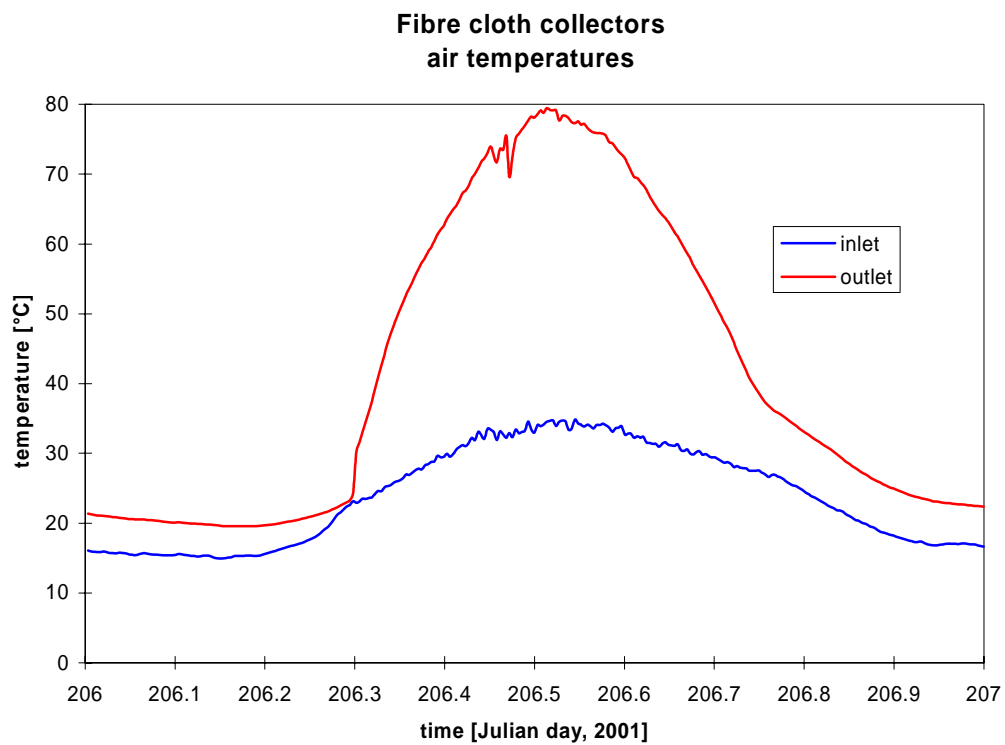
Figure 4.22. The inlet and outlet temperature of the single solar air collector with fibre cloth collector on July 25,

Solar air collectors
inlet temperatures
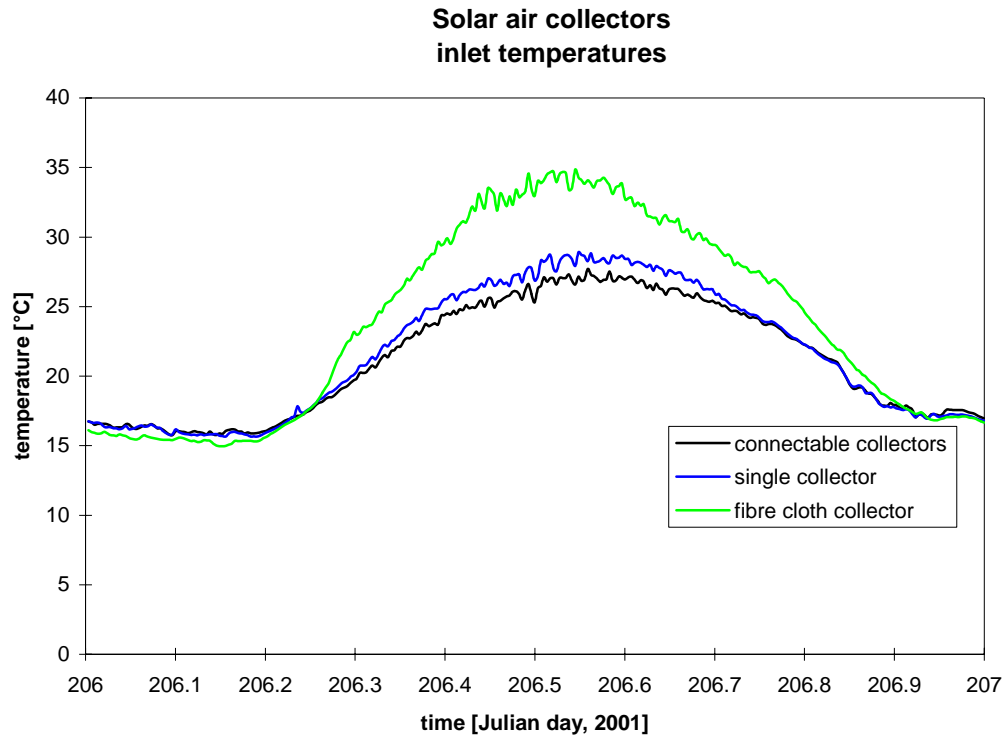
Figure 4.23. The inlet temperature to the three solar air collectors on July 25.

Connectable solar air collectors
air temperatures

Figure 4.24. Air temperatures in the connectable solar air collectors on July 25.

Figure 4.25. Temperature increase across the connectable solar air collectors on July 25.

4.2.3. Absorber temperatures in the connectable solar air collectors

Figure 4.26 shows the location and labelling of the temperature sensors for measuring the absorber temperatures in the connectable solar air collectors. The obtained absorber temperatures are shown in figure 4.27 – figures 4.28-30 show the two absorber temperatures in each collector. Absorber temperature abs 11 of the first collectors is very fluctuating. This was caused by the measuring system. There was some kind of conflict between the reading of this sensor and the tricking of the water draw off of the hot water tank in the system the single solar air collector with fibre cloth absorber was connected to. The reading of abs 11 got regular the reading of zero. So when creating mean values some of the obtained mean values are too low. However, as seen during periods without solar radiation the top value of abs 11 is identical to abs 12. This means that the curve for abs 11 still can be used if only looking at the top values while disregarding the bottom values in the fluctuations.
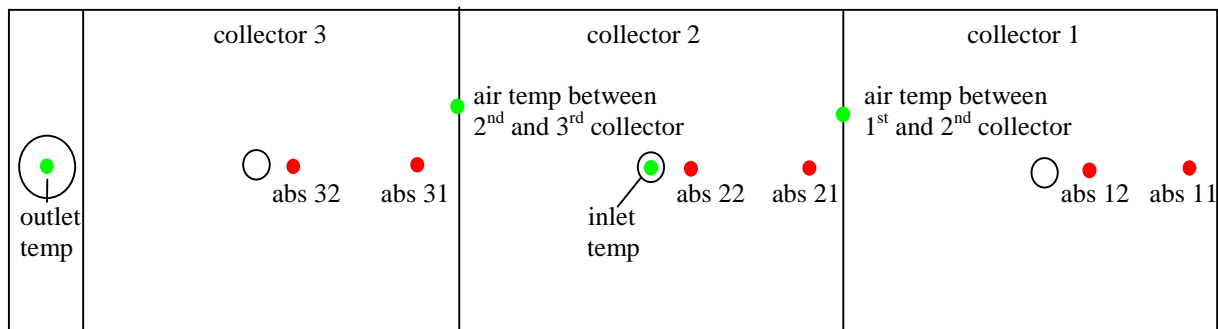
Figure 4.26. The location and labelling of the temperature sensors in the connectable solar air collectors.

Figure 4.27. Absorber temperatures in the connectable solar air collectors on July 25.
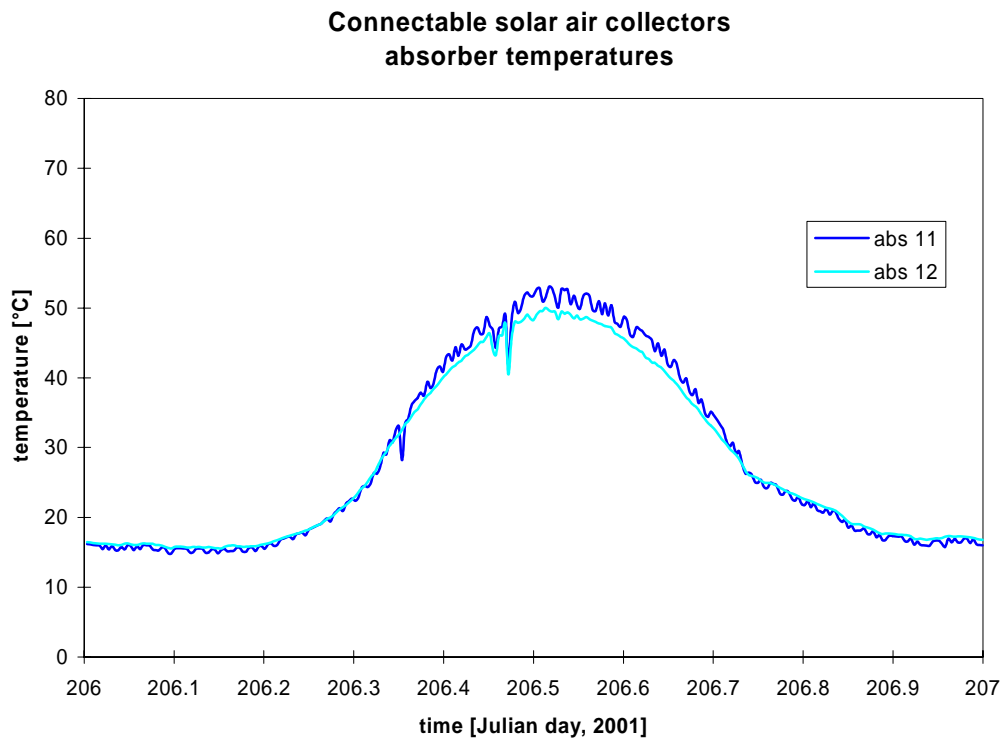
Figure 4.28. Absorber temperatures in the first connectable solar air collector on July 25.
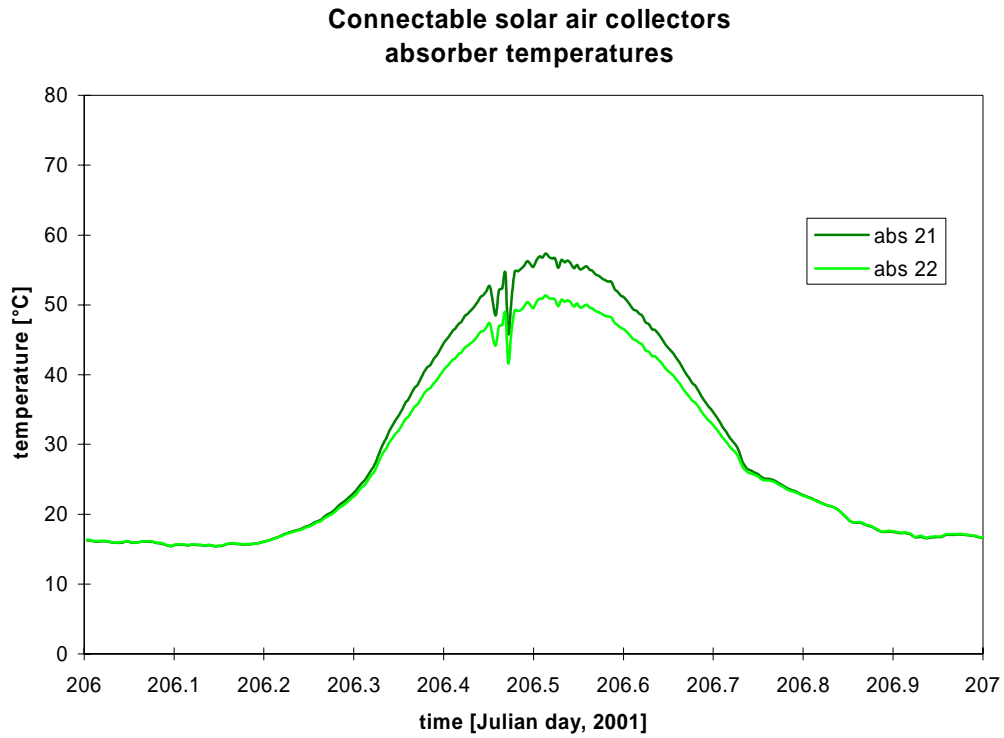
Figure 4.29. Absorber temperatures in the second connectable solar air collector on July 25.
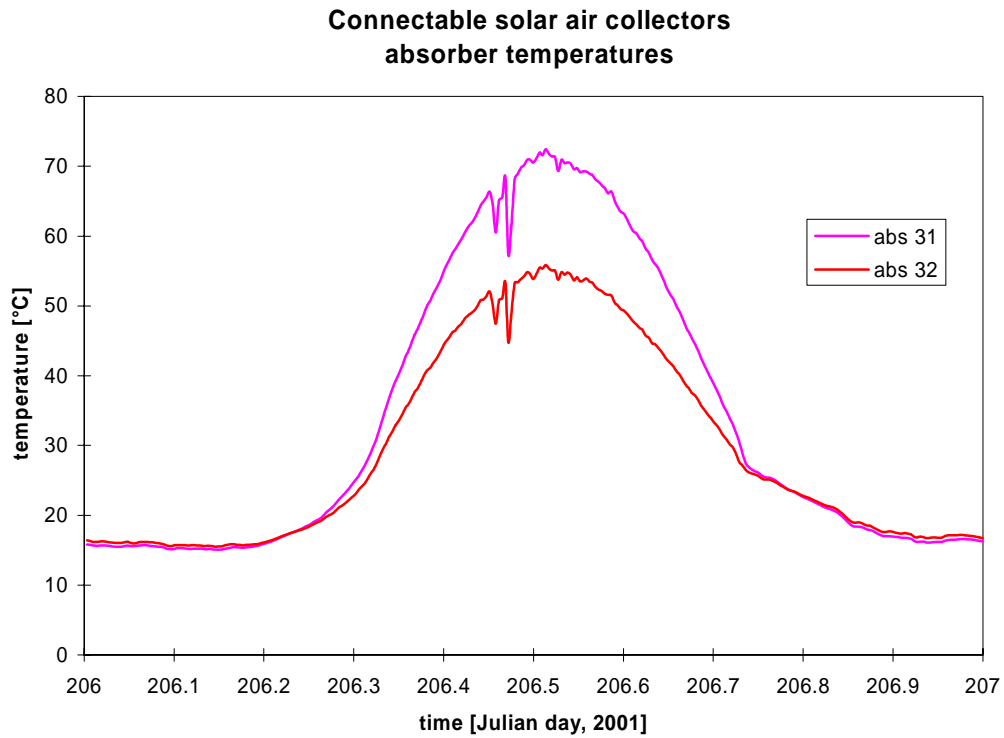
Figure 4.30. Absorber temperatures in the third connectable solar air collector on July 25.

The two absorber temperatures are very close in figure 4.28 indicating an even distribution of the air flow over the absorber. The temperatures are also very close in figure 4.29 while much

more different in figure 4.30. The reason for the higher temperature difference in figure 4.29 than in figure 4.28 is that the temperature of the air behind the absorber is higher in the second collector than in the first collector. This could also be the reason for the even higher temperature difference observed in figure 4.30, however this difference is very large and may, therefore, also be due to a less even distribution of the air flow over the absorber in this collector.

From figures 4.27-30 it seems likely that the air flow is rather even distributed over the absorbers, however, figures 4.27-30 were obtained for a mass flow rate through the connectable solar air collectors of approx. 50 kg/hm³ which is in the middle of the expected operation area of this type of collectors. How will a lower or higher mass flow rate influence the air flow over the absorber? In order to investigate this the absorber temperatures are shown in the following for two other days – July 19 and August 18 where the mass flow rate was around 70 and 20 kg/hm² as seen in figures 4.31-32 – the larger peaks in figure 4.32 is due to some stability problems with the air speed sensor, however, during periods with solar radiation the sensor was stable. Figures 4.33-34 show the total solar radiation and ambient temperature for the same two days. The chosen two days were as July 25 nice sunny and warm days.

Figures 4.35-39 show the air and absorber temperatures in the connectable solar air collectors during July 19 while figures 4.40-44 show the same temperatures for August 18. The absorber temperature abs 11 is in figures 4.41-42 more fluctuating than in the other figures showing this temperature. The reason is that the values in figures 4.40-44 are minutely mean values and not 5 minutely mean values. The occasionally zero reading for this sensor has, therefore, a bigger influence on the mean value where they occur due to fewer values in the minutely mean values compared to the 5 minutely mean values.

The general picture when comparing figures 4.28-30, 4.37-39 and 4.42-44 is that the difference between the two absorber temperatures in each collector increases with decreasing mass flow rate through the solar air collectors. This is more clearly seen in figure 4.45. Figure 4.45 shows the temperature differences between the two absorber temperature sensors in each collector around noon dependent on the mass flow rate during the same period.

There will always be a temperature difference between the two sensor locations due to heating up of the air when passing above the absorber. A temperature difference of 3-7 K at 70 kg/hm² seems reasonable. The difference between the absorber temperatures increases as expected with decreasing mass flow rate through the collectors – however, with major differences between the three collectors. The increase in temperature difference is minor for the second collector while especially the third collectors experiences a very large increase in temperature difference. It is believed that the major reason for the differences shown in figure 4.45 is due to differences in the inlets of the collectors – i.e. the inlet diffusers were handmade and therefor very likely rather different.

Form figures 4.27-45 it is seen that a rather even air flow seems to be obtained at high mass flow rates through the connectable solar air collectors. At low mass flow rates this seems only obtained for the middle collector. It, thus, seems to be possible to obtain a well distributed air flow over the absorber, however, major focus should be put in developing the inlet so that not only the air will be well distributed over the absorber but that the pressure drop across the inlet gets as low as possible in order to save fan energy.
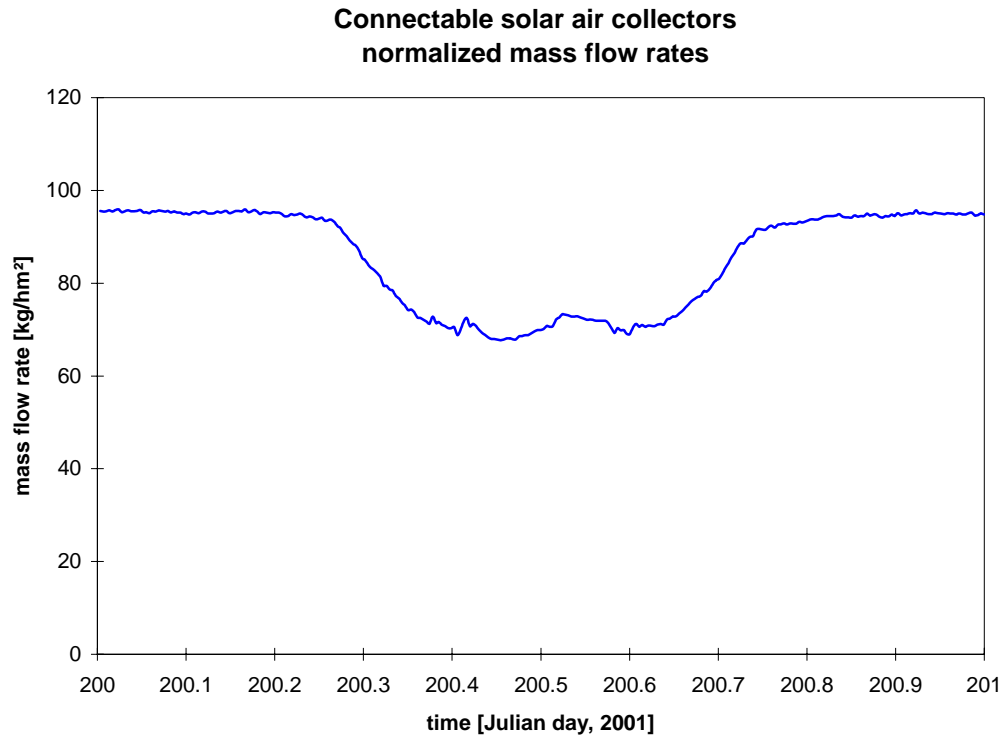
Figure 4.31. Mass flow rate through the collectable solar air collectors on July 19.
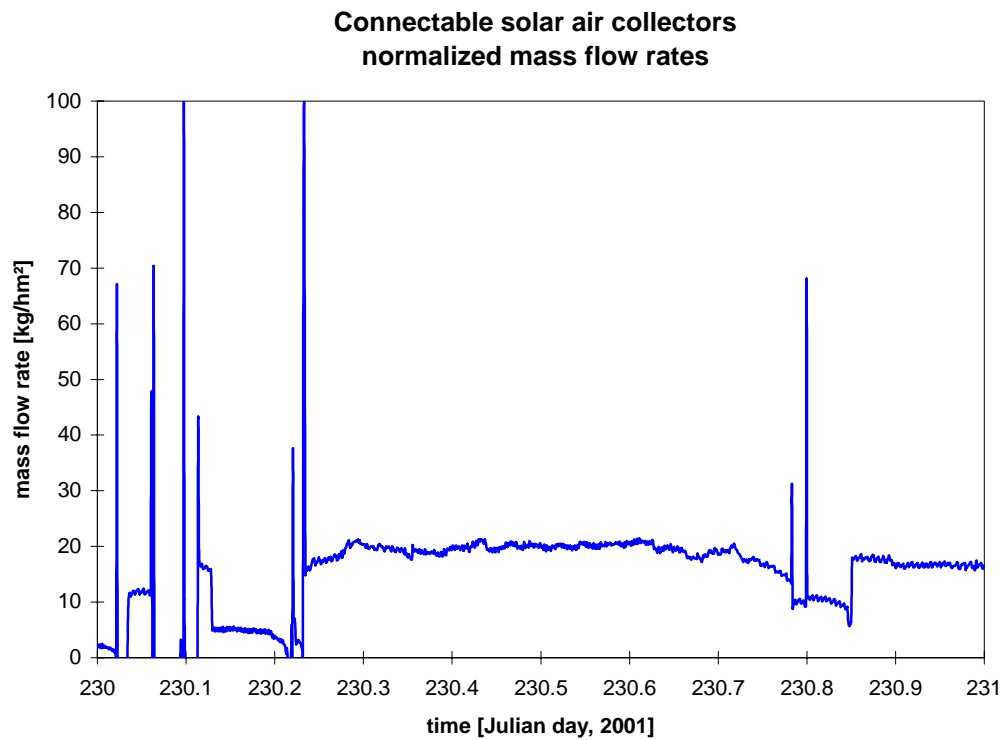
Figure 4.32. Mass flow rate through the collectable solar air collectors on August 18.
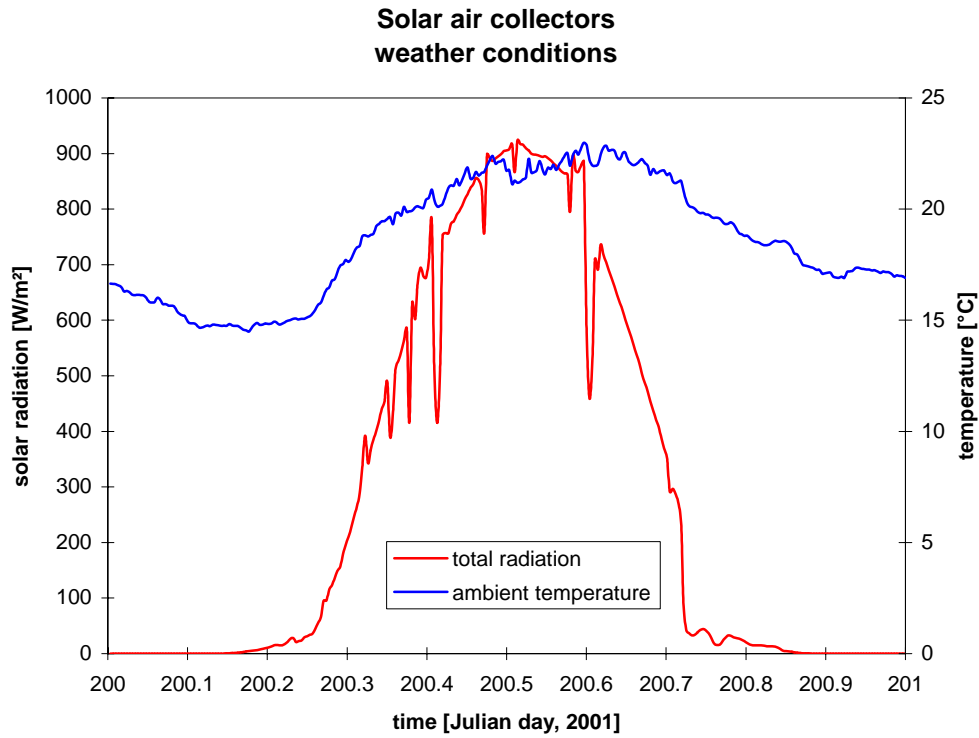
Figure 4.33. The weather conditions on July 19.
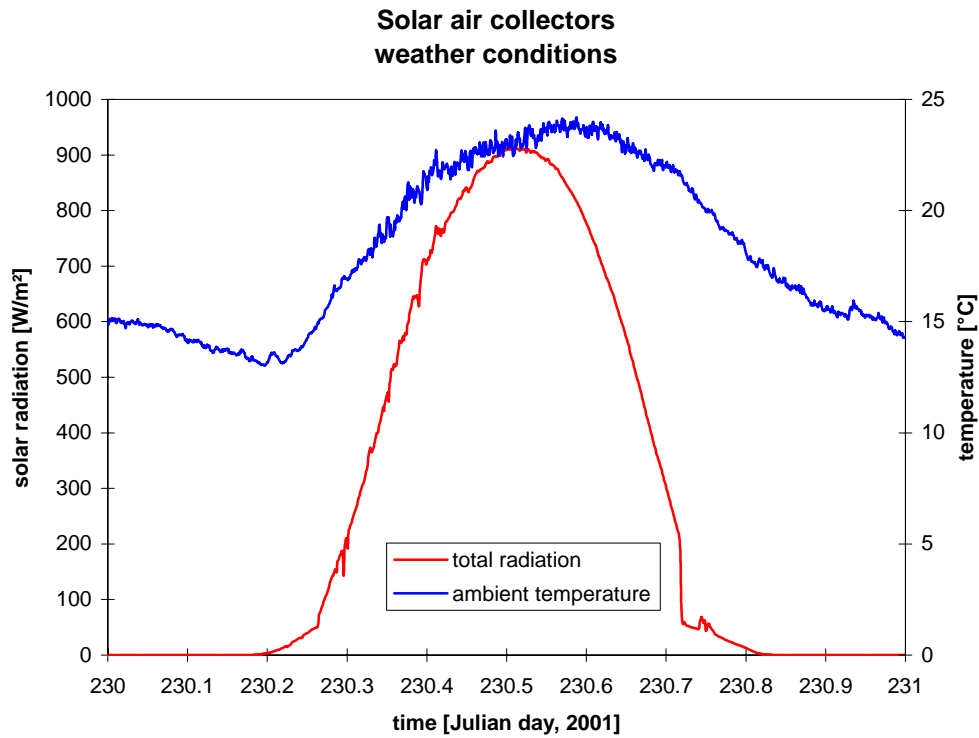
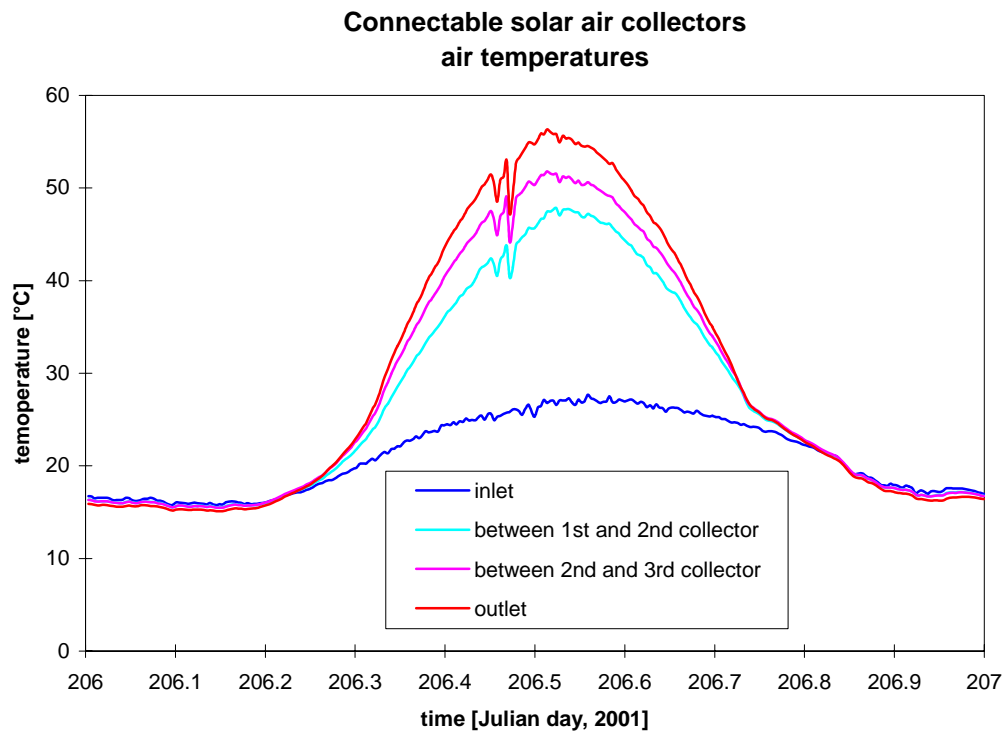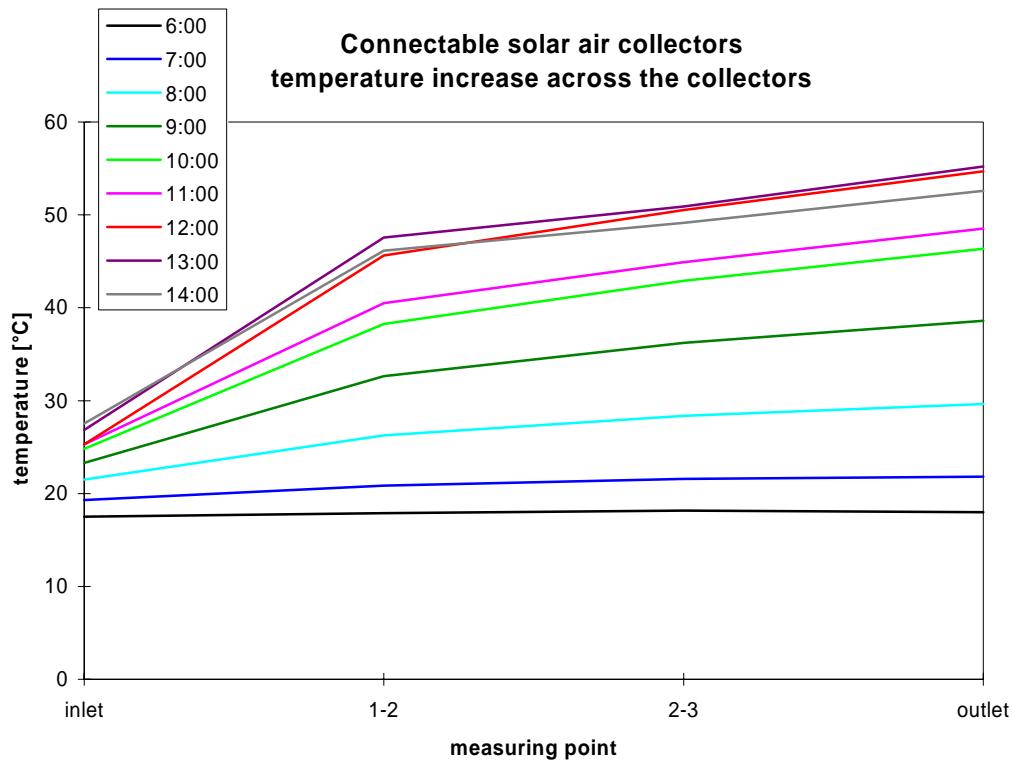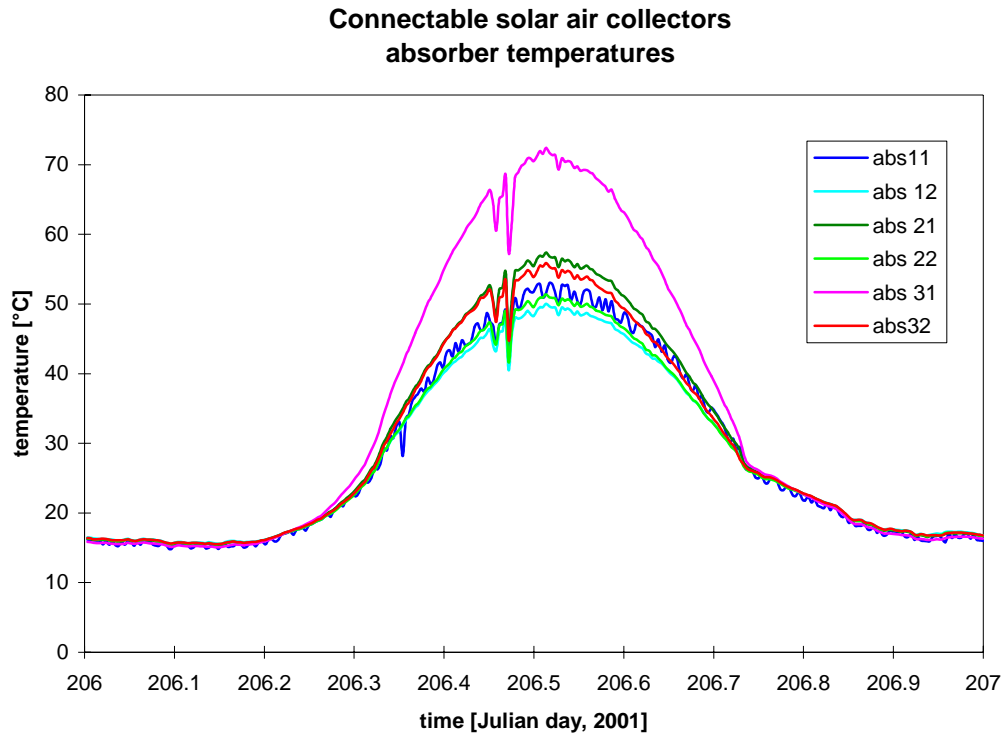Figure 4.34. The weather conditions on August 18.
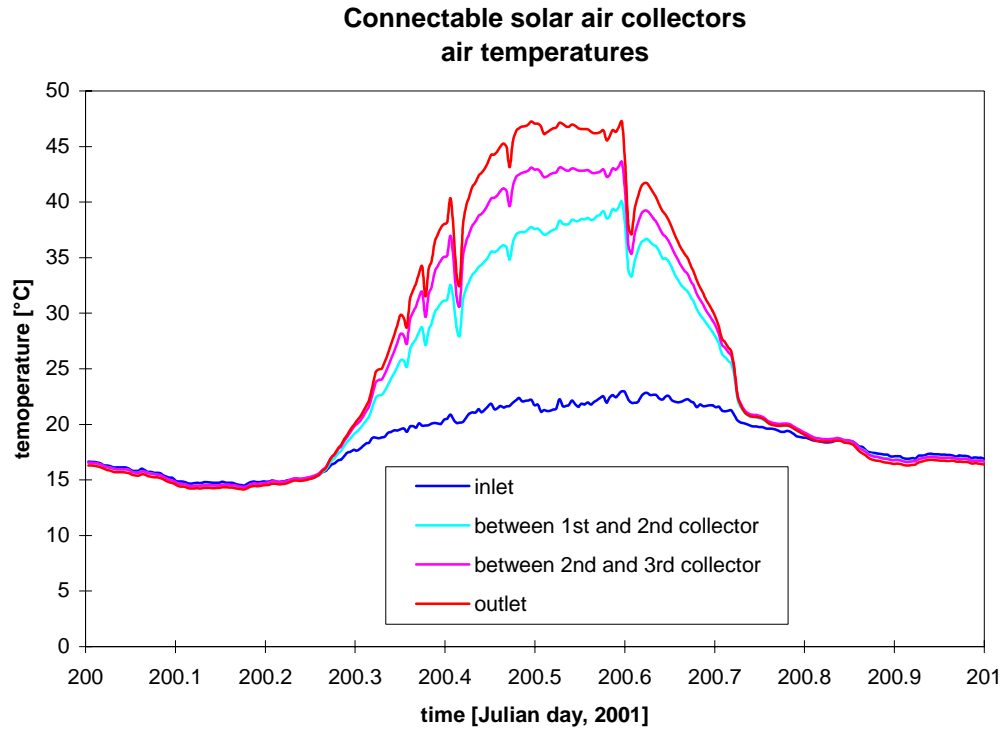
Figure 4.35. Air temperatures in the connectable solar air collectors on July 19.
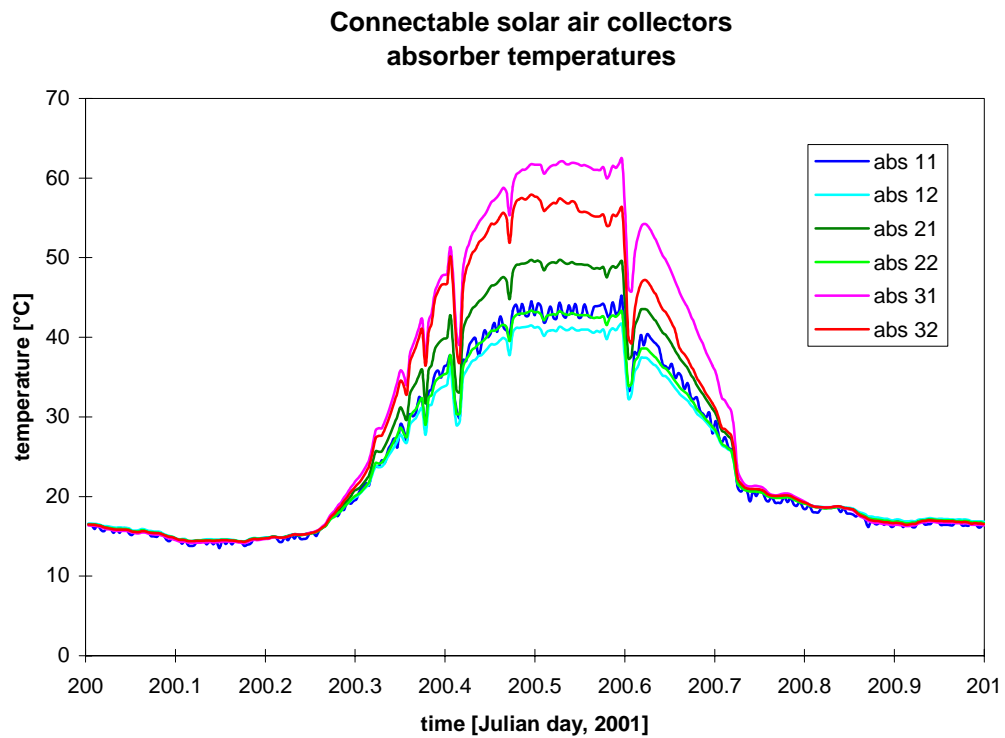
Figure 4.36. Absorber temperatures in the connectable solar air collectors on July 19.
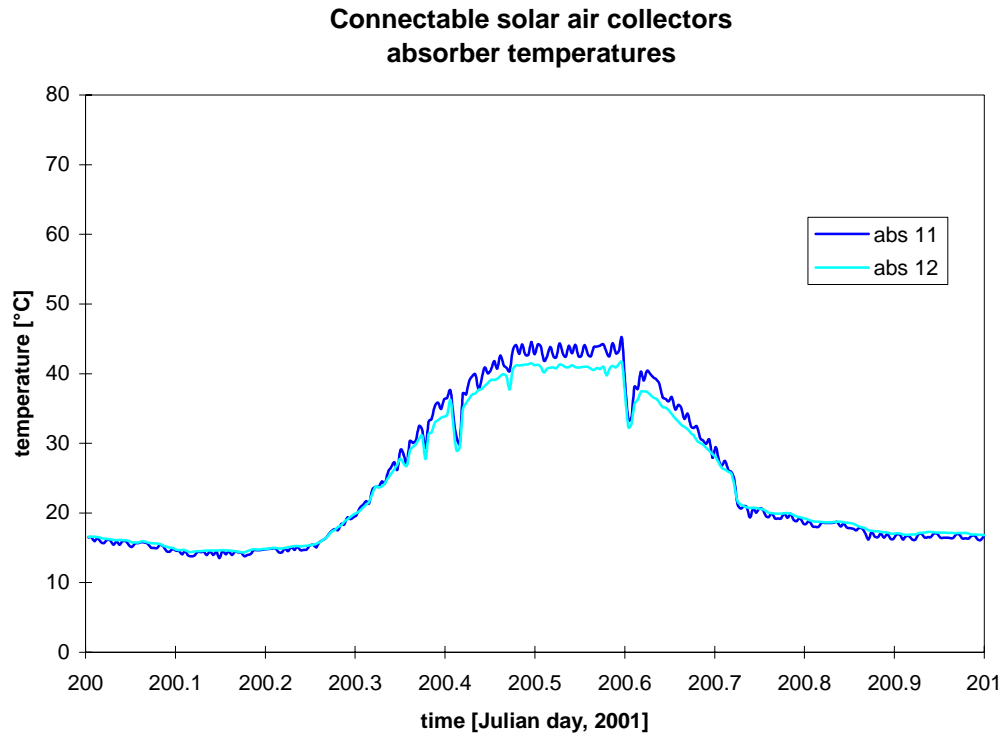
Figure 4.37. Absorber temperatures in the first connectable solar air collector on July 19.
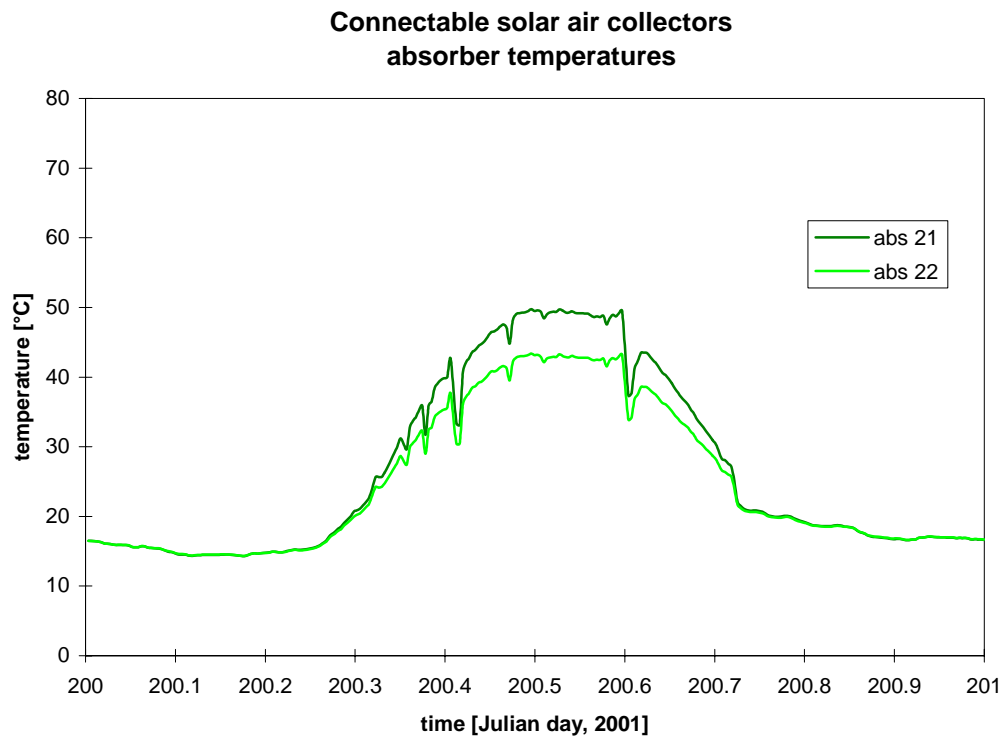
Figure 4.38. Absorber temperatures in the second connectable solar air collector on July 19.
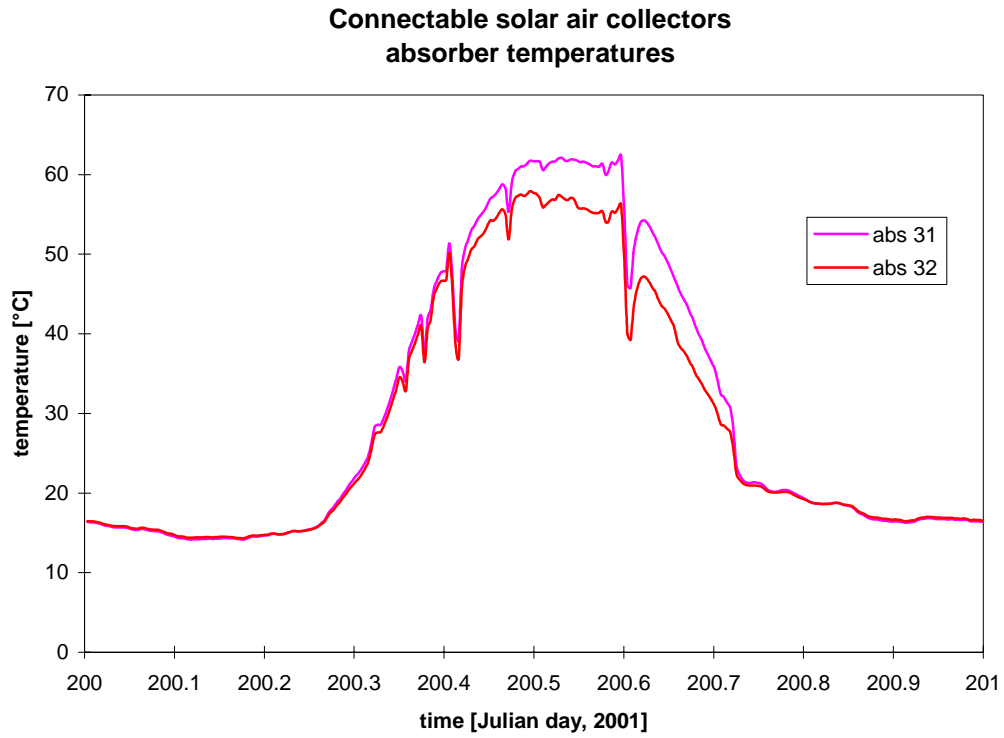
Figure 4.39. Absorber temperatures in the third connectable solar air collector on July 19.
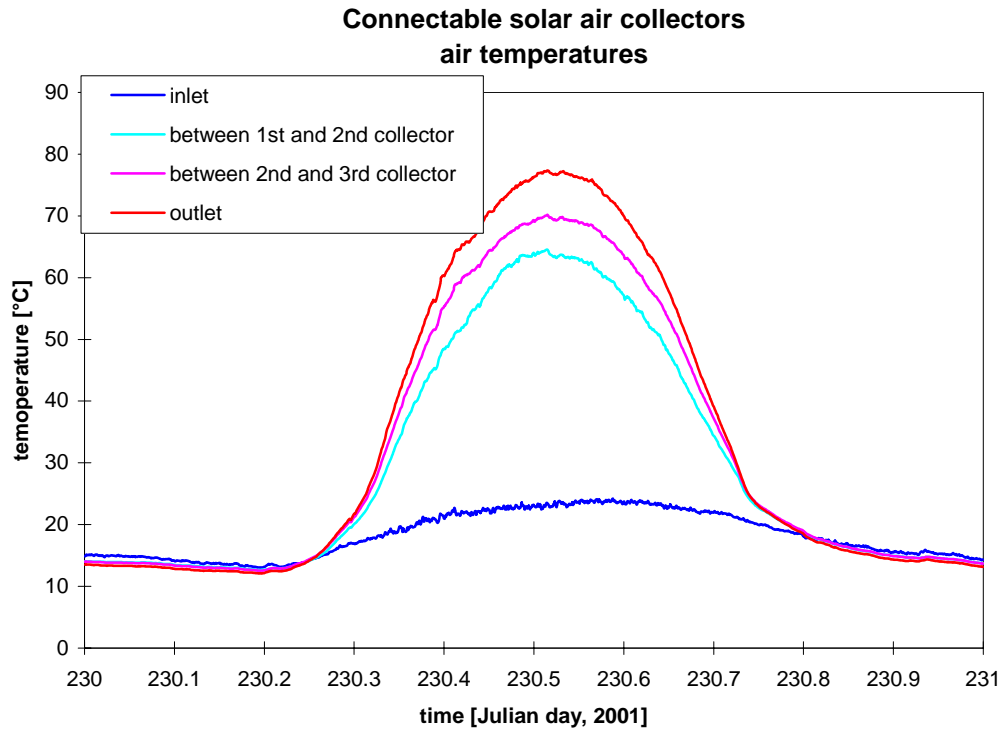
Figure 4.40. Air temperatures in the connectable solar air collectors on August 18.
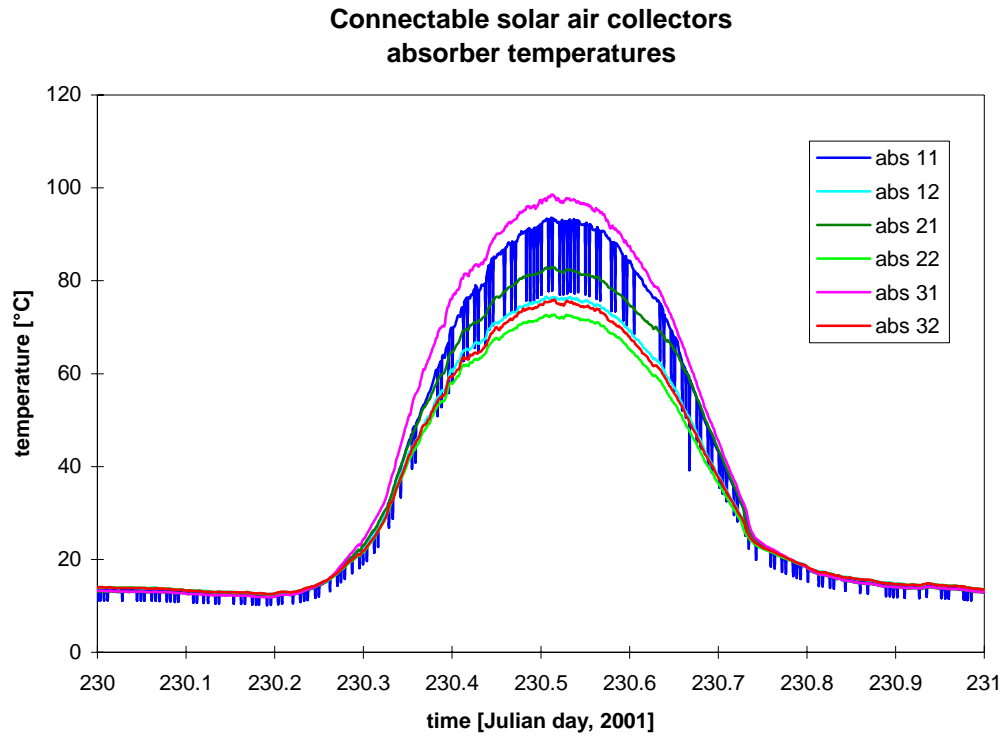
Figure 4.41. Absorber temperatures in the connectable solar air collectors on August 18.
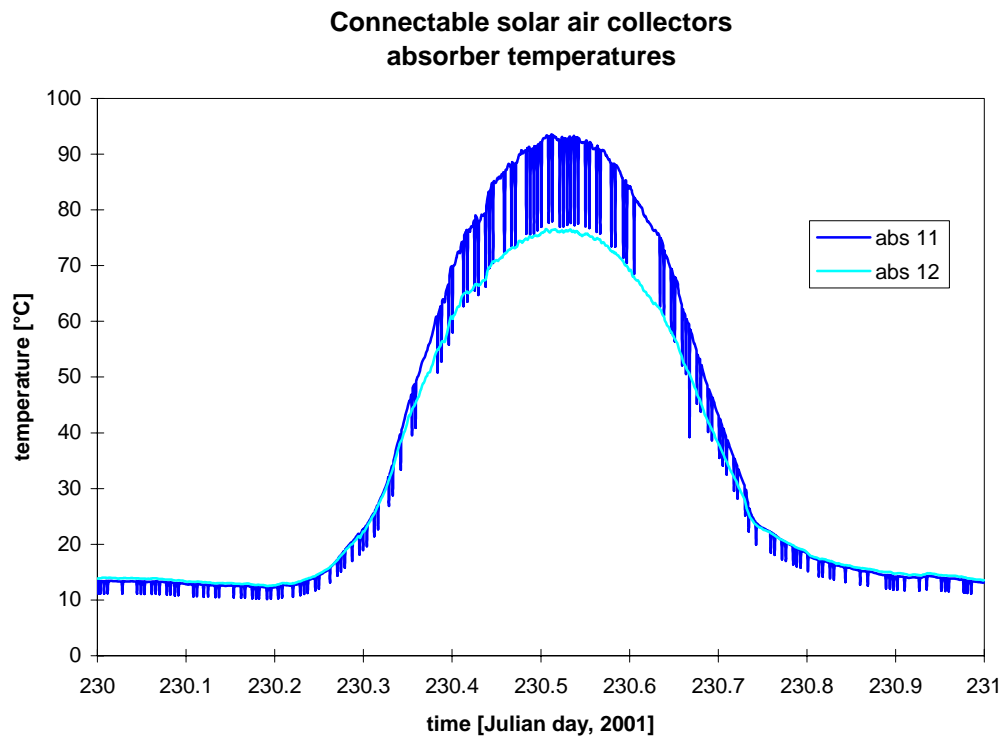
Figure 4.42. Absorber temperatures in the first connectable solar air collector on August 18.

Connectable solar air collectors
absorber temperatures
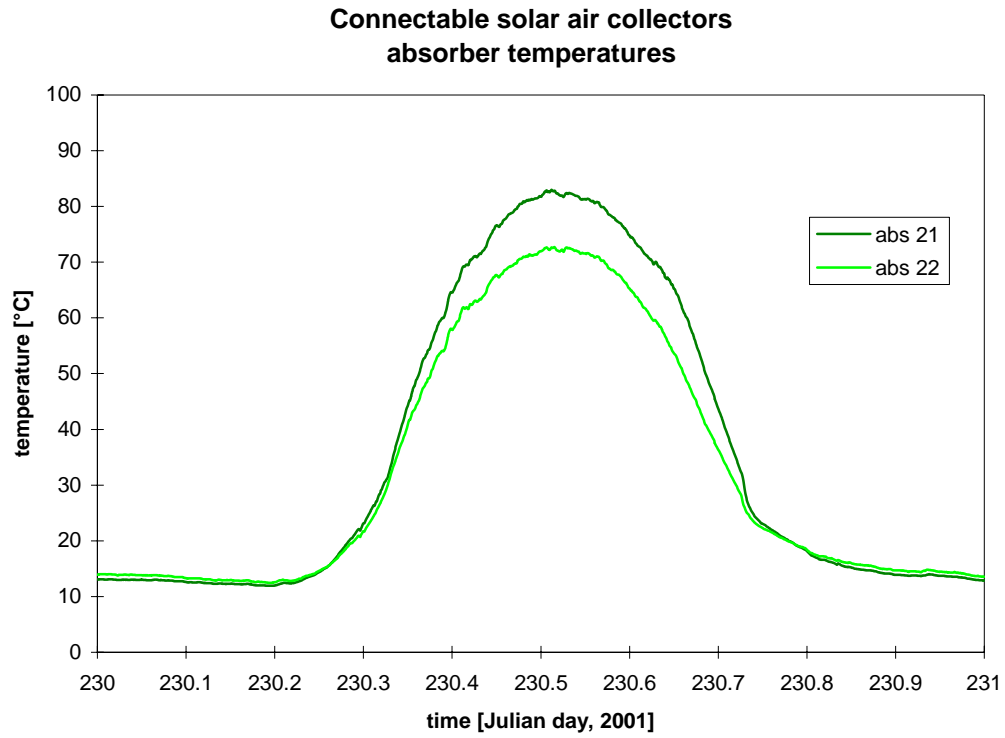
Figure 4.43. Absorber temperatures in the second connectable solar air collector on August 18.

Connectable solar air collectors
absorber temperatures
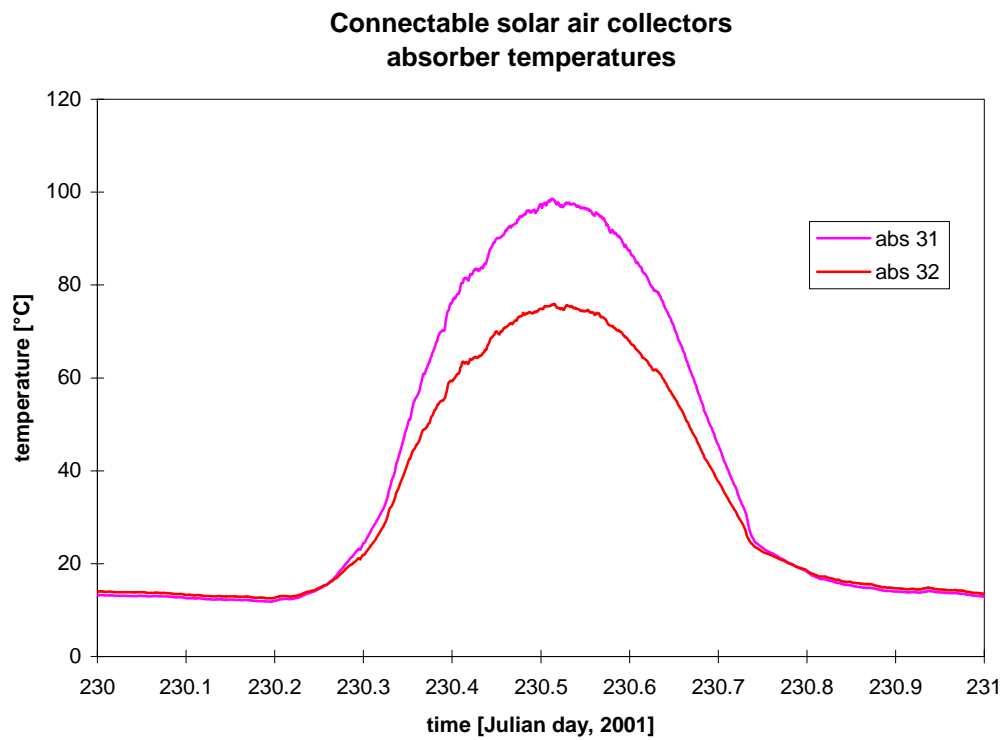
Figure 4.44. Absorber temperatures in the third connectable solar air collector on August 18.
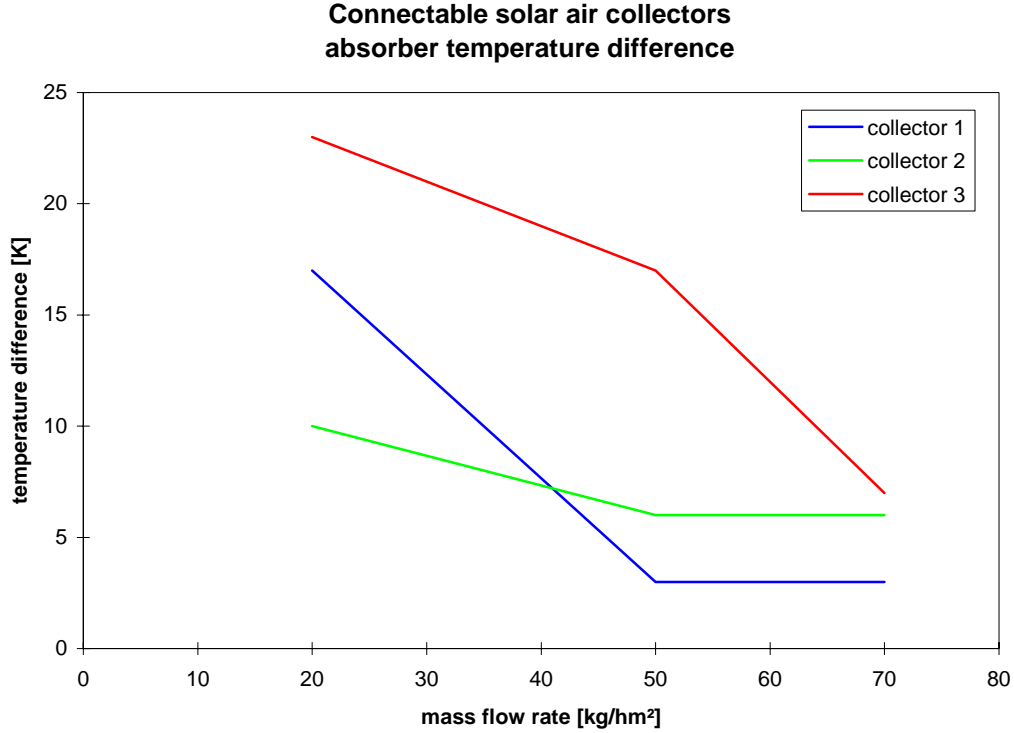
Figure 4.45. Difference between the two absorber temperature sensors of the three connectable solar air collectors at different mass flow rates.

4.2.4. Power from and efficiency of the solar air collectors

The main purpose of the solar air collectors is to heat the fresh air. Figures 4.46-47 shows the power transferred to the air when passing the solar air collectors on July 25. Figure 4.46 shows the total power in the air while figure 4.47 shows the normalized power – i.e. the total power divided with the transparent area of the collectors.

The total power transferred to the air in the solar air collectors is of course largest in the connectable solar air collectors due to this solar air collector being more than three times bigger than the two single collectors. Figure 4.47 shows that the nomalized power is in the same order of magnitude for the three solar air collectors. When comparing figure 4.47 with 4.19 it is seen that the highest normalized power is obtained for the collector with the highest mass flow rate. This is because the efficiency of the solar air collectors increases with the mass flow rate as seen in figure 1.4. Based on the power from figures 4.46-47 and the solar radiation it is possible to calculate the efficiency of the solar air collectors.

The efficiency of the solar air collectors was calculated in the following way:

$$\eta = q_{coll}/(E_{usefull} \cdot A_{coll}) \qquad\qquad [4.1]$$

where q_{coll} is the power transferred to the air [W],
  $E_{usefull}$ is the useful solar radiation [W/m²] – i.e. total solar radiation corrected for reflection losses in the cover of the solar air collectors,
  A_{coll} is the transparent area or the solar air collectors.

Figure 4.46.   Power from the sun to the air in the solar air collectors on July 25.
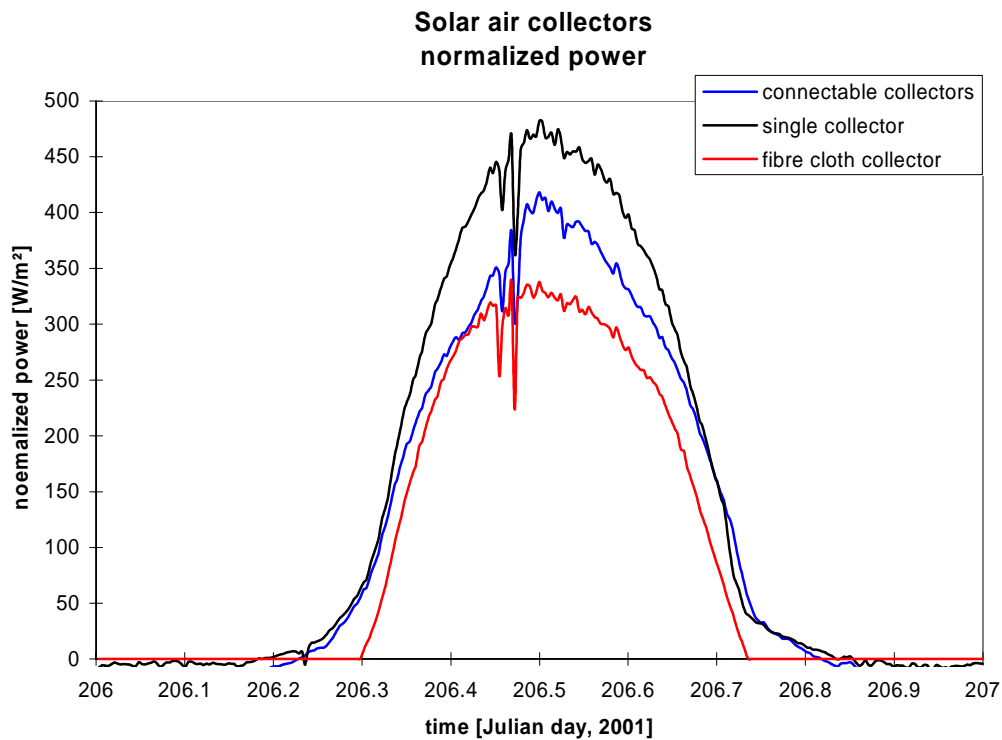
Figure 4.47. Normalized power from the sun to the air in the solar air collectors on July 25.

In the following a simple way of determining the useful radiation as been applied where only the total radiation from the PV pyranometer (see figure 3.15) has been used. The total radia-

tion on the solar air collectors was transformed into useful radiation by taking into account the reflection of the solar radiation in the glazing of the solar air collectors at periods with a non zero incidence angle for the solar radiation. In order to correct for the reflections it is necessary to calculate the split between direct and diffuse radiation based on the measured total radiation. This was done using the equations in (Duffie and Beckman, 1991). The calculated split introduces a small uncertainty compared to a case where both total and diffuse radiation is measured. The following equation has been applied to account for the reflection in the cover – the factor should be multiplied with the direct and diffuse irritation:

$$k = 1 - \tan^a(\theta/2)$$ [4.2]

where θ is the incidence angle for the radiation: the actual incidence angle for the direct radiation and 60° for the diffuse radiation. a is 3.2 (Nielsen, 1995).

Figure 4.48 shows the calculated efficiency of the three solar air collectors on July 25. Figure 4.48 shows clearly the dynamic behaviour of the efficiency of the solar air collectors. The efficiency is very dependent on the solar radiation and mass flow rate – compare with figures 4.17 and 4.19. High efficiencies (even above 100 %) are obtained when the solar radiation decreases and opposite when the solar radiation increases. This is due to the heating up and cooling down of the solar air collectors. During increasing solar radiation part of the heat from the sun is used to heat the materials of the solar air collectors and thereby leading to a lower efficiency, while during decreasing solar radiation the heat stored in the materials is transferred to the air leading to a higher efficiency. Figure 4.48 gives, thus, not a clear picture of the steady state efficiency of the solar air collectors. An even more scattered picture of the efficiency may be obtained if looking at a day with drifting clouds – i.e. very scattered solar radiation. A more thorough investigation of the efficiency of the solar air collectors will be performed in the next chapter.

Figure 4.48 further indicates as also seen in figure 4.47 that the efficiency of the solar air collectors is dependent on the mass flow rate – however, the differences seen in figure 4.48 may also be due to the differences in the construction of the solar air collectors. The latter will also be investigated in the following chapter.

4.2.5. Temperature level of the single solar air collector with fibre cloth absorber

The fan connected to the single solar air collector with fibre cloth absorber was directly driven by PV panels in order to obtain a close match between air flow rate and solar radiation as high temperatures were wished because the air was used to heat domestic hot water in a DHW tank. Figures 4.49-50 show the mass flow rate for two days in August 2001 (August 18 and 27) where the mass flow rate through the single solar air collector with metal absorber was in the same order of magnitude as the max mass flow rate through the single solar air collector with fibre cloth absorber. In this way the variable flow rate through the latter solar air collector may be evaluated. Figures 4.51–52 show the weather condition on August 18 and 27. Figures 4.49-52 show a direct coupling between solar radiation and the mass flow rate through the single solar air collector with fibre cloth absorber.

Figures 4.53-54 show the temperature increase of the air when passing the two solar air collectors on the two considered days.

**Solar air collectors
efficiency**
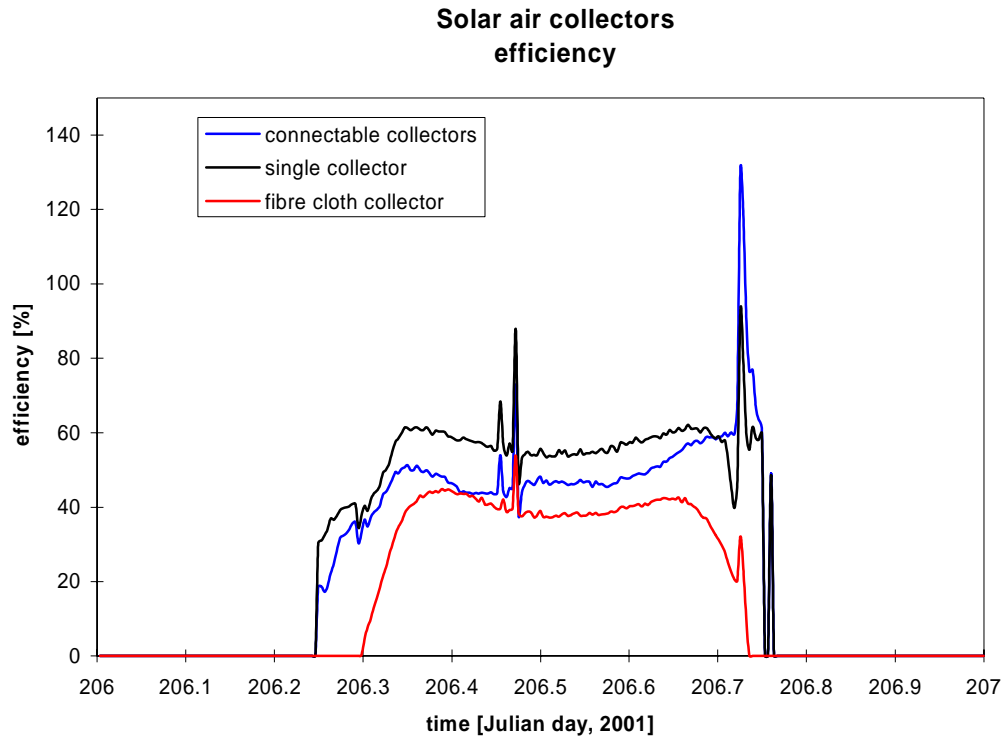
Figure 4.48. Calculated efficiencies of the three types of solar air collectors on July 25.

**Solar air collectors
normalized mass flow rates**
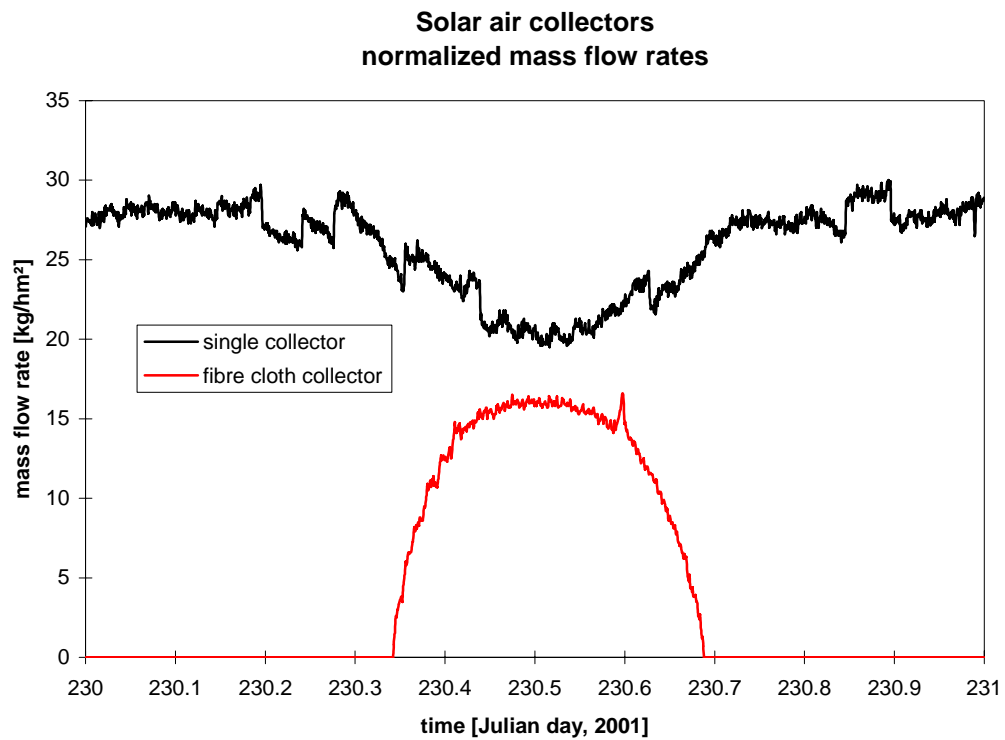
Figure 4.49. Mass flow rate through the single solar air collectors on August 18.

**Solar air collectors
normalized mass flow rates**
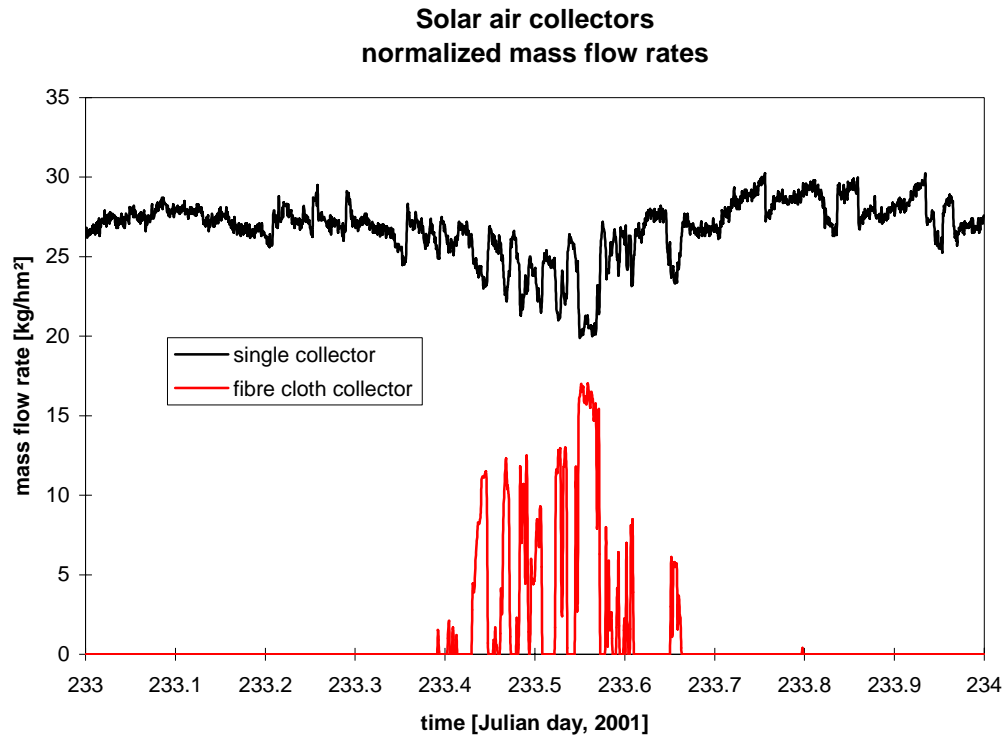
Figure 4.50. Mass flow rate through the single solar air collectors on August 21.

**Solar air collectors
weather conditions**
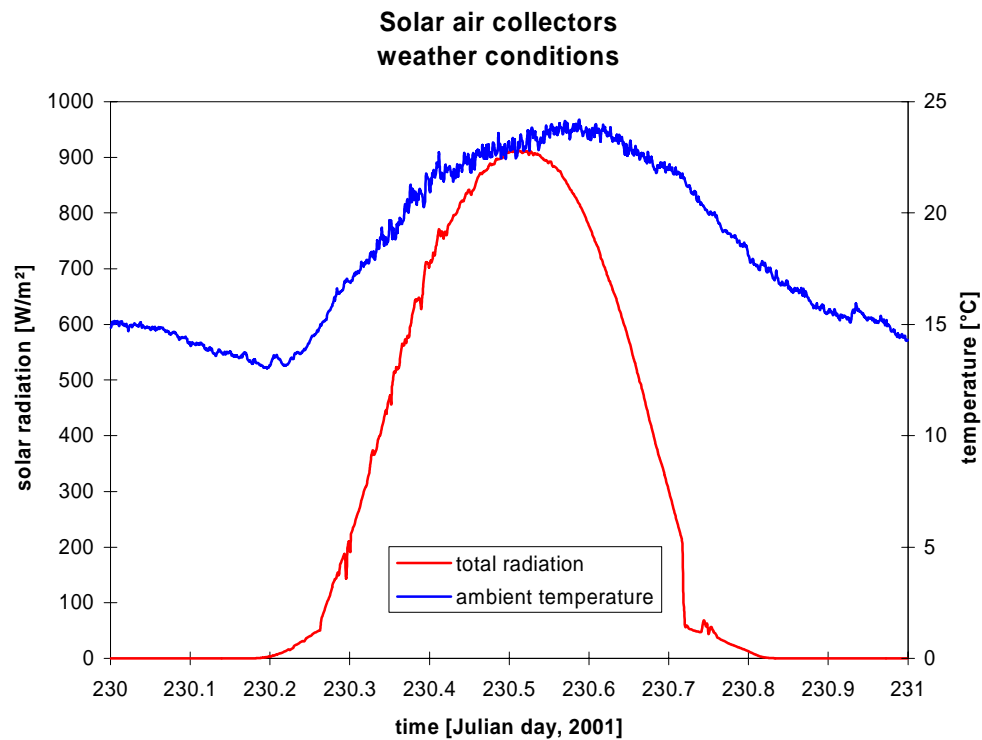
Figure 4.51. Weather conditions on August 18.

Solar air collectors
weather conditions
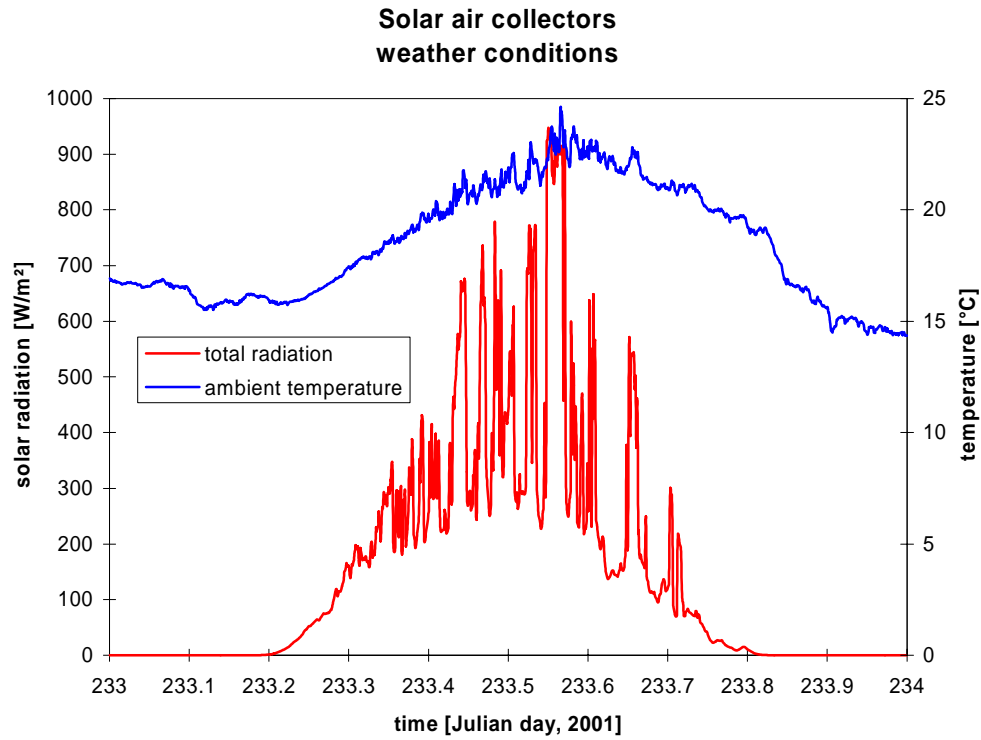
Figure 4.52. Weather conditions on August 21.

Single solar air collectors
air temperatures
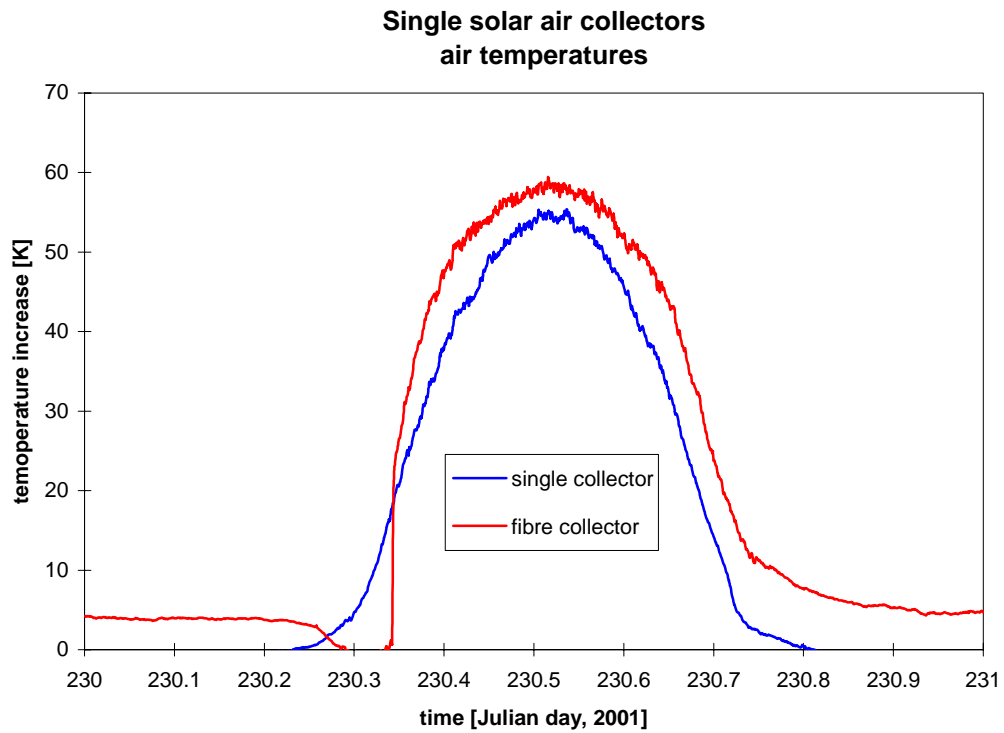
Figure 4.53. Temperature increase across the two solar air collectors on August 18.
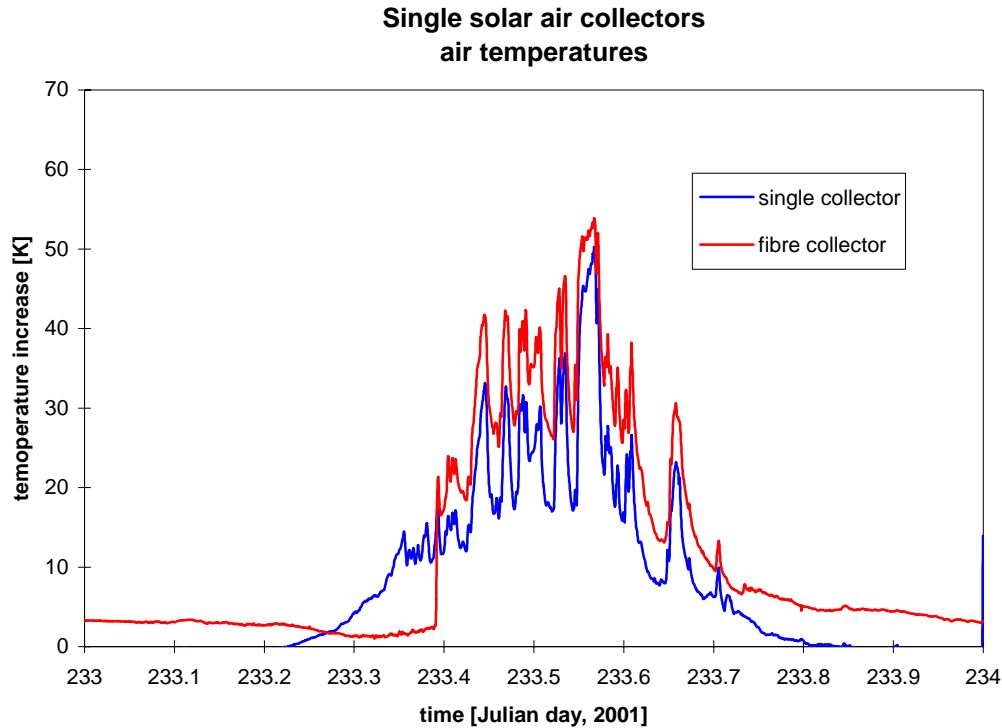
Figure 4.54. Temperature increase across the two solar air collectors on August 21.

Both figures 4.53-54 show a larger temperature increase of the air when passing the single collector with fibre cloth absorber than over the single solar air collector with metal absorber due to the higher mass flow rate through the latter collector. Figure 4.53 shows not too different temperature increases over the two collectors due to the stable solar radiation. The curves show not much difference expect that the temperature increase increases more rapidly in the morning for the fibre cloth collector due to the lower mass flow rate. Figure 4.54 show almost identical scattering for the two collectors, however, the temperature increase over the fibre cloth collectors if most of the time 10 K higher than over the collector with metal absorber. More useful temperatures for heating DHW is, thus, obtained for the fibre cloth collector. However, the higher temperatures due to the lower mass flow rate is not obtained for free. The lower mass flow rate leads to a lower efficiency and thereby to a lower power from the collector. This is illustrated in figure 4.55-56. But it is better to obtain some useful power than a lot of not useful power. In the system with the single solar air collector with fibre cloth absorber the power is only useful when the air reaches a certain temperature level dependent on the actual temperature level of the DHW tank – i.e. higher air temperatures are required when the temperature of the tank increases. The performance of the system with the single solar air collector with fibre cloth absorber is further evaluated in (Jensen and Bosanac, 2002) – please refer to this report if interested.

Figures 4.53-54 show that there is an temperature increase over the single solar air collector with fibre cloth absorber during the night. This is caused by the heat loss from the tank to the solar air collector during the night.
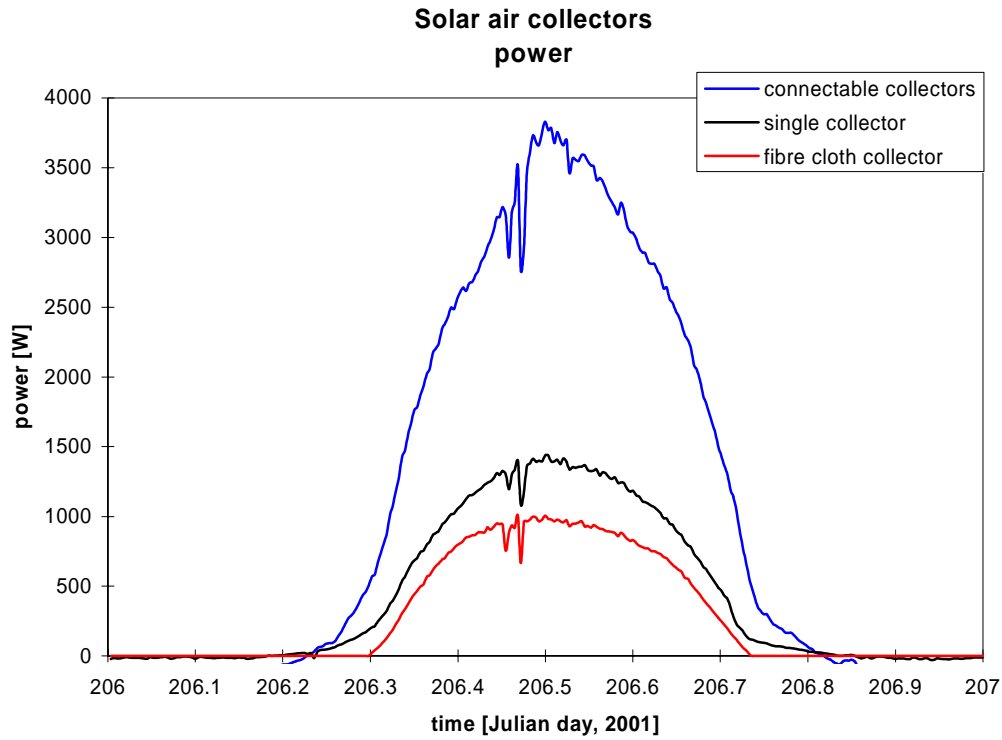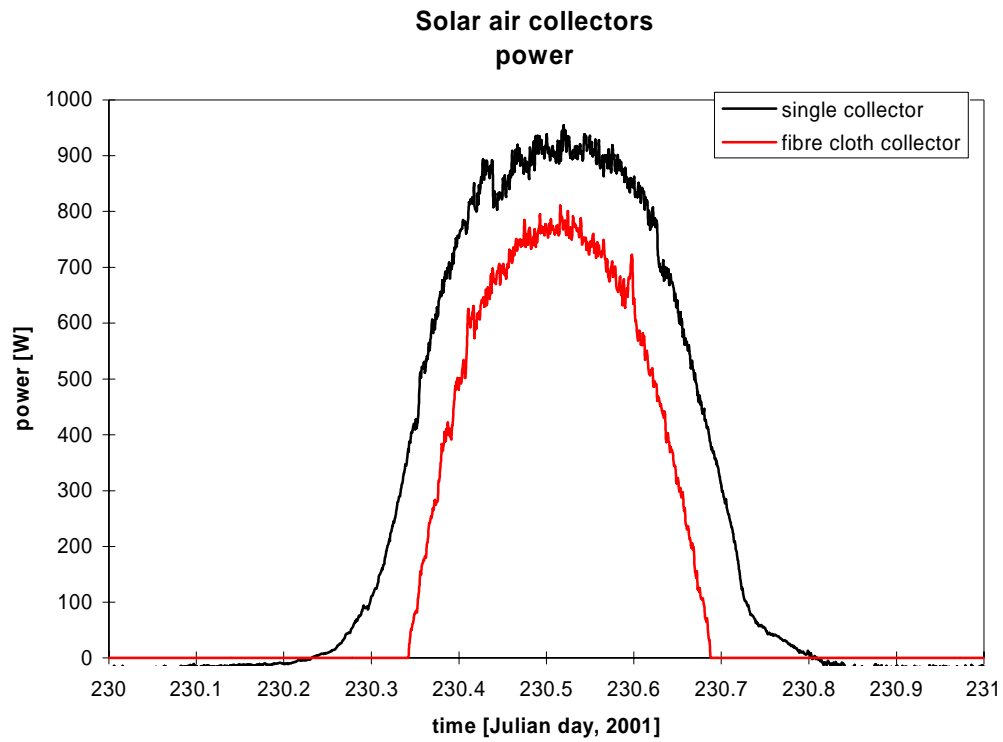
Figure 4.55. Power from the sun to the air in the solar air collectors on August 18.
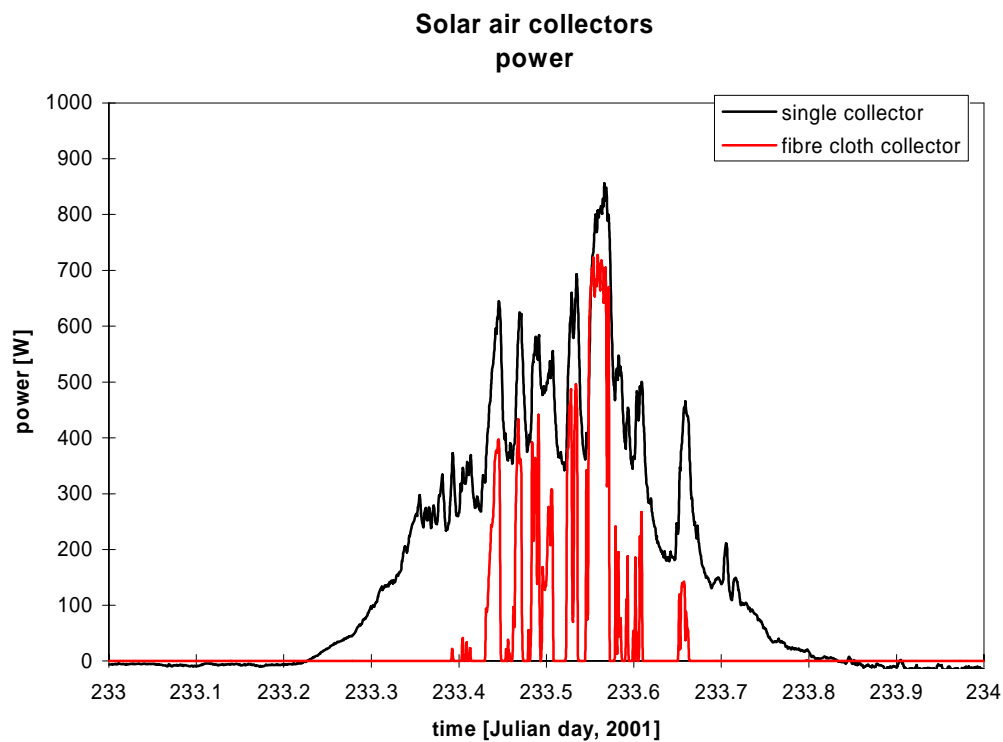
Figure 4.56. Power from the sun to the air in the solar air collectors on August 21.

4.2.6. Smell

The investigated solar air collectors have been developed for pre-heating of fresh air to buildings. It is thus outmost important that the air don't get polluted when passing the solar air collectors. Pollution may be fibres, dust, toxic gasses, smell, microbiologic particles, etc.

The insulation of the collectors is encapsulated and the fibre cloth doesn't give of fibres. Dust should be stopped at the inlets to the collectors by removable filters. It is not expected that microbiological activities will occur in the solar air collectors due to the heating up and thereby drying of the air in the collectors, however, microbiological activity may occur in the inlet filters, which makes it important that the filters can be replaced or cleaned. Smell and maybe toxic gasses is a problem in the investigates solar air collectors. At low air flow rates the temperature of the air out of the collectors may get as high as 90°C. There is a very noticeable smell in the air leaving the solar air collectors at high temperature levels. A smell of warm fibreboard, which of course is due to the heating up of the fibreboard on top of the insulation in the collectors. It has not been determined if toxic gasses also are released. However, the cause of the smell should be removed from the collectors. The fibreboard should – thus be replaced with a material, which don't give off smell – or any other pollution.

4.3. Conclusions on the measurements

The measurements reveal that it is possible to create a rather even distribution of the air flow through the perforated metal absorbers of three interconnected solar air collectors. The tests were carried out for three solar air collectors each of approx. 3 m², however, it should be possible to connect even more collectors into one larger solar air collector as long as the pressure drop in the manifold air gab behind the absorber stays low.

The pressure loss measurements show that the pressure drop across especially the connectable solar air collectors is too high. The high pressure loss will lead to a too high power demand of the fan connected to the solar air collectors. It is believed that it should be possible to decrease the pressure loss of all three solar air collectors without loosing efficiency because of an uneven air flow distribution across the solar air collectors.

Especially the inlet diffuser of the connectable solar air collectors should be modified to allow for a lower pressure drop over this devise. However, also the inlets to the single solar air collectors and the outlets of all the collectors should be examined carefully in order to find measures for reducing the pressure losses.

The connectable solar air collectors are very easy to connect, but the connections were in the present form too difficult to make airtight when installing the collectors. Effort should, therefore, be put in a further development of the connection details in order to maintain the easy connection of the collectors while ensuring air tight connections also when the collectors are mounted at less favourable conditions as on the test rig – i.e. also ensuring air tightness when the connections have to compensate for not straight support for the collectors.

5. Efficiencies

One of the main objectives of the project was to determine and compare the efficiencies of the three solar air collectors. In order to evaluate the efficiencies of the solar air collectors two different methods have been applied: a simple method and an advanced method based on statistical identification. The reason for applying two different methods was to characterize the solar air collectors with the lowest possible uncertainty and further to test the accuracy of the simple method.

- The benefit of the simple method is that it is very easy and fast to use and quickly gives an idea of the steady state efficiency at a certain flow rate – the drawback is that it only gives this value and that clear sky conditions around noon is required.

- The benefit of the advanced method is that it doesn't necessarily require clear sky condition, it not only gives the efficiency of the collectors at inlet temperatures equal to the ambient temperature, it gives the thermal capacity of the collector and the incidence angle modifier for the cover – the drawback is that it is more time consuming and it requires skill to identify the parameters.

It was wished to test the simple method against the advanced method because it often is more applicable to used this method rather than the advanced method, but in order to do so it is important that the method has been validated against a proven method.

5.1. Simple method for determination of the efficiency

The simple method is based on the way to calculate the efficiency described in section 4.2.4. The method was developed in (Jensen, 1999) but was never before validated. The radiation – total radiation - is measured with one pyranometer. Based on this the useful radiation is determined as described in section 4.2.4. However, the obtained efficiency shown in figure 4.48 gives only an indication of the efficiency of the solar air collectors. Due to the dynamic behaviour of the efficiency in figure 4.48 it is not possible to determine the steady state efficiency of the collectors.

The essence of the method is to show the efficiency and mass flow rate as a function of the useful solar radiation on the solar air collectors. The efficiency of the solar air collectors is too low during periods with increasing solar radiation and too high during periods with decreasing solar radiation due to the heating and cooling of the materials in the solar air collectors. Therefore, the steady state radiation must be found just around the time, when the radiation level on a sunny day is at its maximum. The thermal capacity does, however, that the right time is somewhat after the maximum solar radiation occurs dependent on the amount of thermal mass. But on a day with clear sky conditions there is an almost vertical plateau on the curve showing the solar radiation – see e.g. figures 4.51 (and 4.53), which allows for the determination of the steady state efficiency of the solar collectors with a rather good precision as seen later.

Figure 5.1 shows the calculated efficiency for the single solar air collector with fibre cloth absorber from figure 4.48. The method gives an efficiency of 37 % at a flow rate of 26.5 kg/hm² - both values shown at the blue arrows. Due to the clouds just before noon figure 5.1 is not as clear as could be hoped. Figure 5.2 shows the same as figure 5.1 but for August 18

with clear sky conditions. Here an efficiency of 29.5 % was obtained at a flow rate of 16 kg/hm².

**Fibre cloth collector
efficiency - mass flow rate**
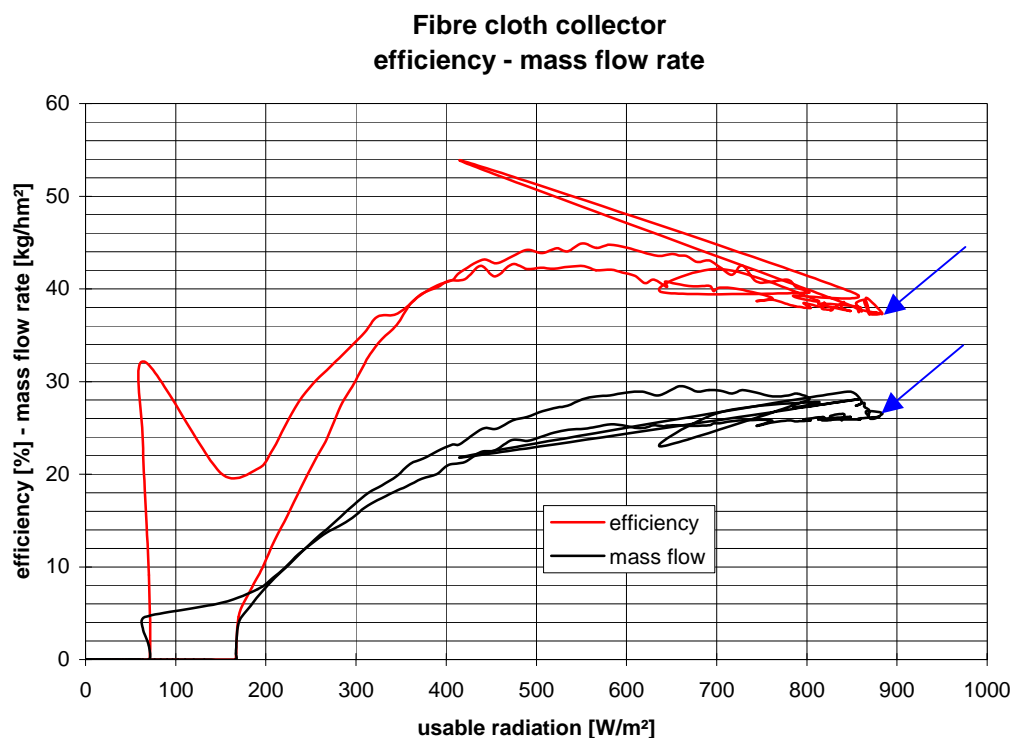
Figure 5.1.   The efficiency and mass flow rate of the single solar air collector with fibre cloth absorber dependent on the useful radiation on July 25.

**Fibre cloth collector
efficiency - mass flow rate**
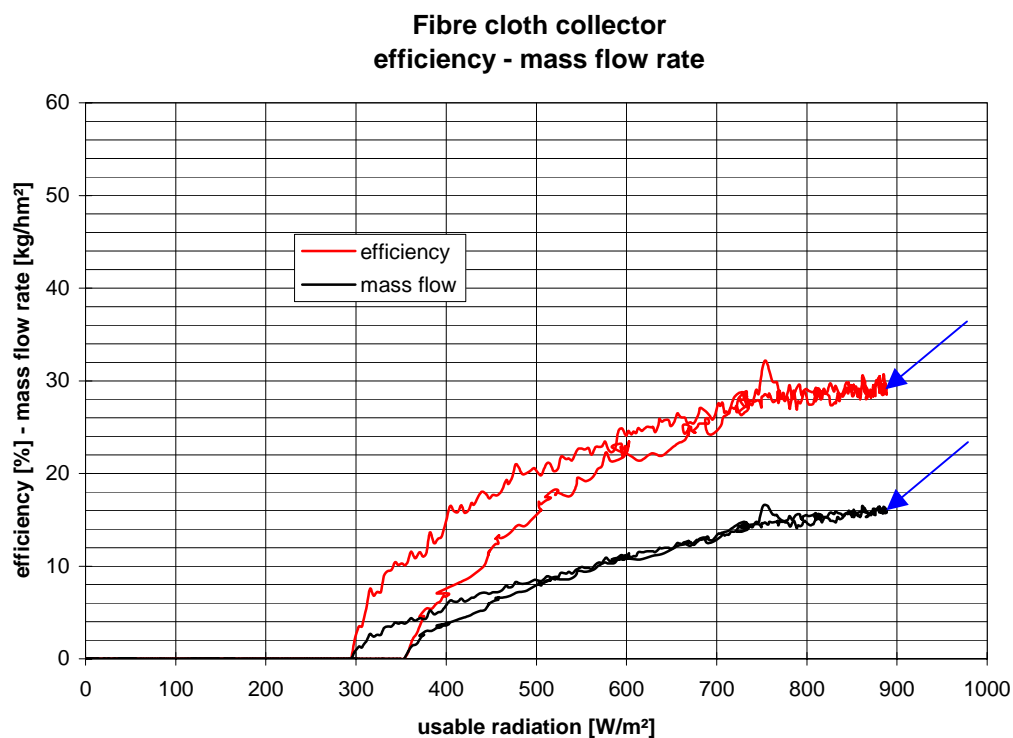
Figure 5.2.   The efficiency and mass flow rate of the single solar air collector with fibre cloth absorber dependent on the useful radiation on August 18.

Table 5.1 shows the obtained efficiencies for 10 useful days with clear sky or almost clear sky conditions – 9 useful days in the period mid July-August is a low number which clearly illustrates one of the drawbacks of the method. The efficiency was only obtained for the single solar air collector with fibre cloth absorber for October 6. The aim of this measurement was to obtain the efficiency for this collector at a higher mass flow rate than could be obtained with the PV panel driven fan. A new fan similar to the fan applied on the single solar air collector with metal absorber was therefore installed.

Day	Connectable collectors		Single collector		Fibre cloth collector	
	mass flow kg/hm²	efficiency %	mass flow kg/hm²	efficiency %	mass flow kg/hm²	efficiency %
July 18	67	55.5	84	58.0	32.5	43.0
July 19	71	55.5	84	59.0	36	48.0
July 25	50	47.0	65	54.5	26.5	37.0
July 26	59	52.5	66	56.5	30	40.5
July 27	42	43.5	52	50.0	15	26.0
August 15	36	43.5	36	44.5	15	28.0
August 16	35	43.5	35	43.5	15.5	28.5
August 18	20	34.0	20	35.0	16	29.5
August 22	20	34.0	20	30.5	16	27.5
October 6	-	-	-	-	69	57.0

Table 5.1.   The efficiency of the solar air collectors dependent on the flow rate obtained by the simple method.

The values from table 5.1 are shown graphically in figure 5.3. Although only data from 10 days the measurements from the simple method for determination of the efficiency of solar air collectors for pre-heating of fresh air gives a good impression of the efficiency of the solar air collectors if the efficiencies are found for mass flow rates which are well distributed over the range of interest. Figure 5.3 further shows that efficiencies for one collector found for identical mass flow rates are almost identical. The reproducibility of the method is thus high – i.e. the measuring and calculation uncertainties are low.

Figure 5.3 shows that the efficiency of the three solar air collectors are almost identical – especially when considering a certain uncertainty on the found uncertainties.

Figure 5.4 shows the same values as figure 5.3 but now including the efficiency of two of the solar air collectors from the IEA Task 19 investigation (Fechner, 1999) – the collector of the Summer House Package with identical absorber as the single solar air collector with fibre cloth absorber and the collector with the highest efficiency – the rather expensive Grammer collector. The blue squares show the values for the collector of the Summer House Package found in (Fechner, 1999). The blue line is a regression line based on these values.

Figure 5.4 shows that the efficiency of the here investigated solar air collectors is almost as high as the collector from the Summer House Package which had the second highest performance of the investigated solar air collectors in IEA Task 19 – see figure 1.4. The aim of obtaining the same high efficiency as the collector of the Summer House Package seems thus to be fulfilled – however, no firm conclusion can be made before the results from the advanced

method for determination of the efficiency of solar air collectors have been investigated and the simple method has been validated.

Solar air collectors efficiencies
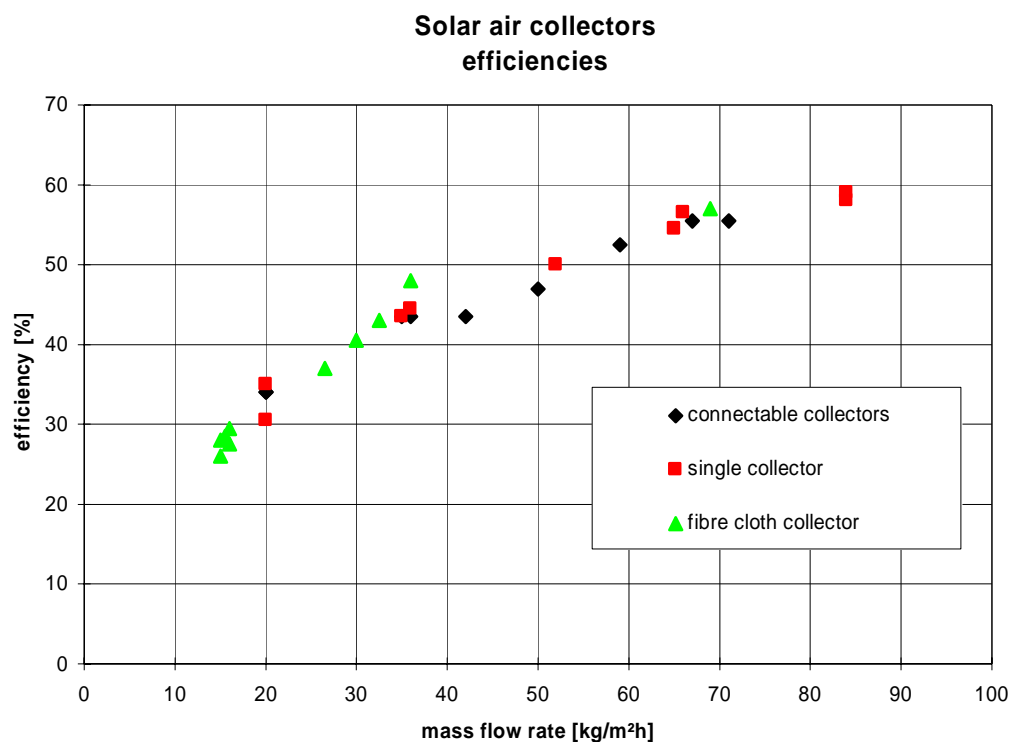
Figure 5.3.   The values from table 5.1 shown graphically.

Solar air collectors efficiencies
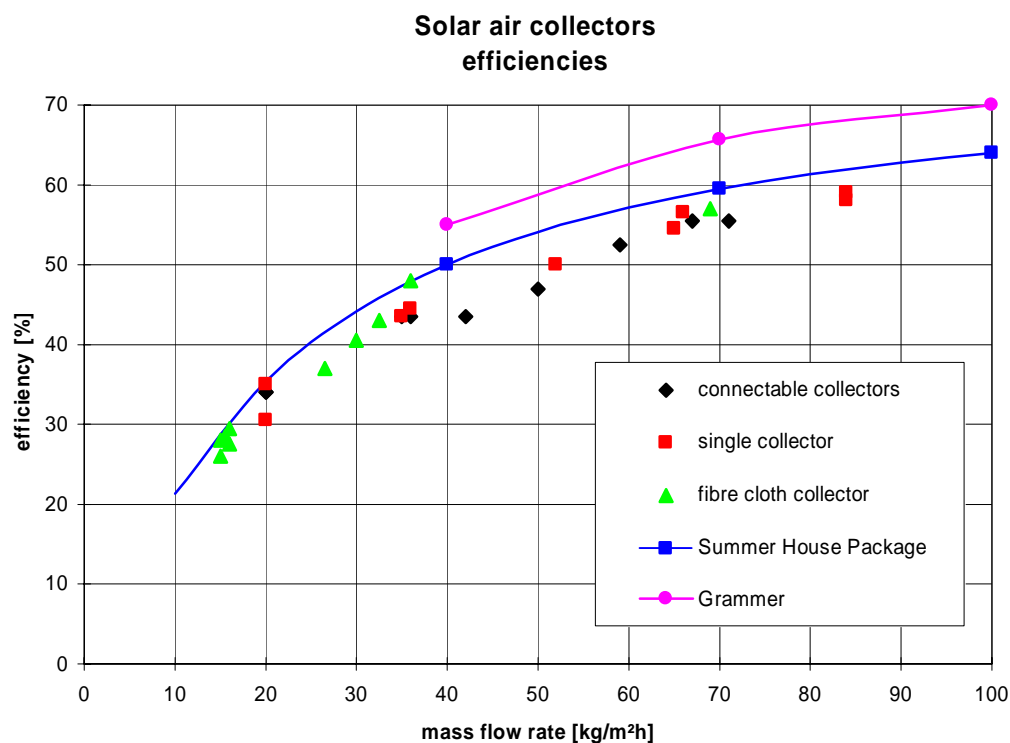
Figure 5.4.   The values from table 5.1 shown together with the efficiency of two solar air collectors measured in IEA Task 19 (Fechner, 1999).

5.2. Advanced method for determination of the efficiency

The advanced method for determination of the efficiency of solar air collectors is based on identification of the parameters characterizing the solar air collectors. The method was developed and validated by Solar Energy Centre Denmark, Danish Technological Insitute and is fully described in (Bosanac and Jensen, 1997) where also the results from the validation may be found. A paper on the method for the EuroSun 2000 conference is included in appendix C. The method is briefly described in the following. A brief description of the validation results may also be found in appendix C.

5.2.1. Brief description of the advanced method

5.2.1.1. Collector model

In order to be able to characterise a solar air collector a modified multi-node collector model (Bosanac et al, 1993) has been applied. The model has the following features:

- The collector is modelled with distributed capacities in the flow direction.
- A linear dependence of the collector efficiency factor on the collector flow rate is assumed.
- A linear dependence of the heat loss coefficient on the surrounding air speed as well as on the temperature difference between collector and ambient is assumed.
- Incident angle modifiers for direct (as a function of incident angle) and diffuse irradiance are used.

The main features of the model are briefly described in the following. For a description of the different parameters please refer to the list of nomenclature in appendix C

Each node of the solar air collector is characterised by:

$$C_n \, dT_n/dt = A_n \, k_m \, F'[(\tau\alpha)_0 G_{eq} - U_L(T_n - T_a)] - q_{u,n} \qquad [5.1]$$

where G_{eq} is the equivalent normal solar radiation taking into account the components of the solar radiation multiplied by the respective incident angle modifiers:

$$G_{eq} = K_{\tau\alpha, \, beam} \, G_{beam} + K_{\tau\alpha, diff} \, G_{diff} + K_{\tau\alpha, alb} \, G_{alb} \qquad [5.2.]$$

U_L is the overall heat loss coefficient:

$$U_L = U_0 + U_v \, v + U_T(T_n - T_a) \qquad [5.3]$$

$q_{u,n}$ is the rate of energy gain by the collector node:

$$q_{u,n} = m_c c_p(T_n - T_{n-1}) \qquad [5.4]$$

The coefficient characterising flow-rate dependence:

$$k_m = 1 + c_m \, m_c \qquad [5.5]$$

$(\tau\alpha)_0$ is the transmittance-absorbtance-product at normal incidence. An incidence angle modifier for direct radiation is defined by the modified Ambrosetti (Ambrosetti, 1983) equation:

$$K_{\tau\alpha, beam}(\theta) = 1 - \tan^{1/r}(\theta/2) \qquad [5.6]$$

The incident angle modifier for diffuse radiation assuming isotropic distribution is used as derived in (Bosanac et al, 1993). The incident angle modifiers for diffuse radiation and for the albedo are assumed to be equal. They are both derived in (Bosanac et al,1993) as a function of the parameter r.

The following parameters fully characterise the presented model:

- The optical efficiency of the collector array: $F'(\tau\alpha)$.
- The overall heat loss coefficient if $T_n=T_a$ and v=0: U_o.
- The coefficient characterising wind dependence of the overall heat loss: Uv.
- The coefficient characterising temperature dependence of the overall heat loss: U_T.
- The total thermal capacity of the collector array: C.
- The incident angle modifier coefficient: r.
- The coefficient characterising the flow-rate dependence; c_m.

5.2.1.2. Principle of the test procedure

The performance of solar air collector arrays depends on their design parameters and on various weather and operating conditions, e.g. irradiance, ambient temperature, wind velocity, inlet air temperature. The method uses detailed, in-situ measured data as a function of time in order to identify the most relevant parameters characterising the performance of the solar collectors.

In order to evaluate long-term system performance and enable diagnosis of sources of array malfunctioning, it is primarily necessary to identify array parameters. Sets of array parameters are not necessarily identical for each array to be tested.

Therefore, in the first step of the procedure, it is necessary to estimate the influence of the array parameters characterising the array performance. For example, if the flow rate in the collector loop is fixed or a majority of data is available for a single, specific flow rate, the parameter characterising flow rate dependence may not be identified.

The basic principle of the procedure is given in figure 5.5.

The parameter estimation involves identification of system parameters described by the mathematical model described in the previous section.

Two sets of criteria are defined in order to assure reliable test results:

- The first set of criteria deals with requirements regarding influencing variables (irradiance level, reduced temperature (mean temperature of the air in the collector minus ambient temperature divided by the solar radiation) range, etc.). These criteria indicate whether enough data have been collected.

- The second set of criteria deals with statistical measures regarding identified array parameters. These criteria being met means that the test is successfully accomplished.
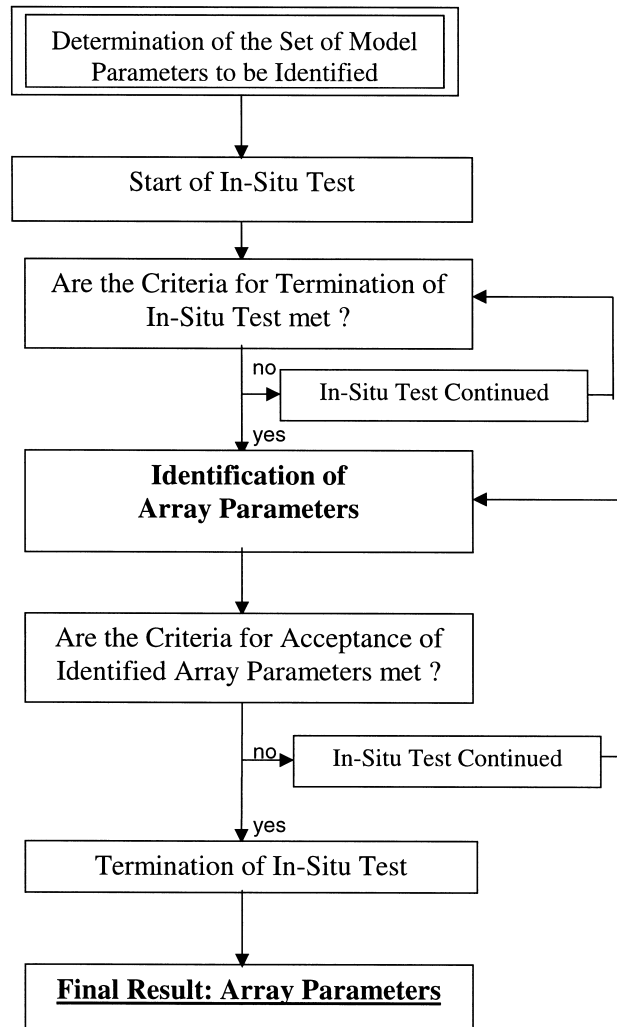
Figure 5.5.   Principle of the test method.

5.2.1.3. Criteria for termination of the measurements

The criteria for accurate identification of the system parameters deal with:

- Available amount of solar energy incident on the collector plane during a measuring period. This criterion assures that enough data with high collector power are available.

- Necessary range of variation of influencing parameters. These criteria should provide more accurate identification of respected parameters.

5.2.1.4. Criterion for the minimal irradiation during a test sequence

The first criterion deals with the amount of solar energy incident on the collector plane during the test sequence. The minimum hemispherical irradiation available on the collector plane during a test sequence is recommended to be:

120 MJ/m^2

assuring that a portion of direct irradiation exceeds 50% of the total and/or that at least 50% of data correspond to a level of hemispherical irradiance higher than 400 W/m² .

This criterion assumes identification of the basic set of parameters including; optical efficiency, incident angle modifier, overall heat loss coefficient and thermal capacity. Depending on the number of additional parameters to be estimated (if considered essential for the system), a longer time period for monitoring might be necessary.

5.2.1.6. Criteria for variability of influencing variables

This request deals with the necessary variability of the influencing variables. The variability determines directly the accuracy of the identified values. However, type and dimension of the array and its operating conditions influence these spans and the listed values should, therefore, be used for orientation only. Table 5.2 gives an indication of the recommended range of variation to be scanned during the measurements (here only data having hemispherical irradiance above a certain level should be considered e.g. 400 W/m²).

Influencing variable	Recommended Range of Variations
$T_m - T_a$	10 – 50 (70) K
Reduced Temperature	0.02 - 0.12 (0.2) K m² /W
Wind Velocity	1 - 5 m/s

Table 5.2.   Recommended range of the variation of influencing parameters (values in brackets correspond to preferable values).

It is reasonable to assume that after a certain measuring period, maximum possible variation of the influencing parameters is reached so that a further prolongation of the measurements would not considerably contribute to the de-coupling of the parameters´ associated errors. For some systems a high correlation between uncertainties can not be avoided. If particular correlation coefficient is too high one should rather use a lumped parameter, if possible, characterising both effects described by the separate parameters. In the case of the heat loss coefficient, it is preferred to avoid identification of the respective components (e.g. U_o, U_v, U_T) whenever the respective correlation coefficient remains being too high.

However, in the case of high coefficient of correlation between uncertainties describing diverse physical effects (e.g. the optical efficiency and the heat loss coefficient) - it is not possible to use lumped parameter and we must notice the correlation as it is. If it is high it means that the array is operating in a small range of reduced temperatures.

5.2.1.6. Identification of array parameters

The identification of the collector parameters is carried out using the Dynamic System Testing (DST) algorithm developed by Spirkl (Spirkl, 1990).

Figure 5.6 shows the DST procedure. The measured variables, i.e. collector inlet and outlet temperature, air mass flow rate, ambient temperature, hemispherical and diffuse irradiance are input variables to the theoretical model. Then, the difference between measured system power and modelled power is minimised by optimising the set of parameters. As a result of this pro-

cedure the estimated errors of the parameters are given. If the same model is used for simulation, the error of the predicted energy output can be estimated. In order to apply dynamic fitting for the identification of the collector array parameters a program subroutine was developed (Bosanac, 1993) characterising a dynamic collector model as described in the previous section.
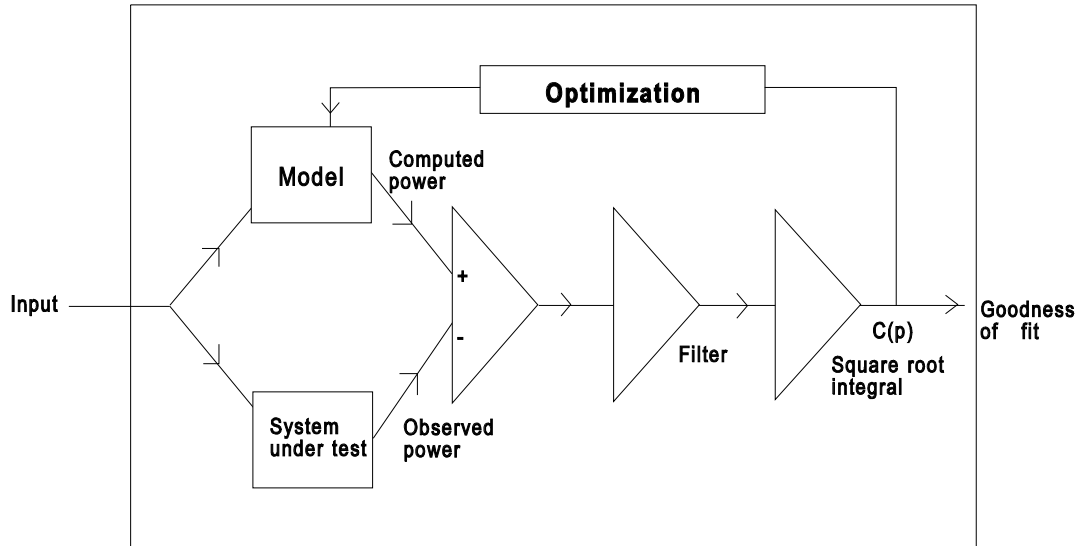
Figure. 5.6.   Schematic diagram of the Dynamic System Testing procedure.

The main benefit of the dynamic test is that stationary (i.e. steady state) conditions of the system are not required. The system is tested under normal, dynamic operation conditions and the monitoring data is used for identification of the system parameters.

5.2.1.7.   Acceptance criteria for test results

The identified parameters themselves have to satisfy general 'acceptance' criteria mainly dealing with statistical measures. The work in (Bosanac and Jensen, 1997) has shown that the identified parameters are reliable if the following statistical requirements are met as stated in table 5.3.

Symbol	Basic parameters	Units	Permitted standard deviation
$F'(\tau\alpha)_0$	Zero-heat-loss efficiency of array	-	10 %
C_m	Flow rate dependence	s/kg	10 %
U_L	Heat loss coefficient of array	W/Km^2	25 %
U_T	Heat loss temperature dependence	W/K^2m^2	35 %
Cc	Collector array capacity	kJ/K	15 %
r	Incident angle modifier coefficient	-	30 %

Table 5.3.   Permitted standard deviations.

If these criteria are not met for the basic set of parameters, an additional test sequence exceeding in total 35 MJ/m² is required. After this has been collected, the identification procedure is to be repeated using all available data.

5.2.2. Application of the advanced method

The list of output from the detailed method shown on page 73 was in the present project altered to the following list.

- The optical efficiency of the collector array: F'($\tau\alpha$).
- The overall heat loss coefficient combining U_o, U_V and U_T into one U-value: U_L
- The total thermal capacity of the collector array: C.
- The incident angle modifier coefficient: r.

The three U values (U_o, U_V and U_T) was combined into one overall heat loss coefficient as it was judge that a more precise determination wouldn't add much information on the performance of the solar air collectors.

The flow rate dependency was taken care of in another way as seen later.

The efficiency of a solar air collector may be defined in several different ways dependent on the temperatures the efficiency is based on. The traditional European way is to define the efficiency based on the mean temperature of the fluid in the collector:

$$\eta_m = F'(\tau\alpha) - U_L \cdot (T_m - T_a)/G \qquad [5.7]$$

where F'($\tau\alpha$) is one of the values identified,
U_L is one of the values identified – defined for the mean temperature of the fluid in the collector,
T_m is the mean temperature of the fluid in the collector,
T_a is the ambient temperature,
G is the useful solar radiation on the collector.

Another way of defining the efficiency of a solar air collector is the American (ASHRAE) way based on the inlet temperature of the fluid to the collector:

$$\eta_i = F_R(\tau\alpha) - U_{Li} \cdot (T_i - T_a)/G \qquad [5.8]$$

where $F_R(\tau\alpha)$ and U_{Li} is based on the inlet temperature,
T_i is the inlet temperature to the collector.

As the inlet temperature to the collector is ambient air $T_i = T_a$, which means that equation 5.8 may be transformed to:

$$\eta_i = F_R(\tau\alpha) \qquad [5.9]$$

$F_r(\tau\alpha)$ may be found in the following way:

$$F_R(\tau\alpha) = F'(\tau\alpha)(\dot{m}Cp/A_c)/(\dot{m}Cp/A_c + F'(\tau\alpha)U_L/2) \qquad [5.10]$$

where $\dot{m}$ is the mass flow rate of the fluid,
Cp is the thermal capacity of the fluid,
A_c is the transparent area of the collector.

$F_R(\tau\alpha)$ is dependent on the mass flow rate of the fluid through the collector:

$$F_R(\tau\alpha) = f(\dot{m}) \qquad\qquad [5.11]$$

Based on the identified parameters $F'(\tau\alpha)$ and U_L and equations 5.9-11 it is possible to determine the efficiency of the solar air collectors dependent on the mass flow rate where equations 5.9-11 are applied at discrete intervals of mass flow rates in order to obtain maximum precision in the dependency on the mass flow rate.

5.2.3. Results from applying the advanced method on the measurements

Figure 5.7 shows the results of applying the advanced method on the obtained measurements while table 5.4 gives the precision of the identification of the parameters $F'(\tau\alpha)$ and U_L.
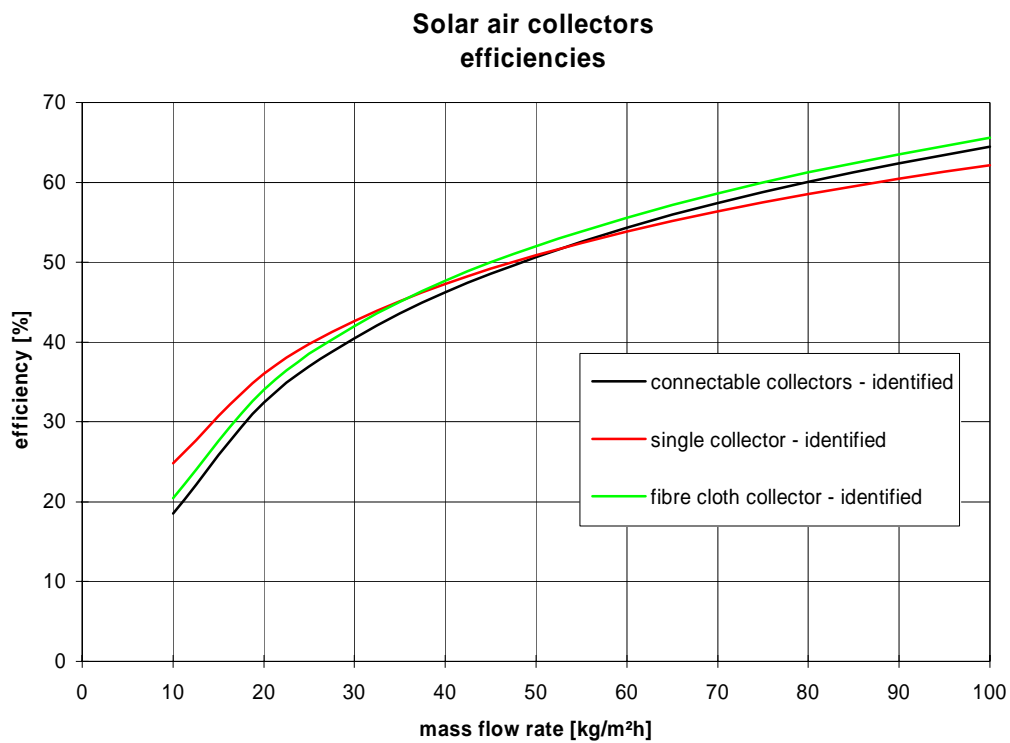
Figure 5.7.   The efficiency of the three solar air collectors found using the advanced method.

Collector	Optical efficiency $F'(\tau\alpha)$	Heat loss coefficient U_L
Connectable solar air collectors	0.9 %	1.0 %
Single solar air collectors with metal absorber	0.5 %	0.9 %
Single solar air collector with fibre cloth absorber	0.8 %	1.1 %

Table 5.4.   The standard deviation when identifying $F'(\tau\alpha)$ and U_L of the three solar air collectors.

Table 5.4 shows that the parameters of the three solar air collectors are identified very precisely – i.e. a much higher precision than the acceptance criteria – compare table 5.4 with 5.3. Figure 5.7 shows as figure 5.4 that the efficiency of the solar air collectors is very similar – especially the efficiency for the connectable solar air collectors and the single solar air collector with fibre cloth absorber – differences of less than 2 % point. The efficiency of the single solar air collector with metal absorber is somewhat higher at low mass flow rates than the efficiency of the other two solar air collectors and lower at high mass flow rates – figure 5.3 doesn't show this difference. The lower efficiency of the connectable solar air collectors compared to the single solar air collector with metal absorber was expected at low flow rates based on the pressure drop measurements in section 4.1.2.

The efficiency of the single solar air collector with fibre cloth absorber is in figure 5.7 really only valid for mass flow rates up to 30 kg/m²h. A measuring sequence with at higher mass flow rate was carried out as seen in figure 5.3 but the data set could not be used to identify the parameters of the solar air collector at this mass flow rate – the standard divinations were too large and the identified parameters were completely out of range. However, as seen in figure 5.3 the efficiency of the three collectors were identical at this mass flow rate. Figure 5.8 shows the results from the simple and the advanced method for determination of the efficiency of the three solar air collectors.
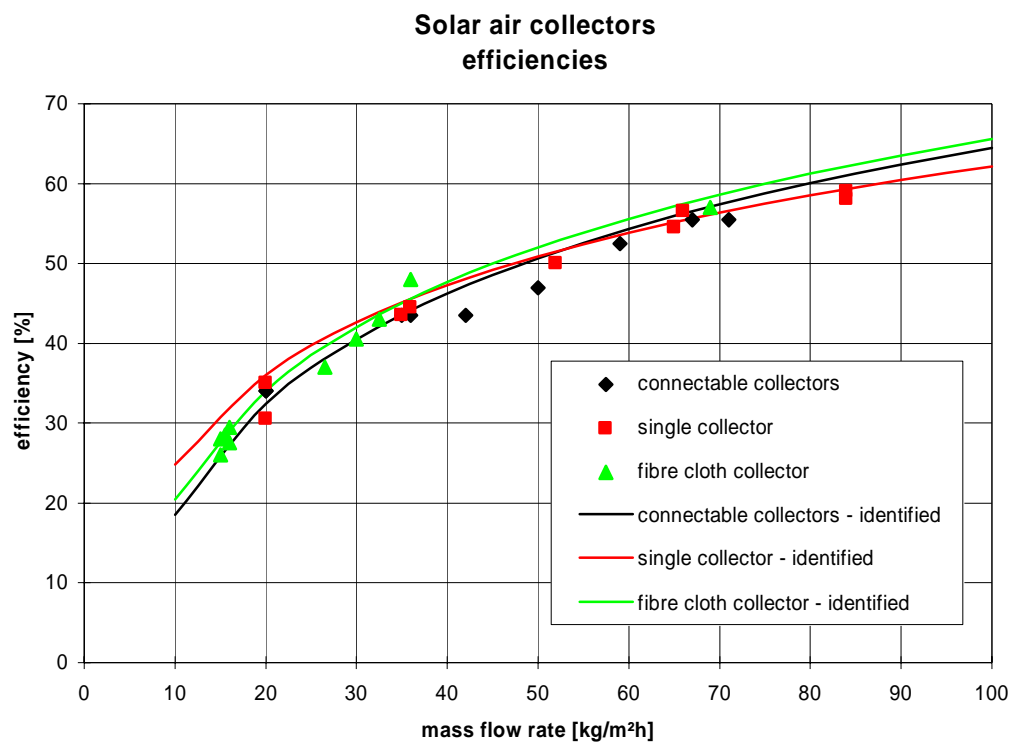
Figure 5.8.   The efficiency of the three solar air collectors found using both the simple and the advanced method.

Figure 5.8 shows that the two method lead almost to the same efficiency for the three solar air collectors except for smaller fluctuations of the simple method. Considering the uncertainty of both methods the results of the two methods are quite similar. Based on figure 5.8 it can be stated that the simple method gives rather correct results maybe with a tendency to be a little conservative in the prediction of the efficiency. The advantage of the advanced method is,

however, that it gives far more information on the considered solar air collectors than the simple method as shown later.

The efficiency of the three curves shown in figures 5.7-8 can be expressed in the following way:

Connectable solar air collectors: $\eta = 0.1994 \cdot \ln(\dot{m}) - 0.2733$ [5.12]
Single solar air collector with metal absorber: $\eta = 0.1621 \cdot \ln(\dot{m}) - 0.1249$ [5.13]
Single solar air collector with fibre cloth absorber: $\eta = 0.1959 \cdot \ln(\dot{m}) - 0.2462$ [5.14]

Figure 5.9 shows the efficiency curves of the three solar air collectors from figure 5.7 together with the efficiency of two of the solar air collectors from the IEA Task 19 investigation (Fechner, 1999) – the collector of the Summer House Package with identical absorber as the single solar air collector with fibre cloth absorber and the collector with the highest efficiency – the rather expensive Grammer collector.

Solar air collectors efficiencies
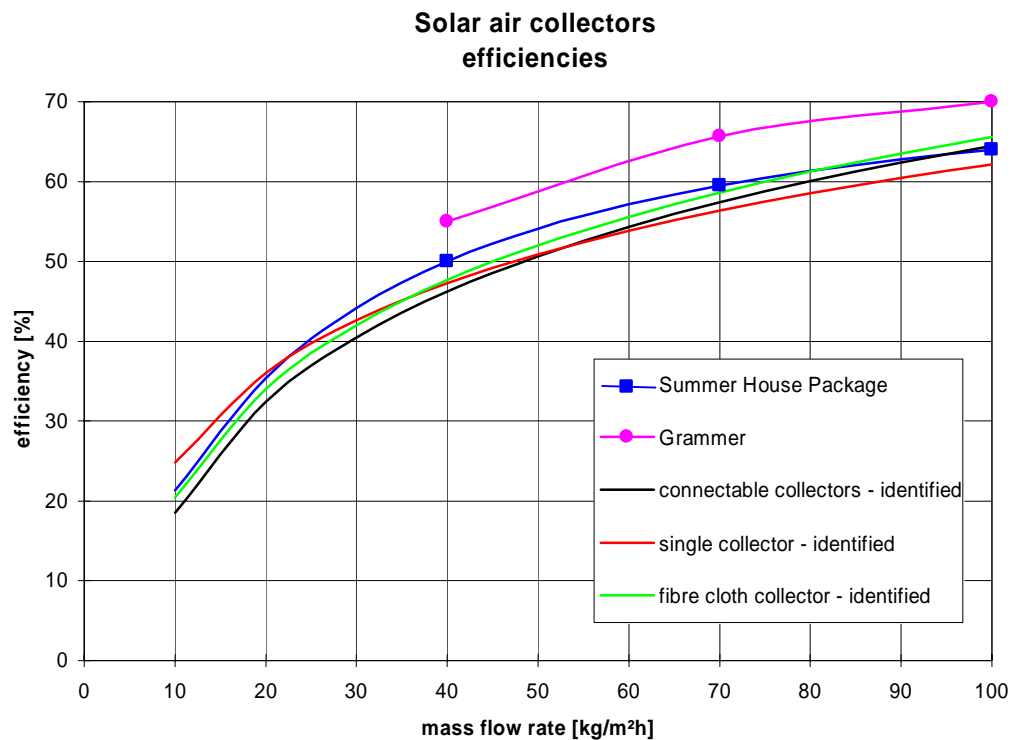
Figure 5.9. The efficiency curves from figure 5.7 shown together with the efficiency of two solar air collectors measured in IEA Task 19 (Fechner, 1999).

Figure 5.9 shows as already shown in figure 5.4 that the three solar air collectors are very efficient and as efficient as the solar air collectors of the Summer House Package which in (Fechner, 1999) proved to have the second highest efficiency of the investigated solar air collectors. The efficiency of the three investigated solar air collectors is very similar to the efficiency of the collector of the Summer House Package except that the efficiency of the collector of the Summer House Package is somewhat higher at mass flow rates in the range of 30-70 kg/m²h. The Summer House Package was, however, tested with a fan both at the inlet and the outlet in order to reduce the influence of leakage (Fechner, 1999). So the efficiency of the Summer House Package may in fact be a little lower if tested in the same way as in this re-

port. However, when considering the uncertainty on the efficiency of the three solar air collectors and the uncertainty of the efficiency of the collector of the Summer House Package it can be stated that the efficiencies are very similar.

Table 5.5 lists the obtained thermal capacity of the three solar air collectors. Table 5.5 shows a very scattered picture of this value. It was expected that the normalized thermal capacity of the two solar air collectors with metal absorber would be almost identical and somewhat higher than the thermal capacity of the single solar air collector with fibre cloth absorber. The latter because aluminium has a higher thermal capacity than the fibre cloth made of plastic. The thermal capacity of the metal absorber alone is about 2 kJ/Km². The metal absorber is as shown in appendix B connected to the casing of the solar air collectors by aluminium profiles. Together with the thermal capacity of the fibreboard the thermal capacity is, therefore, in the order of 4 kJ/km². This means that the identified thermal capacity of the single solar air collector with metal absorber is wrong. The identified thermal capacity of the connectable solar collectors is maybe too small, while the thermal capacity of the single solar air collectors with fibre cloth absorber may be somewhat too high. However, the thermal capacities are identified together with the parameters of the efficiency equations (5.15-17 – see later) for the solar air collectors and should thus be use together with these efficiency equations in order to obtain a correct prediction of the dynamical behaviour of the solar air collectors. When comparing the standard deviation of the identification in table 5.5 and the demands in table 5.3 it is seen that the thermal capacity is very precisely identified

Collector	Total thermal capacity kJ/K	Normalized thermal capacity kJ/Km²	Standard deviation %
Connectable solar air collectors	35.2	3.8	4.4
Single solar air collectors with metal absorber	4.8	1.6	5.4
Single solar air collector with fibre cloth absorber	13.8	4.7	2.6

Table 5.5.   Thermal capacity of the three solar air collectors.

The incident angle modifier coefficient of the three solar air collectors was identified to lay in the area of 3.1-3.5 dependent on solar air collector and mass flow rate. In the simple method a value of 3.2 was used as described in connection with equation 4.2. So here was also a good agreement. The standard deviation is well within the demand given in table 5.3.

It is as mentioned earlier possible to obtain more information on the solar air collectors when applying the advanced method rather than the simple method. The above-described thermal capacity and incident angle modifier are two examples. A more important feature of the advanced method is that it is possible to determine the efficiency of the solar air collectors for situations where the inlet air temperature to the collectors is different from the ambient temperature. This is important if the solar air collectors are applied in a system with a closed loop where the air is returned to the collectors – e.g. if room air is heated in the collectors and blown back into the room. However, the efficiency for cases where the inlet temperature is different from the ambient temperature is also important in order to develop a model of the solar air collector (both for pre-heating and re-circulation of the air) where the thermal capac-

ity of the solar air collectors is taken into account. Figures 5.3-4 and 5.7-8 show the steady state efficiency dependent on the mass flow rate, however, figure 4.48 clearly states the dynamic behaviour of the efficiency of the solar air collectors dependent on the thermal capacity of the solar air collectors – i.e. lower efficiencies when heating up and higher efficiencies when cooling down. This is important to incorporate in a model for simulation of the behaviour of solar air collectors. A model of the single solar air collector with fibre cloth absorber has been developed in (Jensen and Bosanac, 2002). Please refer to this for further details if interested.

The efficiency of the three solar air collectors in the form given in equation 5.7 is shown in figures 5.10-15 and further given in equations 5.15-17 for direct implementation in a model. Figures 5.10-15 show the efficiency dependent on the mass flow rate and either the reduced temperature or the difference between the arithmetical mean air temperature of the air in the collector and the ambient temperature at a solar radiation of 800 W/m². Please notice that the units on the x-axis for the single solar air collector with fibre cloth absorber is different from the two other solar air collectors as are the mass flow rates.

Connectable solar air collectors:

$$\eta = 0.6915 + 0.0327 \cdot \ln(\dot{m}) - (14.46 + 0.641 \cdot \ln(\dot{m})) \cdot \Delta T / G \qquad [5.15]$$

Single solar air collector with metal absorber:

$$\eta = 0.5611 + 0.0334 \cdot \ln(\dot{m}) - (8.569 + 0.2417 \cdot \ln(\dot{m})) \cdot \Delta T / G \qquad [5.16]$$

Single solar air collector with fibre cloth absorber:

$$\eta = -0.2148 + 0.2675 \cdot \ln(\dot{m}) - (2.6424 + 0.2754 \cdot \dot{m}) \cdot \Delta T / G \qquad [5.17]$$
NB! may not be used at higher mass flow rates than 30 kg/m²h.

where $\dot{m}$ is the mass flow rate of the air per m² collector area,
   ΔT is the temperature difference between the arithmetical mean air temperature of the air in the collector and the ambient temperature,
   G is useful the solar radiation on the collector.

Although very similar curves in figure 5.7 the curves for the efficiency based on reduced temperature and T_m - T_a are rather different for the three collectors. Especially is the efficiency for the single solar air collector with fibre cloth absorber different from the two other collectors.

The efficiency curves for the two solar air collectors with metal absorber is nearly not dependent on the air flow rate. This was also found for the Summer House Package in the IEA Task 19 investigation (Fechner, 1999). The dependency of the air flow rate shown in figure 5.7 is due to the fact that ΔT increases over the collectors when going toward lower mass flow rates, which means that the efficiency slides down the curves in figures 5.10-13. The efficiency for the single solar air collector with fibre cloth absorber shows in figures 5.14-15 much more dependency on the mass flow rate. This may be due to the lower pressure crop across the fibre cloth than across the metal absorber – i.e. the fibre cloth may be less able to create an uniform air flow through all of the absorber at low mass flow rates.

**Connectable solar air collectors
efficiency**
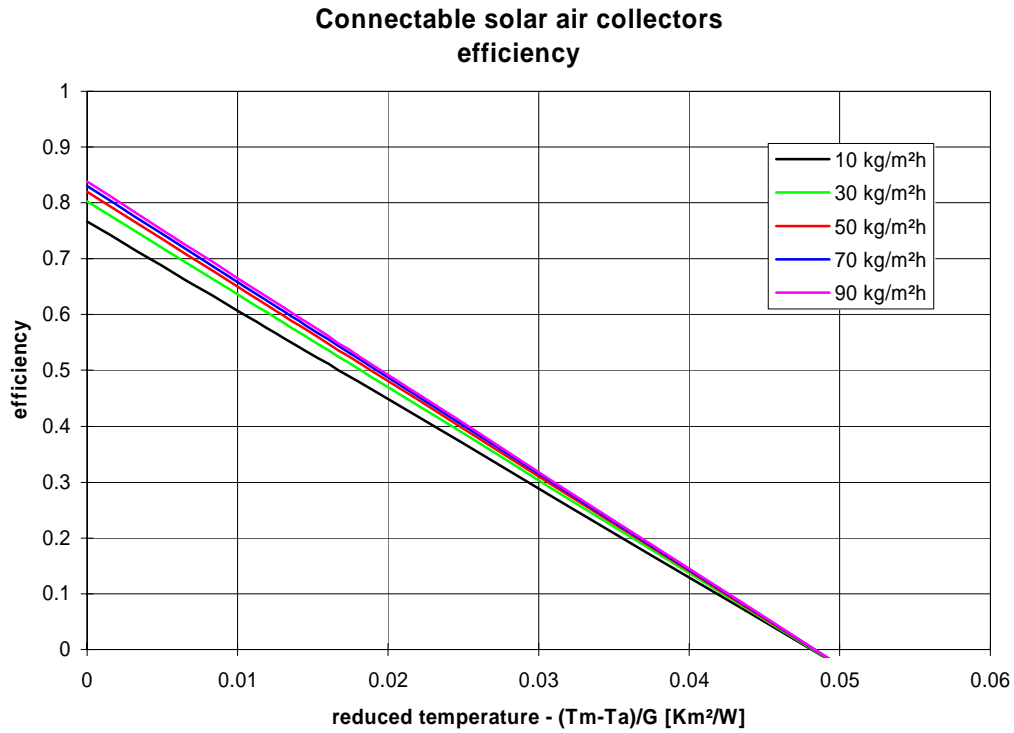
Figure 5.10. The efficiency of the connectable solar air collectors dependent on the mass flow rate and reduced temperature.

**Connectable solar air collectors
efficiency at 800 W/m²**
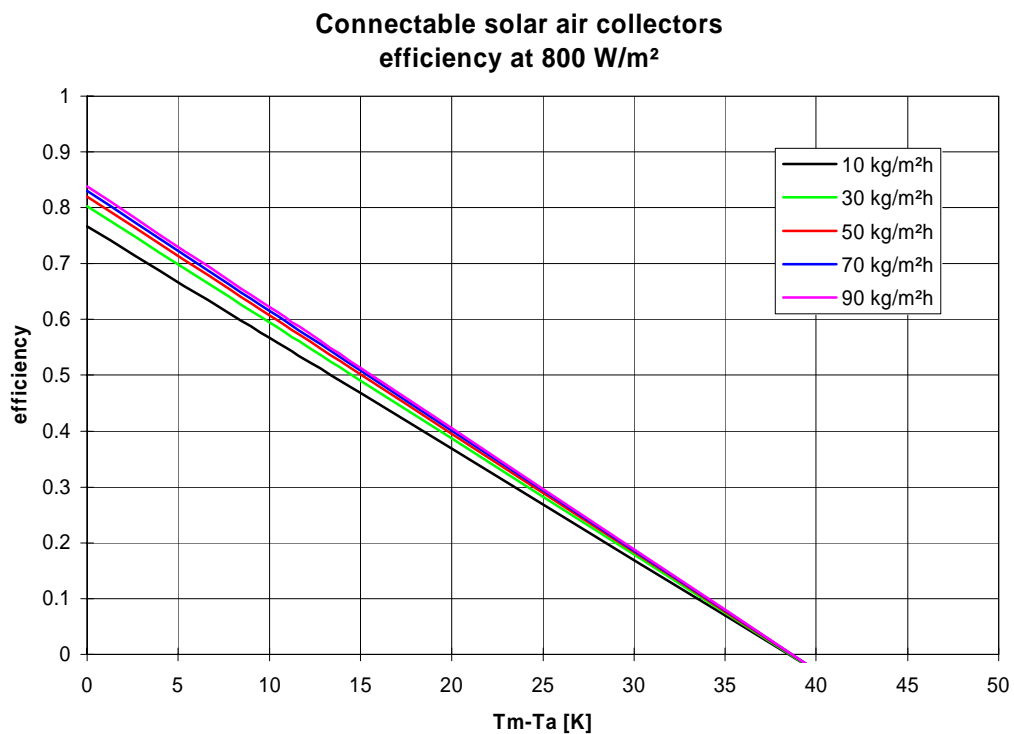
Figure 5.11. The efficiency of the connectable solar air collectors dependent on the mass flow rate and the difference between the arithmetical mean air temperature of the air in the collector and the ambient temperature at a solar radiation of 800 W/m².
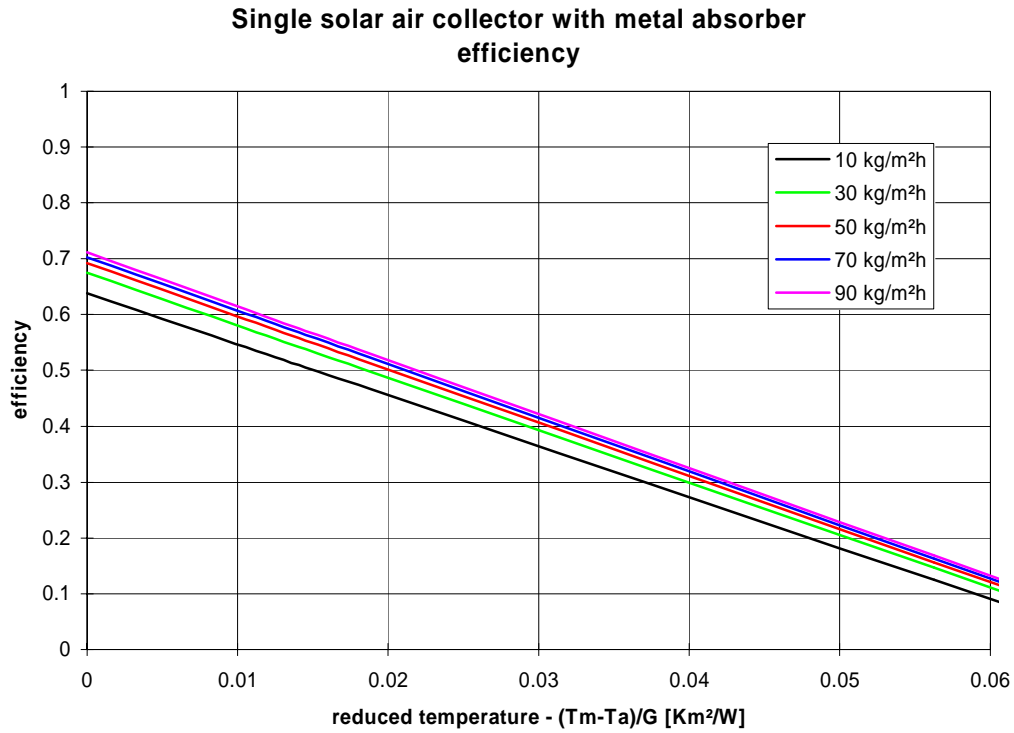
Figure 5.12. The efficiency of the single solar air collector with metal absorber dependent on the mass flow rate and reduced temperature.
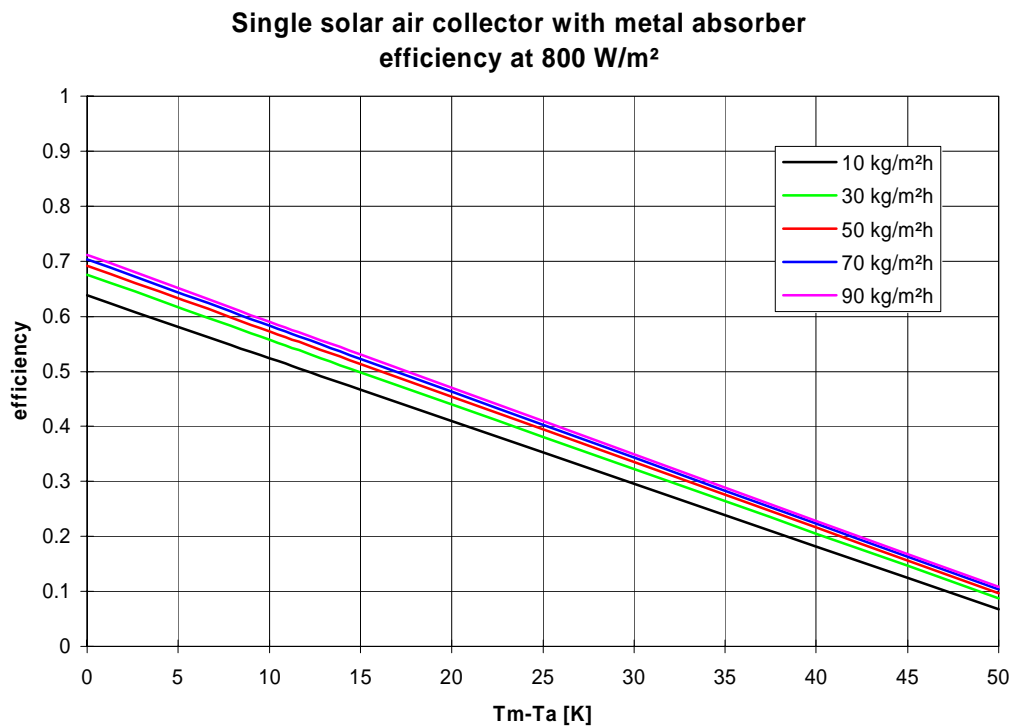
Figure 5.13. The efficiency of the single solar air collector with metal absorber dependent on the mass flow rate and the difference between the arithmetical mean air temperature of the air in the collector and the ambient temperature at a solar radiation of 800 W/m².
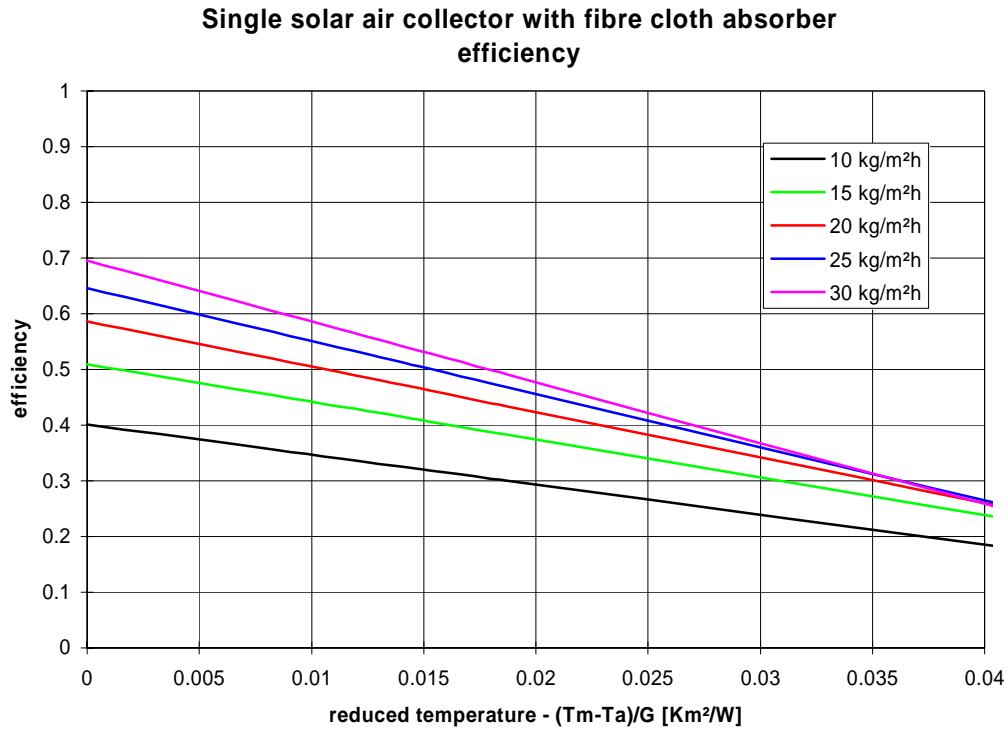
Figure 5.14. The efficiency of the single solar air collector with fibre cloth absorber dependent on the mass flow rate and reduced temperature.
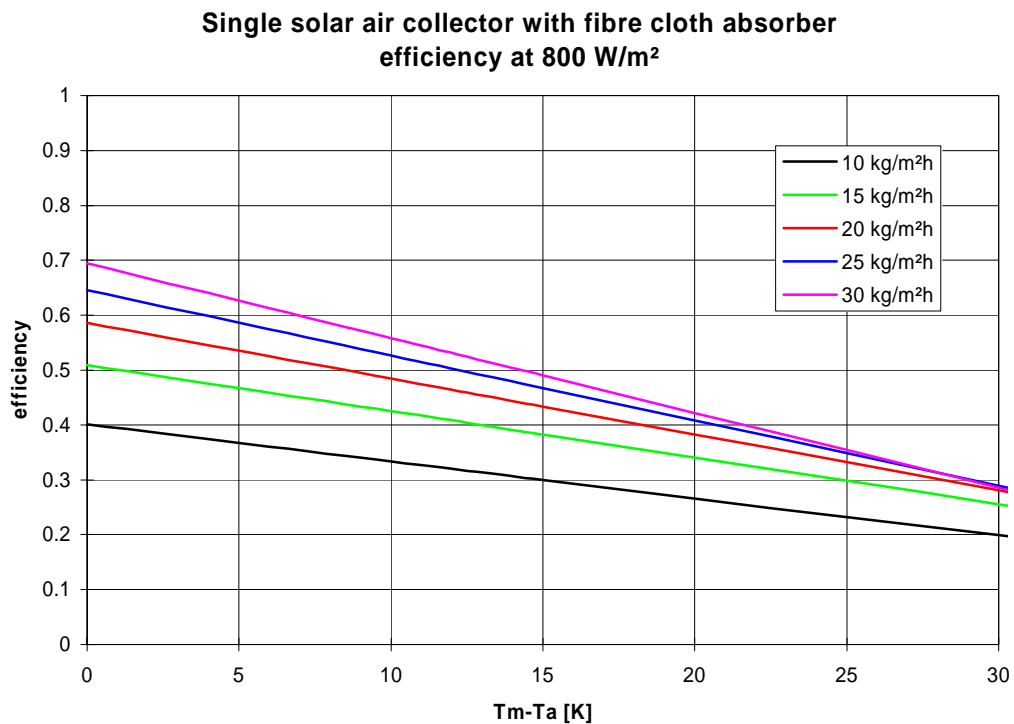
Figure 5.15. The efficiency of the single solar air collector with fibre cloth absorber dependent on the mass flow rate and the difference between the arithmetical mean air temperature of the air in the collector and the ambient temperature at a solar radiation of 800 W/m².

It is surprising that although almost identical efficiency curves in figure 5.7 the efficiency curves based on temperatures show so large differences. Can it, therefore, be trusted that equations 5.12-14 lead to the same efficiencies as equations 5.15-17? This is investigated in the following.

In tables 5.6-8 it is checked if equations 5.12-14 gives the same efficiencies as equations 5.15-17. When comparing the top and bottom lines in tables 5.6-8 it is seen that there is a very good agreement between the two ways of calculating the efficiency for the three collectors - within few percent – except at a mass flow rate of 10 kg/m²h for the two collectors with metal absorber. However, the solar air collectors with metal absorber are supposed to be run at higher mass flow rates – i.e. around 50 kg/m²h.

The agreement between the two ways of calculating the efficiency is very satisfying over the whole range of mass flow rates for the single solar air collector with fibre cloth absorber. This is not a surprise at the identification is valid for a smaller range than for the two other collector. Equation 5.17 should as already mentioned not be used at higher mass flow rates than 30 kg/m²h. In the present investigations (Jensen, and Bosanac, 2002) this is alright as the collector has been tested in a system where the mass flow rate doesn't go above 30 kg/m²h but varying between 0 and 30 kg/m²h dependent on the solar radiation. It would, however, had been nice if equation 5.17 was valid for a larger range of mass flow rates as equations 5.15-16 are. But this is not possible based on the present measurements.

Parameter	mass flow rate			
	10 kg/m²h	20 kg/m²h	50 kg/m²h	90 kg/m²h
efficiency from equation 5.12 [%]	18.6	32.4	50.7	62.4
Power transferred to the air at 800 W/m² [W/m²]	149	259	406	499
ΔT [K]	26.7	23.2	14.5	9.9
Efficiency from equation 5.15 [%]	23.4	31.4	51.2	62.4

Table 5.6.   Check of the agreement between equation 5.12 and 5.15.

Parameter	mass flow rate			
	10 kg/m²h	20 kg/m²h	50 kg/m²h	90 kg/m²h
efficiency from equation 5.13 [%]	24.8	36.1	50.9	60.5
Power transferred to the air at 800 W/m² [W/m²]	198	289	407	484
ΔT [K]	35.6	25.9	14.5	9.6
Efficiency from equation 5.16 [%]	23.2	36.0	51.9	59.6

Table 5.7.   Check of the agreement between equation 5.13 and 5.16.

Parameter	mass flow rate		
	10 kg/m²h	20 kg/m²h	30 kg/m²h
efficiency from equation 5.14 [%]	20.5	34.1	42.0
Power transferred to the air at 800 W/m² [W/m²]	164	273	336
ΔT [K]	29.4	24.4	20.1
Efficiency from equation 5.17 [%]	20.3	33.8	42.1

Table 5.8.   Check of the agreement between equation 5.14 and 5.17.

Based on table 5.6-8 it can be stated that equations 5.12-14 lead to the same efficiencies as equations 5.15-17. The equations represents, therefore, the efficiency of the three investigated solar air collectors, and may be used in simulation programs for determination of the performance of the solar air collectors connected to a system or a house.

5.3. Conclusions on the efficiencies

Two different method for determination of the steady state efficiency of solar air collectors for pre-heating of fresh air has been has been examined: a simple easy to apply method and an advanced method based on statistical identification of the parameters determining the efficiency of the solar air collectors.

Within the uncertainty the two methods have proved to lead to almost identical efficiencies for the three investigated solar air collectors. For an easy evaluation of the steady state efficiency of solar air collectors for pre-heating of fresh air the simple method may thus be used instead of the advanced method. However, the advanced method gives more information on the solar air collectors than the simple method. With the simple method it is only possible to compare the efficiencies of different solar air collectors while it with the results of the advanced method is possible to simulate the dynamic behaviour of the solar air collectors.

The steady state efficiency of the three solar air collectors dependent on the mass flow rate proved to be very similar with really no important discrepancies, which cannot be explained by means on the uncertainty on the measurements and the determination of the efficiencies. It has thus successfully been shown that it is possible to manufacture easy connectable solar air collectors which in larger collector arrays still is as efficient as smaller solar air collectors.

All three solar air collectors are further very efficient – among the most efficient today. The high efficiencies show that a good air distribution over the solar air collectors has been established.

Although the curves of the steady state efficiency based on mass flow rates of the three investigated solar air collectors are very similar the identified efficiency curves based on temperature differences and the identified thermal capacity shows large discrepancies. In spite of the large discrepancies in the identified efficiencies based on temperature differences these leads to the same efficiencies as can be found using the steady state efficiency based on mass flow

rates. However, the combined set of efficiencies based on temperature differences and the thermal capacity should be used together when simulating the dynamic performance of the solar air collectors as the identification with very high precision showed that the found equations, the thermal capacity and the incidence angle modifier where those which best characterize the solar air collectors in the investigated areas – i.e. within the measured range of mass flow rates and reduced temperatures. Other measurements on the same collectors may lead to other sets of identified parameters, which just as well characterize the performance of the solar air collectors as described in section 5.2.1.

6. Conclusions

The project has proved that it is possible to manufacture solar air collector panels, which in an easy way can be connected into large collector arrays with integrated ducting without loss of efficiency.

The developed connectable solar air collectors are based on the use of matrix absorbers in the form of perforated metal sheets. Three interconnected solar air collectors of the above type - each with an transparent area of approx. 3 m² - were tested and compared with parallel tests on two single solar air collectors also with a transparent area of approx. 3 m². One of the single solar air collectors has an identical absorber as the connectable solar air collectors while the absorber of the other single solar air collector was a fibre cloth. The efficiency of the three solar air collectors proved to be almost identical in the investigated range of mass flow rates and temperature differences. The solar air collectors further proved to be very efficient – as efficient as the second most efficient solar air collectors tested in the IEA task 19 project Solar Air Systems.

Some problems remain although to be solved:

- the pressure drop across especially the connectable solar air collectors is too high – mainly across the inlets of the solar air collectors. It should, however, be possible to considerably reduce the pressure losses with a more aerodynamic design of the inlet and outlet of the solar air collectors.

- the connectable solar air collectors are easy connectable but the air tightness of the connections in the present form is not good enough. As leakage leads to lower efficiencies focus should be put on making the connections more air tight without loosing the easiness in connecting the solar air collectors.

- The fibreboard used internally in the solar air collectors should be replaced with another material, which don't give off smell.

As a spin off of the project a simple and easy way to determine the steady state efficiency of solar air collectors for pre-heating of fresh air has been validated. The simple method of determining the efficiency has with success been compared with an advance method applying statistical identification of the parameters characterizing the solar air collectors. The two methods lead to identical steady state efficiencies for the three investigated solar air collectors. The simple method is mainly applicable when comparing efficiencies of different solar air collectors. If simulation of the dynamical behaviour of the solar air collectors is the aim, the advanced method is still needed.

7. References

Ambrossetti, J.P., 1983. Das neue Bruttowärme-ertragsmodel für Sonnenkollektoren. Technical Report. EIR Würenlingen. ISBN-3-85677-012-7.

Bosanac, M., 1993. TYPE 59, TRNSYS Module for Dynamic Simulation of Collectors and Collectors Arrays. Expert Meeting IEA Task XIV. Rome 1993.

Bosanac, M., Brunotte, A., Spirkl, W. and Sizmann, R., 1994. Use of Parameters Identification for Flat Plate Collector Testing under Non Stationary Conditions. J. Renewable Energy Sources, 4, pp 217-222.

Bosanac, M. and Jensen, S.Ø., 1997. In-situ Solar Air Collector Array Test. Solar Energy Laboratory, Danish Technological Institute Energy Division. ISBN 87-7756-480-4.

Duffie, J.A. and Beckman, W.A., 1991. Solar Engineering of Thermal Processes. John Wiley & Sons, New York. ISBN 0-47-51056-4.

Fechner, H., 1999. Investigations on Series Produced Solar Air Collectors. IEA Task 19 Solar Air Systems. Arsenal Research, Austria.

Jensen, S.Ø., 1999. Solar Shutter – a movable solar panel. Solar Energy Centre Denmark, Danish Technological Institute. ISBN 87-7756-549-5.

Jensen, S.Ø. and Bosanac, M., 2000. In-situ Determination of the Efficiency of Solar Air Collectors. In proceedings from EuroSun 2000, Copenhagen, Denmark, June 19-22, 2000. ISBN 87-7756-625-4.

Jensen, S.Ø. and Bosanac, M, 2002. Solar air heating system for combined DHW and space heating – phase 2. Solar Energy Centre Denmark, Danish Technological Institute. ISBN

Jensen. S.Ø., Kristensen. E.F and Forman, T., 2001. Test of a solar crop dryer. Solar Energy Centre Denmark, Danish Technological Institute, Danish Institute of Agricultural Sciences and Aidt Miljø. ISBN 87-7756-583-5. www.risoe.dk/solenergi/rapporter/sec-r-6.htm.

Nielsen, J.E., 1995. Dokumentation of KVIKSOL – a program for simulation of solar heating systems (in Danish). Version 5.0. Solar Energy Laboratory, Danish Technological Institute Energy.

Spirkl, W., 1992. Dynamic SDHW System Testing, Program Manual. Sektion Physik der Ludwig-Maximilians Universität München.

Appendix A

Data sheet for the
Summer House Package

Summer House Package

The system consists of

Solar air collector

Warm dry air

Fan

Solar cell panel

Ventilation with heating
- for your health and comfort

The fan has a capacity of 60 m³/h. The air in the building will be exchange by fresh, warm and dry air - humidity and smell will be removed. The system further gives a surplus for heating of the building. Simple, efficient and cheap.

Ventilation without running costs
- solar controlled, solar maintained

Each time the sun shines the fan will start to blow fresh warm and dry air into the building. The fan is controlled and driven by a solar cell - so no running cost.

Self regulating and safe
- functions even in your absence

The system starts and stops automatically controlled by the sun. The system is totally independent on the public electrically supply - ideal for house which in periods is unoccupied. Nothing to leak and no damage possible.

AIDT miljö

- keep your house nice and dry with solar energy - all year round

Technical data

Solar Air Collector

Dimensions:	1.99 x 0.71 x 0.1 m
Weight:	23 kg
Frame:	Sturdy aluminium
Cover:	Shockproof polycarbonate
Insulation:	30 mm mineral wool
Absorber:	Special felt mat
Base:	Wood fiber

Solar Cell

Dimensions:	0.92 x 0.31 x 0.008 m
Rated tension:	14.2 Volt
Power:	11 Watt
Rated current:	759 mA

Ventilator with build-in regulator

Dimensions:	0.175 x 0.175 x 0.05 m
Rated tension:	12 Volt
Power:	5 Watt

The Siting

A south, south east or south west facing site, with minimum shade is ideal. The solar air panel and the solar cell can be wall mounted directly or to special brackets provided. The fan is installed inside the house, connected to the solar air panel via a special flex-tube.

Easy to install

The system can be fitted within a few hours, either by our operatives or by a do it yourselves enthusiast. The only tools required being a power drill, a screwdriver and a hammer and chisel. Full installation instructions enclosed with the system.

Our range of solar energy products covers:

- Low flow systems for hot water and central heating supply
- Combined system, hot water/dehumidification
- Solar dehumidifier
- Pool heating systems
- Under ground storage system

Rights to make alterations reserved
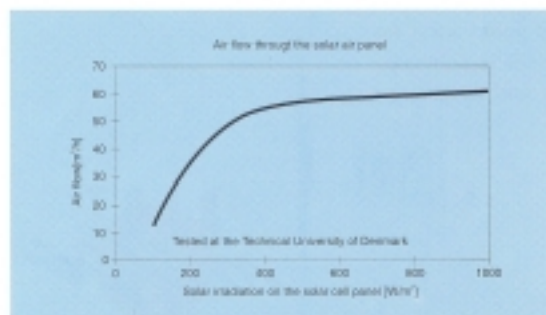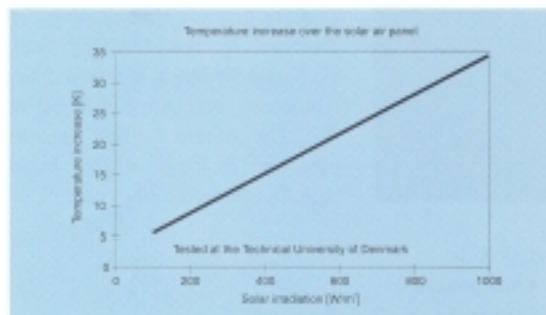
- keep your house nice and dry with solar energy - all year round

Appendix B

Working drawings for the connectable solar air collectors

(10 mm double walled ribbed polycarbonate)

SolarWall glat (perforated metal absorber)

10 mm PC plade

(heated air) Gennemgang af opvarmet luft

(insulation)

0,7 mm aluplade
(0.7 mm aluminium sheet)

3,5 mm træfiber
(3.5 mm woden fibreboard)

20 x 30 mm lærk
(20 x 30 lath)

Luftindtag
(ambient air)
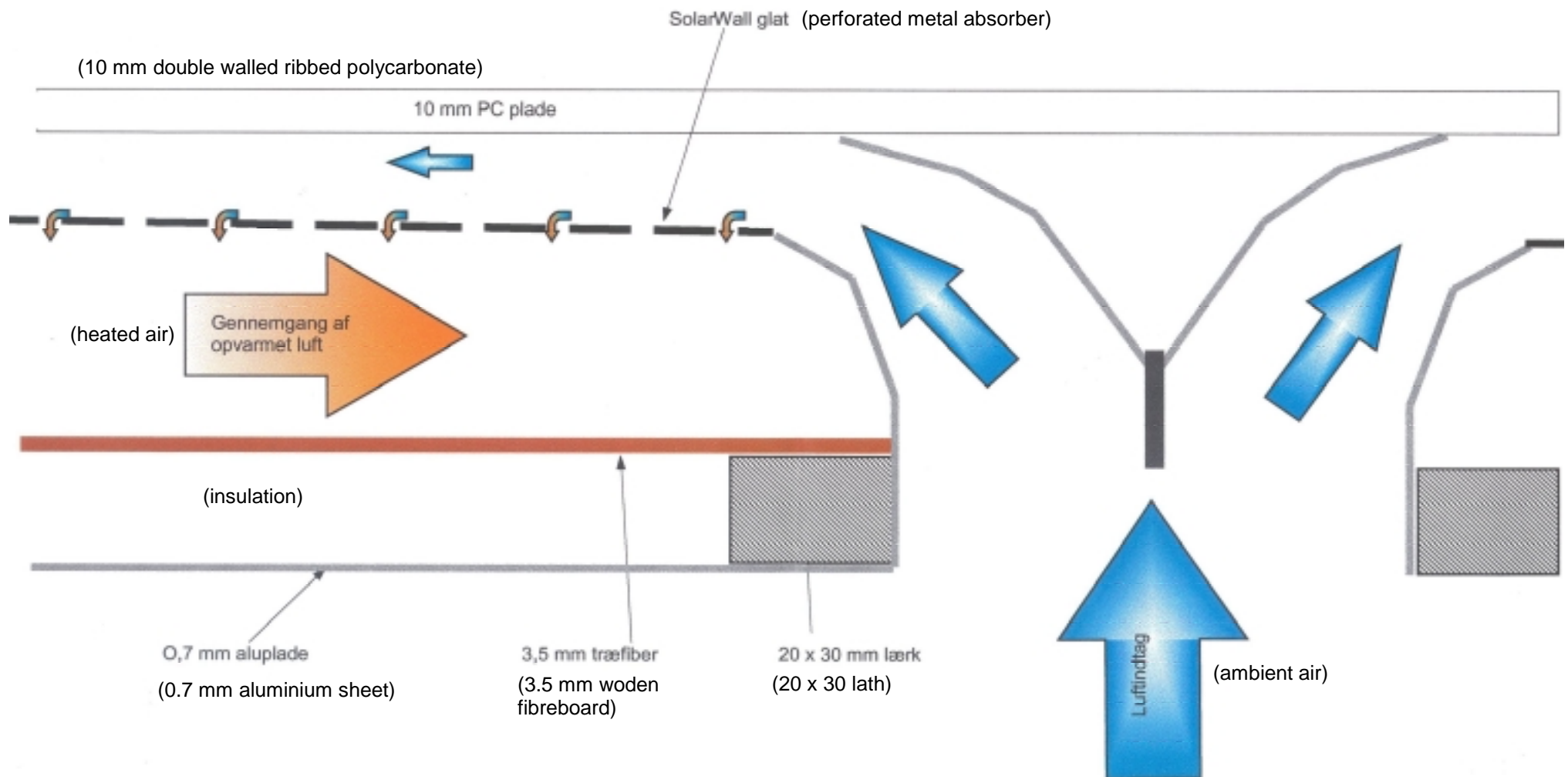
Figure 3.1. Inlet to the connectable solar air collector.

Solfanger standard alu-profil (standard aluminium casing profile)

(perforated metal absorber)
SolarWall glat

(10 mm double walled ribbed polycarbonate)
10 mm PC plade

(weather strip)

(aluminium profile for assembling)

(heated air)
Gennemgang af opvarmet luft

Isolering
(insulation)

O,7 mm aluplade
(0.7 mm aluminium sheet)

3,5 mm træfiber
(3.5 mm wooden fibreboard)

20 x 30 mm lærk
(20 x 30 lath)
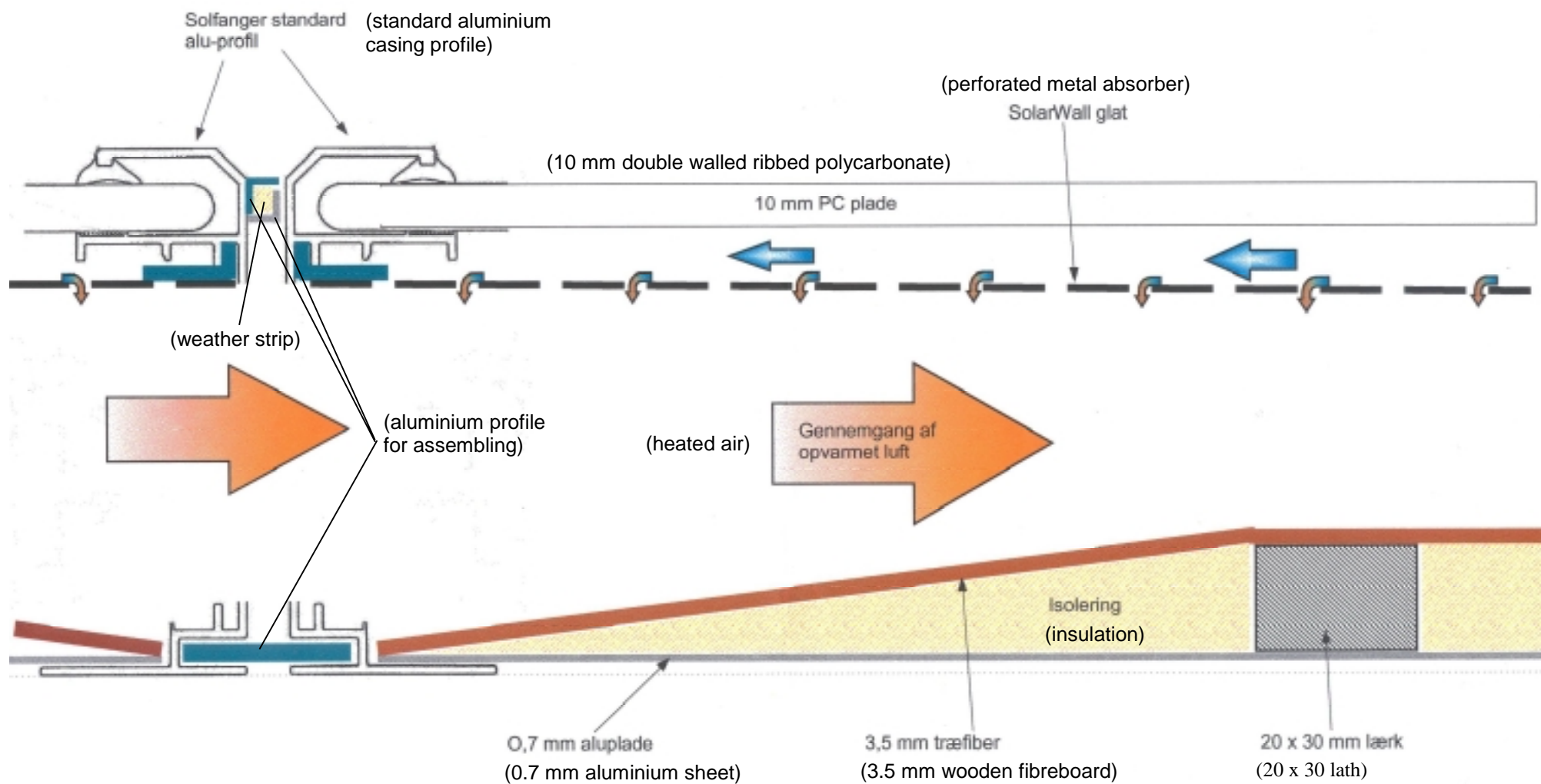
Figure B.2. Connection between two connectable solar air collectors.

Solfanger standard alu-profil top/bund (standard aluminium casing profile)

(10 mm double walled ribbed polycarbonate)

10 mm PC plade

SolarWall glat (perforated metal absorber)

(3.5 mm wooden fibreboard) 3,5 mm træfiber

(insulation)

Isolering (insulation)

Figure B.3 Not connectable side walls

Appendix C

Paper to EuroSun 2000

In-situ determination of the efficiency of solar air collectors

IN-SITU DETERMINATION OF THE EFFICIENCY OF
SOLAR AIR COLLECTORS

Søren Østergaard Jensen and Miroslav Bosanac
Solar Energy Centre, Danish Technological Institute, Gregersensvej, P.O.Box 141, Taastrup, DK 2630,
Denmark, phone: +45 72 20 24 88, fax: +45 72 20 25 00, e-mail: Soren.O.Jensen@teknologisk.dk

Abstract – A method for in-situ determination of the efficiency of solar air collectors has been developed and tested on two larger Danish solar air collectors. A method for in-situ determination of the efficiency of solar air collectors is an important tool in the ongoing development of solar air collectors. The efficiency of solar air collectors is opposite liquid solar collectors much influenced by the actual mass flow rate inside the collector. It is, therefore, often difficult/impossible to extrapolate from tests on small modules of solar air collectors in test rigs to larger solar air collector areas. The chosen method is based on identification of the parameters characterizing the collector. The method has been tested on two very different solar air collector in order to test the method on a larger range of collector types. In both systems the heat from the air is transferred to a liquid loop by an air to water heat exchanger. In this way the method was tested against measurements performed on the liquid side of the systems where good accuracy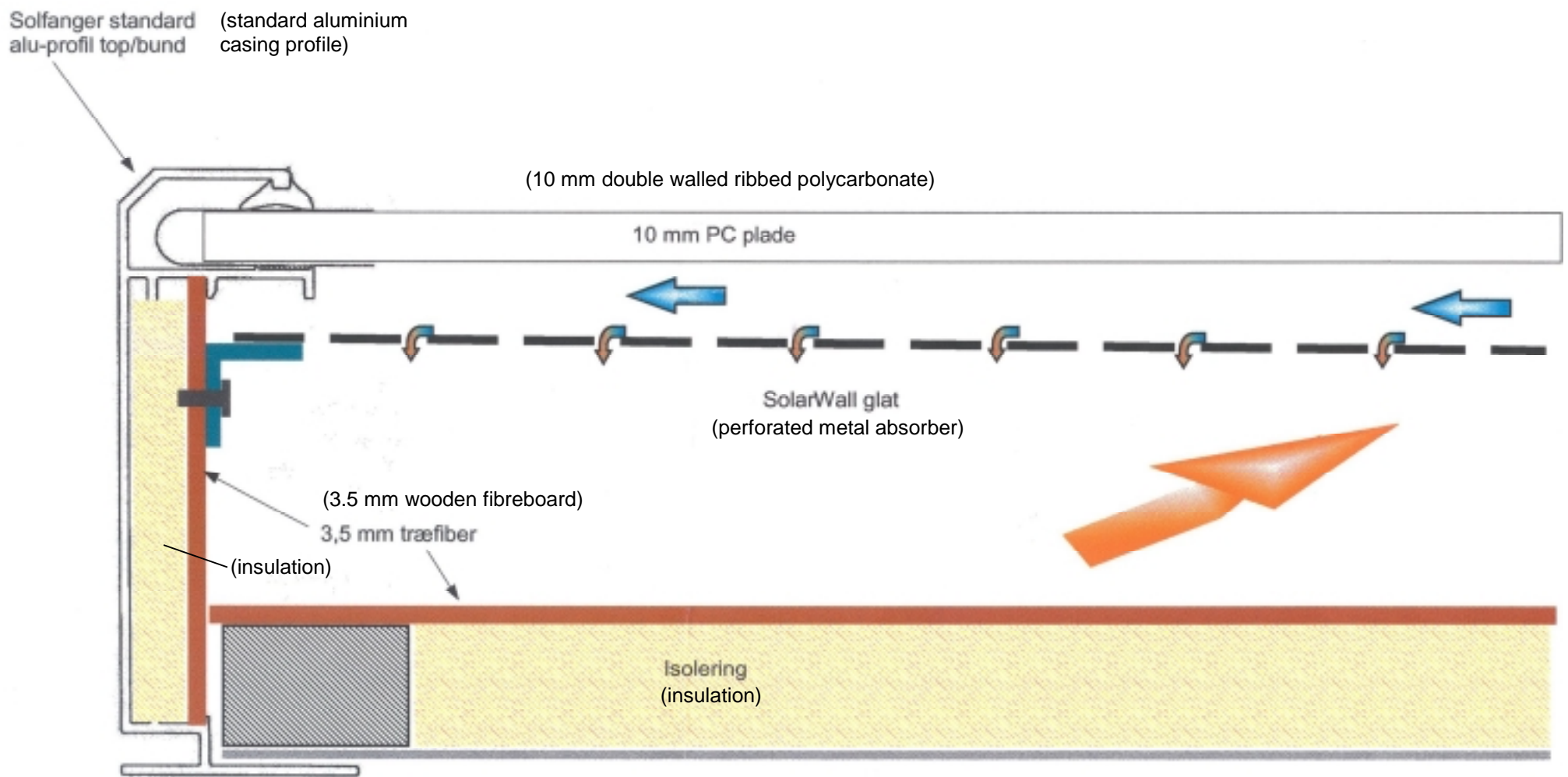 is easier obtainable. Within the area of interest the difference in the measured energy flows is below 2-3% between the air and liquid measurements. This is a surprisingly good agreement as it is difficult to obtain accurate measurements in air flows. The most important feature of the method is its ability to accurately predict long-term energy yield. Prediction of monthly energy yield shows encouraging accuracy, e.g. better than 5 % for the two test cases.

1. INTRODUCTION

The efficiency of solar air collectors is opposite liquid solar collectors much influenced by the actual mass flow rate inside the collector due to the often rather low heat transfer coefficient between absorber and air. The heat transfer coefficient is highly dependent on the air speed. It is, therefore, often difficult/impossible to extrapolate from tests of small modules of solar air collectors in test rigs to larger solar air collector arrays as the air speed will change.

A method for in-situ determination of the efficiency of solar air collectors has, therefore, been developed at the Solar Energy Centre, Danish Technological Institute (Bosanac and Jensen, 1997).

The main problems in in-situ determination of the efficiency of solar air collectors are:

- Accurate measurements, which do not disturb the flow pattern in the collector loop as this may influence the efficiency of the collector.
- The efficiency has to be determined based on measurements carried out under dynamic conditions.

2. MEASURING OF TEMPERATURES AND FLOW RATES

As a temperature profile often – differently to liquid pipes – occurs across the cross section of air ducts it is necessary to establish a mean air temperature by measuring a number of air temperatures located at

different positions within the same cross section of the duct as shown in figure 1. The temperature measurements of the method are, therefore, based on calibrated temperature sensors located in a well-defined grid in the duct. The sensors should be chosen in order to have only a small influence on the flow pattern in the duct – ie small sensors (eg thermocouples connected to a thermopile) only creating a small pressure drop.
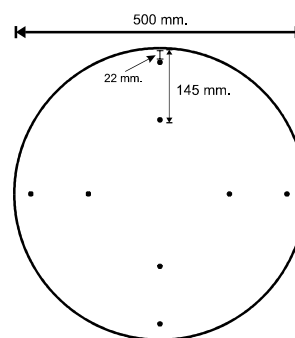
Figure 1. Example of the locations of air temperature sensors for determination of the mean air temperature in a duct.

The measuring method is for the air flow measurements based on either a calibrated pressure drop or a calibrated air speed. The calibrated pressure drop should preferably be an already existing pressure drop like e.g. an existing bending of the ducts. An orifice may also be used but introduces an extra pressure drop in the system, which may change the flow rate noticeable. Pito tubes and air speed sensors

can be used in straight duct with a developed flow pattern.

The measurement accuracy of the temperature difference should be below 0.1 K and for flow rates it should be below 10%.

3. IDENTIFICATION OF THE PARAMETERS DESCRIBING THE COLLECTOR

3.1. Collector Array Model

In order to be able to characterise a collector a modified multi-node collector model (Bosanac *et al.* 1993) has been used. The model has the following features:

- The collector is modelled with distributed capacities in the flow direction.
- A linear dependence of the collector efficiency factor on collector flow rate is assumed.
- A linear dependence of the heat loss coefficient on the surrounding air speed as well as on the temperature difference between collector and ambience is assumed.
- Incident angle modifiers for beam (as a function of incident angle) and diffuse irradiance are used.

Here are briefly described the main features of the model.

Each node of a flat-plate collector is characterised by:

$$C_n \, dT_n/dt = A_n \, k_m \, F'[(\tau\alpha)_0 \, G_{eq} - U_L(T_n - T_a)] - q_{u,n}$$

where G_{eq} is the equivalent normal irradiance taking into account irradiance components multiplied by respective incident angle modifiers:

$$G_{eq} = K_{\tau\alpha, beam} \, G_{beam} + K_{\tau\alpha,diff} \, G_{diff} + K_{\tau\alpha,alb} \, G_{alb}$$

U_L is the overall heat loss coefficient:

$$U_L = U_0 + U_v \, v + U_T(T_n - T_a)$$

$q_{u,n}$ is the rate of energy gain by the collector node:

$$q_{u,n} = m_c c_p(T_n - T_{n-1});$$

Coefficient characterising flow-rate dependence:

$$k_m = 1 + c_m \, m_c$$

$(\tau\alpha)_0$ is the transmittance-absorbtance-product at normal incidence. An incidence angle modifier for beam irradiance is defined by the modified Ambrosetti (Ambrosetti 1983) equation:

$$K_{\tau\alpha, beam}(\theta) = 1 - \tan^{1/r}(\theta/2)$$

The incident angle modifier for diffuse irradiance assuming isotropic distribution is used as derived in (Bosanac *et al.*1993). The incident angle modifiers for diffuse irradiance and for albedo are assumed to be equal. They are both derived in (Bosanac *et al.*1993) as a function of the parameter r.

Hence, the following parameters fully characterise the presented model:

- The optical efficiency of the collector array, $F'(\tau\alpha)$.
- The overall heat loss coefficient if $T_n=T_a$ and $v=0$, U_o.
- The coefficient characterising wind dependence of the overall heat loss, U_v.
- The coefficient characterising temperature dependence of the overall heat loss, U_T.
- The total thermal capacity of the collector array, C.
- The incident angle modifier coefficient.
- The coefficient characterising the flow-rate dependence, c_m.

3.2. Principle of the Test Procedure

The performance of large collector arrays depends on their design parameters and on various weather and operating conditions, e.g. irradiance, ambient temperature, wind velocity, inlet air temperature. The method uses detailed, in-situ measurement data as a function of time in order to identify the most relevant parameters characterising array performance.

In order to evaluate long-term system performance and enable diagnosis of sources of array malfunctioning, it is primarily necessary to identify array parameters. Sets of array parameters is not identical for each array to be tested.

Therefore, in the first step of the procedure, it is necessary to estimate the influence of the array parameters characterising array performance. For example, if the flow rate in the collector loop is fixed or a majority of data is available for a single, specific flow rate, the parameter characterising flow rate dependence may not be identified.

The basic principle of the procedure is given in figure 2.

The parameter estimation involves identification of system parameters described by the mathematical model described in the previous section.

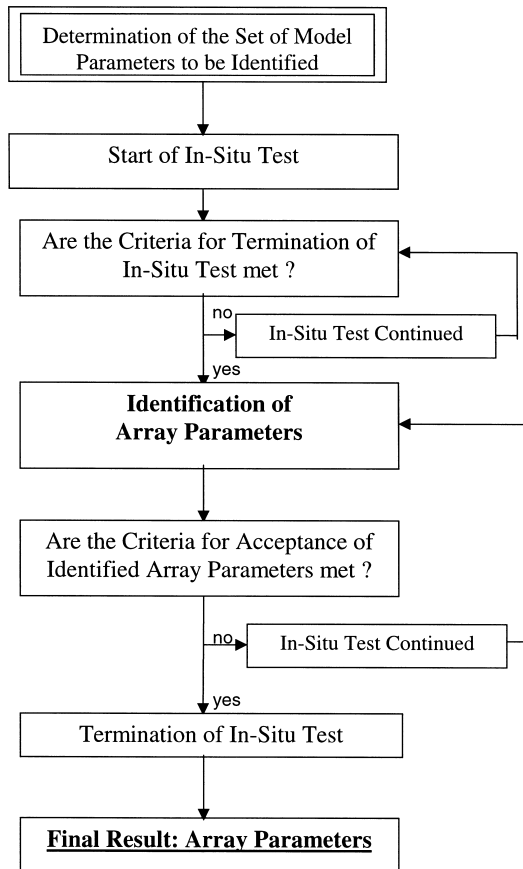Two sets of criteria are defined in order to assure reliable test result:

Figure 2. Principle of the test method.

- The first set of criteria deals with requirements regarding influencing variables (irradiance level, reduced temperature range etc.). These criteria indicate whether enough data are being collected.
- The second set of criteria deals with statistical measures regarding identified array parameters. These criteria being met means the test is successfully accomplished.

3.3. Criteria for Termination of In-Situ Tests

The criteria for accurate identification of system parameters deal with:

- Available amount of solar energy incident on the collector plane during an in-situ test. This criterion assures that enough data with high collector power will be available.
- Necessary range of variation of influencing parameters. These criteria should provide more accurate identification of respected parameters.

3.4. Criterion for the Minimal Irradiation during Test Sequence

The first criterion deals with the amount of solar energy incident on collector plane during an in-situ test. The minimum hemispherical irradiation available

at collector plane during a sequence is recommended to be:

$$120 \text{ MJ/m}^2$$

assuring that a portion of direct irradiation exceeds 50% of the total and/or that at least 50% of data correspond to level of hemispherical irradiance higher than 400 W/m² .

This criterion assumes identification of the basic set of parameters including; optical efficiency, incident angle modifier, overall heat loss coefficient and thermal capacity. Depending on the number of additional parameters to be estimated (if considered essential for the system under the test), a longer time period for monitoring might be necessary.

3.6. Criteria for Variability of Influencing Variables

This request deals with the necessary variability of the influencing variables. The variability determines directly the accuracy of the identified values. However, type and dimension of the array and its operating conditions influence these spans and the listed values should, therefore, be used as an orientation only. Table 1 gives an indication about the recommended range of variation to be scanned during in-situ monitoring (here only data having hemispherical irradiance above certain level should be considered e.g. 400 W/m²).

Influencing variable	Recommended Range of Variations
Tm-Ta	10 – 50 (70) K
Reduced Temperature	0.02 - 0.12 (0.2) K m² /W
Wind Velocity	1 - 5 m/s

Table 1. Recommended range of the variation of influencing parameters (values in brackets correspond to preferable values).

It is reasonable to assume that after a certain monitoring period, maximum possible variation of the influencing parameters is reached so that a further prolongation of the measurements would not considerably contribute to the de-coupling of the parameters´ associated errors. For some systems a high correlation between uncertainties can not be avoided. If particular correlation coefficient is too high one should rather use a lumped parameter, if possible, characterising both effects described by the separate parameters. In the case of the heat loss coefficient, it is preferred to avoid identification of the respective components (e.g. U_o, U_v, U_T) whenever the respective correlation coefficient remains being too high.

However, in the case of high coefficient of correlation between uncertainties describing diverse physical effects (e.g. the optical efficiency and the heat loss

coefficient) - it is not possible to use lumped parameter and we must notice the correlation as it is. If it is high it means that the array is operating in a small range of reduced temperatures.

3.6. Identification of Array Parameters
The identification of collector parameters is carried out using the Dynamic System Testing (DST) algorithm developed by Spirkl (Spirkl, 1990).

Figure 3 represents the DST procedure. The measured variables, i.e. collector array inlet and outlet temperature, air mass flow rate, ambient temperature, hemispherical and diffuse irradiance are input variables to the theoretical model. Then, the difference between measured system power and modelled power is minimised by optimising the set of parameters. As a result of this procedure the estimated errors of the parameters are given. If the same model is used for simulation, the error of the predicted energy output can be estimated. In order to apply dynamic fitting for the identification of collector array parameters a program subroutine was developed (Bosanac, 1993) characterising a dynamic collector model as described in the previous section.

The main benefit of the dynamic test is that stationary (i.e. steady state) conditions of the system are not required. The system is tested under normal, dynamic operation conditions and the monitoring data is used for identification of the system parameters.
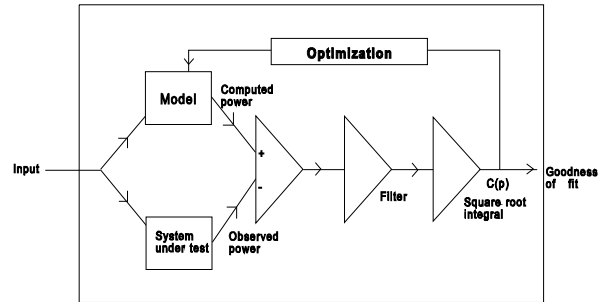

Figure. 3. Schematic diagram of the Dynamic System Testing procedure.

3.7. Acceptance Criteria for Test Results
The identified parameters themselves have to satisfy general ´acceptance´ criteria mainly dealing with statistical measures. The test results have shown that identified parameters are reliable if the following statistical requirements are met as stated in table 2.

If these criteria are not met for the basic set of parameters, additional test sequence exceeding in total 35 MJ/m² is required. After it has been collected, the identification procedure is to be repeated using all available data.

The above criteria are proposed for testing the similar systems as presented in the section below. The technical description of these systems is given in the next section. If other types of systems being addressed, it may be suggested to carry out at least two consecutive tests. That will enable a check of the repeatability of the identified parameters and it will enable cross prediction of the system power.

Symbol	Basic parameters	Units	Permitted standard deviation
$F'(\tau\alpha)_0$	Zero-heat-loss efficiency of array	-	10 %
C_m	Flow rate dependence	s/kg	10 %
U_L	Heat loss coefficient of array	W/Km^2	25 %
U_T	Heat loss temperature dependence	W/K^2m^2	35 %
Cc	Collector array capacity	kJ/K	15 %
r	Incident angle modifier coefficient	-	30 %

Table 2. Permitted standard deviations.

4. TEST OF THE METHOD

The in-situ method have been applied and tested on two larger Danish solar air collectors: Havrevangen and Tjørnegade. Common for the two systems is that the heat from the collector is transferred to a liquid circuit via an air to water heat exchanger making it possible to compare the accuracy of the measurements on the air side with the measurements on the liquid

side where high accuracy normally is more easily accessible.

4.1. Havrevangen
The Havrevangen system is located on the outskirts of Hillerød north of Copenhagen. The row houses are fully exposed to the sun and placed in an appropriate distance to avoid shading.

The solar air collector at Havrevangen is a traditional solar air collectors with the air flowing behind the absorber and fins from the absorber down into the air stream. The absorber is made of aluminium. The absorber has a selective surface and the cover consists of a single layer of glass. The area of the tested collector is 84 m². The tilt and azimut is 45° and 6° to the east respectively. Two-speed fans are used in order to save electricity in periods with low energy yield.

The air flow rate at low temperature differences between storage and collector is approximately 850 m³/h while at higher temperature differences it is approximately 6200 m³/h.

The location of the collector on the roof is shown in figure 3, while figure 4 shows a picture of the building with the solar air collector.
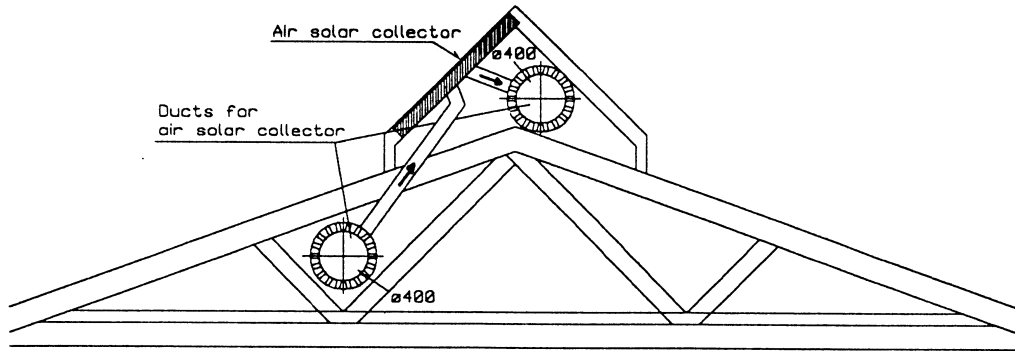

Figure 3.   Schematic presentation of the roof with the solar air collector.

Figure 4.   The building in Havrevangen with the solar air collector.

Table 3 shows the identified parameters using the developed method.

The cross correlation coefficient between the uncertainties of parameters U_0 and U_T is highest (0.88). Responsible for that is the small variability of temperature difference between collector air temperature and ambient temperature.

In fact the variability of the independent variables depends on the system design and its operation conditions. The correlation coefficient between the uncertainties of the heat loss coefficient and the optical efficiency is high as well.

The repeatability of the parameters is closely coupled with the system design and/or the operating conditions. The complete set of parameters is meaningful rather than separate values of parameters for long-term performance prediction. For example, a lower array optical efficiency in combination with a lower array heat loss coefficient will result in similar predicted system savings (supposing limited range of variability of reduced temperature) as a combination of higher array optical efficiency with higher array heat loss coefficient.

Parameters	Optical efficiency	Thermal capacity	Heat loss coefficient, U_O	Heat loss coefficient, U_t
Identified Parameters	0.650±0.021	(28.0±3.2) kJ/Km²	(3.21±0.30) W/K²m	(0.022±0.004)W/K²m²

Table 3.   Identified set of parameters for the Havrevangen collector

4.1.1. Comparison of the Simulated with the Observed Array Power

The key figure characterising the reliability of the set of identified parameters is the precision of the long-term performance prediction.

In order to estimate the accuracy of the long-term performance prediction an investigation on how close each set of the identified parameters is able to predict the monitored array power was carried out. To improve the reliability of this analysis, the prediction is made for the time period other than the period taken for identification of the parameters.

Table 4 shows the comparative results for energy yield prediction for September 1996 using sets of parameters identified. In general, the identified parameters based on airside data predict the power more precisely. Nevertheless, the maximum deviation is 4.2 % computed by the set of parameters derived from the waterside data (here the thermal capacity being set to 28 kJ/K/m²).

If monthly power is being predicted, it is estimated that for the particular system the accuracy of energy yield prediction is 5%.

Test Sequence	Difference between Predicted and Observed Array Power for September 1996
August 22nd – September 2nd Airside	+ 0.7 %
September 1st – September 10th Airside	+ 0.5 %
September 10th – September 19th Airside	+ 0.4 %
September 16th –October 1st Airside	- 0. 4 %
September 1st – September 20th Waterside	+ 2.3 %
August 20th – September 10th Waterside	+0.2 %
September 10th – September 30th Waterside	+ 4.2 %
September 20th – October 10th Waterside	+ 2.0 %

Table 4. The difference between predicted and observed array power for various sequences for data collected at airside and waterside of the heat exchanger

4.2. Tjørnegade

Tjørnegade is situated just outside the centre of Copenhagen in an urban location with surrounding buildings of 4-5 storeys.

The solar air collector at Tjørnegade is a roof space collector where the southern part of the attic is utilized as a solar air collector. The cover consists of triple walled ribbed sheets of UV stabilized polycarbonate. Behind the cover is a black felt mat acting as absorber. The inlet air to the collector is blown into the space between the cover and the felt mat and sucked through the felt mat – see figure 5. The area of the collector is 150 m². The tilt and azimut is 40.5° and 15 ° to the west respectively. A photo of the building is shown in figure 6.

The system is equipped with a two-speed fan in order to save electricity. The flow rate (at low temperature differences between storage and collector) is approximately 1750 m³/h while at higher temperature differences it is approximately 3750 m³/h. The fan starts at low speed at a ΔT between storage and collector of 4 K and switches to high speed at a $\Delta T = 10$ K. The fan switches back to low speed at a $\Delta T = 7$ K and stops at a $\Delta T = 2$ K.
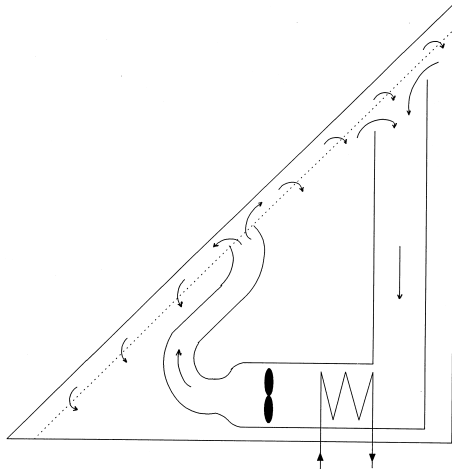
Figure 5. The principle of the roof space collector at Tjørnegade.

Figure 6. The building in Tjørnegade with the roof space collector.

Table 5 shows the identified parameters using the developed method.

Parameters	Optical efficiency	Thermal capacity	Heat loss coefficient, U_0	Heat loss coefficient, U_t
Identified Parameters	0.62 ± 0.03	(31.2 ± 2.3) kJ/Km²	(3.13 ± 0.35) W/Km²	(0.032 ± 0.005) W/K²m²

Table 5. Identified set of parameters for the Tjørnegade array

As for the Havrevangen system, the correlation coefficient between the uncertainties of parameters U_T and U_0 is high (0.92) implying that parameter U_T is not necessary.

Several short-term (up to 20 days) measurement sequences were selected for identification of the collector parameters in order to investigate their accuracy and repeatability.

The repeatability of the parameters is considered important for diagnostic purposes. For the particular system the repeatability of the key parameters is not satisfactory using short-term test sequences. The optical efficiency is repeatable within 15%, and the effective heat loss coefficients differ up to 25% and the thermal capacities up to 40%. The repeatability of the optical efficiency is considerably lower than for the Havrevangen system. The main reason for the relatively low repeatability of the optical efficiency is due to the limited operating range of reduced temperatures, T*. That is a reason for a high correlation coefficient between the uncertainties of the optical efficiency and the heat loss coefficient.

4.2.1. Comparison of the Predicted with the Measured Array Power

The comparison of measured with predicted power is considerably better if longer periods are considered as may be expected. Table 6 shows the comparative results for the energy yield prediction for August, September and October 1996 using sets of parameters identified from different periods. The maximum deviation is 5.3 % induced by an eleven day sequences. Especially critical is the prediction of the energy yield for October, as more precise prediction requires a long-term (2 months) test period. If the identified parameters are based on long-term (two months) testing, the maximum deviation of the prediction is estimated to only 1.1%.

5. CONCLUSION

Two primary goals have been fulfilled within the work:

- It has been demonstrated that with a careful measuring procedure it is possible to achieve satisfactory accuracy of energy flow measurements in air ducts - comparative with the accuracy of energy flow measurements in liquid.
- The method for in-situ characterisation of air heating collectors has been validated.

The method has been demonstrated on two different types of solar air heating systems (Havrevangen and Tjørnegade) showing a wide applicability range of the method.

.Test Sequence	Difference between Predicted and Observed Array Power (month / 1996)		
Time Period	August	September	October
July 30th - August 9th	+ 1.3 %	- 0.2 %	- 5.3 %
August 1st - August 20th	+ 0.4 %	- 0.4 %	- 2.7 %
August 20th - September 10th	+ 2.0 %	- 2.7 %	- 4.6 %
September 1st - September 10th	+ 3.0%	- 2.8 %	- 4.9 %
August	+ 0.6 %	- 0.9 %	- 4.9 %
August & September	- 0.4 %	+ 0.2 %	- 1.1 %
September & October	+ 1.1 %	- 0.1 %	+ 0.1 %

Table 6. The difference between predicted and observed array power for various sequences

The most important feature of the method is its ability to accurately predict a long term energy yield. Prediction of energy yield shows encouraging accuracy, e.g. better than 4.2 % for the Havrevangen collector and 5.3 % for the Tjørnegade collector. If longer measuring periods are used for the identification, the accuracy will increase in both cases.

As the parameters obtained from the test have their physical meaning. The application of the test results is, therefore, not restricted to performance prediction, it allows also diagnostics on system malfunctions.

The potential of the method as a diagnostic tool was demonstrated when the Havrevangen system had a periodic malfunction during the measuring period (Bosanac and Jensen, 1997). This feature of the method may be used to develop a tool for permanent monitoring of system performance and on-line detection of any system malfunctioning. Measured and simulated collector output may continuously be compared (using apriori identified collector parameters). Such a tool would especially be suitable for larger systems where a prompt identification of system malfunctioning would be cost effective.

Accordingly the in-situ method has a potential as a useful tool in scope of quality assurance for large solar systems.

The method was in 1998 accreditated and implemented in line with the already existing certified test methods at the Solar Energy Centre.

7. REFERENCES

Ambrossetti, J P (1983). Das neue Bruttowärme-ertragsmodel für Sonnenkollektoren. Technical Report, EIR Würenlingen, ISBN-3-85677-012-7.

Bosanac M, (1993). TYPE 59, TRNSYS Module for Dynamic Simulation of Collectors and Collectors Arrays, Expert Meeting IEA Task XIV, Rome 1993.

Bosanac M, Brunotte A, Spirkl W and R. Sizmann (1994). Use of Parameters Identification for Flat Plate Collector Testing under Non Stationary Conditions. J. Renewable Energy Sources, 4, pp 217-222.

Bosanac M, Jensen S. Ø. (1997). In-situ Solar Air Collector Array Test. Solar Energy Laboratory, Danish Technological Institute.

Spirkl W (1992). Dynamic SDHW System Testing, Program Manual, Sektion Physik der Ludwig-Maximilians Universität München.

8. NOMENCLATURE

A — total collector (aperture) area of the array

C — collector array total thermal capacity, NC_n

C_n — the heat capacity of each collector node

c_p — specific heat coefficient of the fluid in the collector loop

F' — collector array efficiency factor

G — incident total radiation on a flat surface per unit area

$G_{beam}, G_{diff}, G_{alb}$ — incident direct, diffuse and ground reflected radiation

$K_{beam}, K_{diff}, K_{alb}$ — incidence angle modifiers, beam, diffuse and ground reflected radiation

m_c — collector fluid mass flow rate

r — parameter for incident angle modifier

N — number of nodes

$q_{u,n}$ — rate of energy gain by collector node

T_a — ambient air temperature in vicinity of collector array

T_m — collector mean fluid temperature

T_n — collector node temperature

T^* — reduced temperature

U_L — overall heat loss coefficient

U_o — overall heat loss coefficient when $T=Ta$, and $v=0$

U_v — coefficient characterising wind dependence on the heat loss coefficient

U_T — coefficient characterising temperature dependence of the heat loss coefficient

v — wind speed in the collector plane

dt — time step

dT — increment in node temperature over the time step

$(\tau\alpha)_0$ — product of cover(s) transmittance and absorber absorptance for normal incident angle

θ — incident angle of radiation